Decellularized Wharton's jelly matrix as a three dimensional scaffold for wound healing and hair regeneration applications

By

Sushma Jadalannagari

M.E. (Hons.), Biotechnology, Birla Institute of Technology and Science, India, 2011

Submitted to the graduate degree program in Department of Bioengineering and the Graduate Faculty of the University of Kansas in partial fulfillment of the requirements for the degree of Doctor of Philosophy.

_____
Chairperson Dr. Candan B Tamerler

_____
Dr. Omar S Aljitawi

_____
Dr. Arghya Paul

_____
Dr. Dhaval Bhavsar

_____
Dr. Lynda Bonewald

Date Defended: 17th June 2016

The Dissertation Committee for Sushma Jadalannagari certifies that this is the approved version of the following dissertation:

Decellularized Wharton's jelly matrix as a three dimensional scaffold for wound healing and hair regeneration applications

_____

Chairperson - Dr. Candan B Tamerler

_____

Co-Chair - Dr. Omar S Aljitawi

Date approved: 17th June 2016

Abstract

The repair and management of full-thickness skin defects such as those resulting from burns and chronic wounds remains a significant challenge. The shortage of donor sites makes it impractical to treat with autologous skin grafts for defects exceeding 50-60% of the total skin area. Thus, the most promising approach for the repair of full thickness wound is using a tissue-engineered skin graft with the primary goal is to restore lost barrier function. However, regeneration of appendages like hair follicles and sebaceous glands has not yet been achieved. Previously, we have shown that maintaining WJMSCs seeded onto DWJM in osteogenic media induces ectodermal differentiation evident by generating CK 19 positive cells. WJMSCs are easily accessible non-controversial source of MSCs with self-renewal ability and extended proliferation potential, making them excellent candidates for tissue engineering. This dissertation presents a novel method to promote complete skin regeneration. To achieve this, we ectodermally differentiate Wharton's jelly mesenchymal stem cells (WJMSCs) by seeding these cells onto a three-dimensional decellularized Wharton's jelly matrix (DWJM) and maintaining them in osteogenic differentiation (OD) media. The combination of WJMSCs, DWJM, an acellular dermal graft (DG) (Alloderm®) and the ectodermally differentiated cells were investigated in a wound healing mouse model. The extraction, characterization and use of DWJM in skin tissue engineering as a bioactive, biocompatible and biodegradable scaffold were demonstrated. WJMSCs cultured on DWJM or DG in both regular and OD media generated cytokeratin19 (CK19), collagen I, and alpha-smooth muscle actin (αSMA) positive cells demonstrating ectodermal differentiation. Further, hair-like structures were generated only when WJMSCs were cultured in OD media on DWJM. We explored the underlying molecular mechanisms for ectodermal differentiation in our model and observed up-regulation of β-catenin,

noggin, VCAN, and SMAD genes. Mice with full thickness wounds when transplanted with *in vitro* differentiated/undifferentiated WJMSCs on DWJM demonstrated no skin regeneration. However, mice transplanted with *in vitro* differentiated WJMSCs on DG demonstrated complete skin regeneration along with skin appendages like hair follicles and sebaceous glands. Further, the combination of DWJM and DG with *in vitro* differentiated WJMSCs also showed complete skin regeneration but skin appendages were not as developed. Thus, this current dissertation demonstrates the use of differentiated WJMSCs in combination with DWJM and DG as a novel approach for complete skin regeneration of full thickness wounds in a mouse model.

Keywords –Wharton's jelly mesenchymal stem cells, decellularized Wharton's jelly matrix, osteogenic differentiation media, ectodermal differentiation, and hair-like structures.

Acknowledgments

I would like to thank Drs. Omar S Aljitawi, Candan B Tamerler, Dhaval Bhavsar, Lynda Bonewald and Arghya Paul for serving on my dissertation committee and providing me with continual support and guidance in developing my research and dissertation. I would like to thank Drs. Tara Lin, Brea Lipe and Omar Aljitawi, supported by division director Dr. Joseph McGuirk, for making the Hematology and Transplantation lab a great place to work and for accepting me to be a part of this lab. I am eternally grateful to my mentor and advisor, Dr. Omar S Aljitawi, for providing scientific advice, continual daily guidance, and support in terms of professional and personal needs. He encouraged independent thinking and enabled me to develop into a skilled researcher. Dr. Dhaval Bhavsar has played a crucial role in my research by providing advice in developing research goals, imparting his expertise on mice wound healing surgeries, and constantly encouraging and supporting through all animal experiments.

I greatly appreciate the efforts and continual support of Dr. Richard Hopkins and his lab members especially, Christopher McFall and Eric Buse, who provided training and provided me with decellularized matrix whenever required. I would like to thank Dr. Lynda Bonewald for providing me with GFP-Dmp mice and her constant support, criticism and encouragement in writing my dissertation and preparing my thesis. I am extremely grateful to Dr. Jinxi Wang and Dr. Yi Feng for their training, technical assistance and scientific advice related to mice craniotomies. I would like to give special thanks to Marsha Danley for her help, patience and support related to making and the histological sections and their examination. I would also like to take this opportunity to thank all the nursing staff at the Labor and Delivery unit of KUMC, especially Pearlette Davis, Juanita Harris and Laura Muehlman for helping me with umbilical cord collection on a regular basis. The veterinarians and staff of KUMC LAR were very helpful

and cooperative in maintaining our mice and enabling a major part of my research.

A special thanks to Dr. Brenda Rongish, Dr. Charlie Little and Michael Filla for their assistance with live cell imaging and helping me gain important insights into my research. Additionally, I would like to acknowledge those who were active in helping me conduct my research by providing assistance with equipment and instruments like Drs. Peter S Rowe, Dan A Dixon, Sufi Thomas, Ranjan Preet, Vikalp Vishwakarma and Dhruv Kumar. I greatly appreciate Dr. Lisa Stehno-Bittel for giving me the opportunity to conduct my initial experiments in her lab and sincere thanks to Sonia Rawal for her technical expertise on the confocal microscope and her constant support and encouragement. I would like to acknowledge the efforts of Megan Swink, Gerrie Nowak, Bea Coelton and Amanda Wise in ordering the supplies and enabling my research. I would also like to thank Dr. Sara Wilson and Denise Bridwell, for handling everything at the departmental end. Thanks to my fellow lab-mate Dr. Dandan Li, for her encouragement, support and assistance in continual lab maintenance. Very special thanks to Abigale Berry for her assistance with research and patience during extensive surgery days. She has been a great friend who provided emotional support. Also, thanks to Mathew Allan for being very cheerful and motivating me during low times.

Most Importantly, I want to thank my parents, Pedda Hussainaiah Jadalannagari and Usha Jadalannagari, for their continual love and enabling me to dream big. Thank you for believing and constantly supporting me. I would like to convey my special gratitude to my husband Dr. Chaithanya Ponnaluri, for his unconditional love, support, encouragement, motivation, scientific advice and professional guidance. Thank you for trusting me and motivating me to achieve and accomplish more. I would also like to thank my in-laws Durga Prasad Ponnaluri and Anantha Gowri Ponnaluri, my brother Satish, and Lakshmi, Sagar for their

love and support. Lastly, a special thanks to all my friends for their friendship, support and motivation through my academic journey.

DEDICATED TO MY BELOVED PARENTS AND HUSBAND

Table of Contents

List of Figures

List of Tables

Chapter 1: Introduction

A full-thickness wound to a complex tissue such has skin, results in damage to many structures, cell layers and all lineages. A wound could damage the outermost epidermal keratinocyte layer with its associated epidermal components such as hair follicles, sweat glands, the underlying basement membrane, and the dermis which is comprised of fibroblasts, extracellular matrix, nerves, blood and lymphatic systems [1]. Wounds could be caused by trauma, medical conditions, and burn among others. According to the Centers for disease control and prevention, burns and fires are the third leading cause of death at home. In 2010, a fire injury occurred every 30 minutes, while a fire-related death occurred every 169 minutes [2]. As per the American burn association, about 450,000 patients receive treatment in hospitals and emergency rooms each year. Forty four percent of burn center admissions are a result of fire, while 33 percent are scalding injuries resulting from wet or moist heat and 9 percent from contact with a hot source, 4 percent are electric burns, 3 percent are chemical burns and the remaining 7 percent are due to other miscellaneous sources like vehicle crashes etc. [3]. Burn and fire hospitalizations in the US cost $1billion per year, while non-hospitalized burn and fire injuries cost $3 billion. Although burns differ from other wounds in the degree of systemic inflammation, the healing and repair of burns is an essential dynamic physiological process required for maintaining tissue homeostasis. Healing and management of full-thickness wounds is a dynamic, complicated, and coordinated series of hemostasis, inflammation, and proliferation/granulation and matrix formation/remodeling.

Wound Healing

Wound healing and repair occurs in various stages are described below and in Figure 1.

Hemostasis

Hemostasis is the immediate response to a skin wound, where damaged and stressed cells activate stress signal pathways such as SAP/JNK and p38, which result in phosphorylation of a cascade of signaling molecules that can alter gene expression, cell survival and metabolism [4, 5]. The damage to blood vessels is combated by platelet activation and aggregation and fibrin clot formation. Several growth factors such as platelet derived growth factor, CXCL4, basic fibroblast growth factor, vascular endothelial growth factor and transforming growth factor – β are released into the serum and several interleukins, TNF-α, Interferon-γ to induce transcription of immediate and early genes to assist with the repair process including angiogenesis, inflammation and migration of keratinocytes and fibroblasts [6].

Inflammatory response

The inflammatory response to wounding begins with passive leakage of circulating leukocytes such as neutrophils from damaged blood vessels into the wound. Immune cells such as mast cells [7], and Langerhans cells [8] are released which in turn release a variety of chemokines and cytokines. Neutrophils and macrophages are also recruited to trigger local endothelial cell activation followed by tethering of leukocytes to the vessel wall [9, 10].

Angiogenesis

Angiogenesis involves sprouting of wound-edge capillaries followed by their invasion into the site of damage which helps in formation of new micro-vascular networks throughout the wound to provide nutrients and oxygen to the growing tissues and aid in the formation of provisional wound matrix, also known as granulation tissue [11]. A clot/scab is formed as a temporary mechanism to restore the function by acting as a protective barrier to skin. The proliferation, migration and contraction are the final mechanism that the body adopts to close the

wound gap and replenish lost tissue. This process is initiated within hours, but the time required to heal is highly variable and depends on size and location of wound as well as on the age and health of tissue.

Re-epithelialization

Re-epithelialization of a wound begins with cell-cell and cell-matrix adhesions between keratinocytes, fibroblasts and the surrounding stem cells from the epidermis and bulge region of hair follicles [12]. These enable deposition of matrix proteins such as laminin V, fibronectin and collagen IV that help in regenerating an epidermis [13-15]. The fibroblasts and myofibroblasts from the close vicinity of wound respond by forming weakly contractile actin bundles, which enable connective tissue contraction, and synthesis, bundling collagen fibers thereby, constituting the primary scar tissue and dermis [16, 17].

Remodeling

During the final stage, blood vessels within the scar are refined and mature to form a functional network [18]. The dense extracellular matrix is remodeled to restore normal architecture to dermis through collagen synthesis, bundling and degradation. Neutrophils are cleared by apoptosis and subsequent phagocytosis by macrophages [19]. Imperfect regulation of wound resolution can result in hyper-proliferation, persistence of inflammatory reaction, fibrosis and excessive scar formation [20].

The treatment of patients with severe burn exceeding 50-60% of the total body surface area such massive deep burns or chronic ulcers, has been the biggest challenge despite of refinements in burn shock resuscitation, improvements in surgical techniques, advances in intensive care medicine and the availability of expert surgeons [21]. A major problem associated with the treatment of these burns injuries is the limited availability of autologous skin for

transplantation and the creation of additional donor site morbidity [21]. Harvesting a split thickness skin graft with epidermis and a part of dermis is a viable possibility, but this could lead to keloid formation and increased scarring, especially in children [22].

Natural Scaffold Materials in Skin Repair and Wound Healing

To assist in wound healing, there are variety of naturally obtained scaffold materials such as collagen, gelatin, silk fibroin, fibrin and elastin along with polysaccharide polymers like chitosan, starch, alginate, hyaluronan, chondroitin sulphate that can assist in the process of wound healing and skin regeneration.

Collagen is regarded as an ideal scaffold as it is a major protein component of extracellular matrix, providing support and transducing essential signals for regulation of cell anchorage, migration, proliferation and differentiation for connective tissues like skin, tendons, bones, cartilage, blood vessels and ligaments [23-26]. Collagen also has high mechanical strength, good biocompatibility, and low antigenicity and is easily cross-linked [23]. Apligraf® (Organogenesis, USA) is a bi-layered collagen gel seeded with human fibroblasts in the lower part and human keratinocytes in the upper layer and is being used as a dermal matrix for artificial skin. Although collagen has some great applications, it also linked with some disadvantages such as sterilization drawbacks, difficulty in processing, disability to control the rate of degradability and also the potential for viral and prion contamination since they are derived from animals and the associated high cost of purification techniques [27].

Gelatin is a natural polymer derived from collagen and is commonly used as a carrier for drug delivery and tissue engineering applications due to its biodegradability, biocompatibility and the possibility of poly-ion complexation. Ito *et al.* developed a novel biodegradable hydrogel by cross-linking gelatin with transglutaminase (TGase) in an aqueous solution. They showed that

incorporating cell adhesion factors like vitronectin, fibronectin and two RGD peptides - RGDLLQ and RGDLLG in the hydrogels enhanced proliferation of NIH3T3 fibroblasts and this biomaterial can be used for wound dressing and tissue engineering applications[28].

Silk Fibroin is a protein polymer from Lepidoptera larvae such as silkworms, spiders, scorpions, mites and flies, which are spun into fibers [29]. These fibers are light in weight, extremely strong, and are an excellent biomaterial because of their biocompatibility [30, 31], slow biodegradability [32] and great mechanical properties. Min *et al.* developed an electro spinning method to fabricate silk fibroin nano-fiber nonwovens for cell culture of normal human keratinocytes and fibroblasts and showed that these fibers are a good candidate for tissue engineering and wound dressing applications [33].

Fibrin is a protein matrix produced from fibrinogen, which can be autologously harvested from the patient [34]. Fibrin glue is a biological adhesive used in abdominal, thoracic, vascular, oral and endoscopic surgeries due its hemostatic, chemotactic and mitogenic properties[35]. Neidert *et al.* developed scaffolds of fibrin gels with entrapped tissue cells to improve collagen content and enhance mechanical properties to develop robust fibrin based tissue equivalents for soft connective tissue applications [36].

There are also other protein-based biopolymers such as elastin and soybean, which have been used as scaffolds in tissue engineering. Elastin is an extracellular matrix protein deposited in the arterial wall and synthesized by vascular smooth muscle cells and secreted as a tropoelastin monomer that is soluble, non-glycosylated and highly hydrophobic [37]. Soybean is a leguminous plant, which produces soy protein, a renewable, inexpensive, and biodegradable material with potential tissue engineering applications.

Polysaccharidic polymers

This class of biopolymers includes chitosan, alginate, hyaluronan and chondroitin sulphate, which are constituted by simple sugar monomers [38]. They can be obtained from different sources like microbes, animals, and plants. They share chemical similarities to heparin, show good hemocompatibility, are non-toxic, and have low costs in comparison with other biopolymers like collagen [39, 40]. Chitin is a natural polysaccharide obtained from crustacean shells, inset cuticles or fungal cell walls. Chitosan is the fully or partially deacetylated form of chitin and is used in a variety of applications like skin, bone, cartilage and vascular graft tissue engineering. They are biologically renewable, biocompatible, biodegradable, non-antigenic and bio functional biomaterials [41]. Owing to the wound healing properties of chitosan, bandages containing chitosan are commercially available as HemCon® bandages (HemCon Medical Technologies, Portland, OR). Kweon *et al.*, has proved that a water-soluble chitosan/heparin complex can be an effective wound healing accelerator [42] and Mayol *et al.* reported that a sterile and biocompatible chitosan gel increased proliferation of human foreskin fetal fibroblasts at 24h and accelerated wound healing in an *in vivo* model of pressure ulcers [43]. In a mice model Burkatovskaya *et al*., stably infected the open excision wounds with Pseudomonas and Staphylococcus bacterial and compared the antimicrobial activity by treating the wound with HemCom™ bandage and a chitosan acetate bandage with alginate sponge bandage and silver sulfadiazine cream. They demonstrated that chitosan acetate rapidly kills bacterial in the wound before systemic invasion and are superior to alginate bandages and silver sulfadiazine. Burkatovskaya *et al*. also showed that chitosan acetate bandages could effectively control the growth of bacteria in burns and prevent systemic sepsis [44-46]. Ong *et al*. demonstrated that refining chitosan dressings with polyphosphate and silver improves the hemostatic and

antimicrobial effects by accelerating blood clotting, increasing platelet adhesion and thrombin generation. They also show that testing this dressing in suitable animal models significantly reduced mortality from 90% to 14.5% in *P.aeruginosa* wound infection [47]. Cakmak *et al*. showed that meshes coated with triclosan loaded chitosan gels could be effective for preventing graft infections [48]. Although chitosan gels and bandages are shown to improve wound healing, they have been reported to cause lethal pneumonia in dogs and intra-tumor injection of chitosan to mice bearing tumors increases the rate of tumor metastasis and growth [49].

Hyaluronan is a naturally occurring glycosaminoglycan and a major macromolecular component of the intracellular matrix of connective tissues such as vitreous of the human eye, umbilical cord, cartilage and synovial fluid. Hyaluronan has many physiological roles including tissue and matrix water regulation, structural and space-filling properties, lubrication etc. [50]. Pianigiani *et al*. developed a three-dimensional model based on fragments of human de-epidermized dermis to study micro-perforated, hyaluronan-based membrane as a carrier of cultured epidermal cells and demonstrated that human epidermal cultures migrated from the hyaluronan membrane with growth resembling "*in vivo*" re-epithelialization [51]. Mineda *et al*. showed that the injection of 3D cultured mesenchymal stem cells in a non-cross linked hyaluronic acid gel on an ischemia-reperfusion injury to the fat pad in SCID mice promoted angiogenesis and tissue regeneration, thus proving a potential application of hyaluronan for wound healing [52].

Chondroitin sulfate is another glycosaminoglycan found in the lubricating fluid of joints and is a component of cartilage, synovial fluid, and bone and heart valves. Chondroitin sulfate is a component of the dermal layer of FDA-approved skin substitute for treating burns [53] and a constituent of Integra® bilayered dermal regeneration template (Integralife, Plainsboro, NJ). It is

composed of collagen and chondroitin-6-sulfate for skin replacement by acting as a scaffold for dermal regeneration.

Engineered Grafts

There are also new biomaterials developed from the combination of several polymers such as, a novel three dimensional multilayered fibrous constructs developed from chitosan and hyaluronic acid on Poly (ε-caprolactone (PCL) by Reis *et al*. for application as wound dressing materials [54]. Wang *et al*. developed a biomimetic bi-layered gelatin-chondroitin 6 sulfate-hyaluronic acid biopolymer with keratinocytes in the upper layer and dermal fibroblasts in the lower layer, resembling autologous skin equivalents [55].

Tissue engineered autologous dermoepidermal skin grafts such as Permaderm (Regenicin Inc., New Jersey), denovoSkin and denovoDerm (University of Children's Hospital, Zurich) and Epidermal autografts like Epicel (Genzyme Corp., New Jersey), MySkin (Altrika Ltd., New Jersey) and dermal epidermal autografts such as Hylograft 3D + Laserskin (Fidia Farmceutici, Abano Terme, Italy) have been recognized as promising alternatives to autografts [56]. These grafts use autologous fibroblasts and keratinocytes on a variety of scaffold materials like collagen-glycosaminoglycan substrate, collagen type I hydrogel or hyaluronic acid sheets and have the ability to close wounds by preventing dehydration and infections alongside avoiding any tissue availability concerns [56, 57].

Although a new epidermis and dermis are formed during the repair and healing process, epidermal appendages such as hair follicles and sebaceous glands cannot be regenerated in these kinds of wounds [58]. The lack of hair in grafted sites has psychosocial, psycho-emotional and physiological impacts on the patient [59]. The loss of hair in cases like telogen effluvium and androgenetic alopecia is known to be associated with anxiety and distress with patient suffering

comparable to a severe chronic or life-threatening disease [59-61]. Since hair follicles are developed only during embryonic development and no new hair follicle formation occurs in the adult, and they cannot regenerate on their own after damage without a proper stimulus, new and healthy hair follicles or trichogenic cells need to be introduced to the affected area for regeneration of hair [62]. Hair cycling also serves as a self-protecting system, removing rapidly proliferating keratinocytes in the catagen and preventing oxidative stress and malignant degeneration [63]. Hair follicles may also have paracrine and endocrine function on various cells and structures within the skin. The factors secreted by follicles are also involved in wound healing, re-epithelialization and tissue expansion [64, 65].

Hair Regeneration

Hair follicles are highly regenerative, complex, ectodermal-mesodermal structures enriched with stem cells [62]. They consist of dermal papilla or follicular papilla, which determines the thickness, length and life cycle of hair. The hair bulb surrounds the dermal papilla and produces melanin granules along with hosting keratinocytes that are important for growth and regeneration of hair follicle and epidermis. The interactions between dermal papilla cells (mesenchymal) and follicular keratinocytes (epithelial) play an essential role in normal hair growth [66].

Hair Follicle Formation

Hair follicle is a complex organ formed during the first trimester of pregnancy. During embryonic development, after gastrulation, a single layer of pluripotent ectoderm covers the embryo surface. Following this, mesenchymal cells populate the skin and form the epidermis and its appendages. The basement membrane separates the skin epithelium from its underlying dermal mesenchyme. The dermal cue signals the overlying epithelium to thicken and form a

placode that grows downward to form hair germ while, the epithelial cells cue the underlying mesenchyme to organize the dermal papilla (DP) **(**Figure 2**)**. The interactions between hair germ epithelium and dermal papilla stimulate the epithelium to proliferate and produce hair follicle. As the follicle grows downward, the developing hair germ cells that lose contact with dermal papilla become the outer root sheath (ORS), while the cells that maintain contact become matrix cells that form the inner root sheath (IRS). Sebaceous glands emerge on the upper segment as appendages, which secrete lipids (sebum) into the hair canal at the skin surface.

As the hair follicles fully mature, the matrix cells at the base of the follicle proliferate and differentiate to yield a period of active hair growth (anagen). Due to the limited proliferative ability of the matrix cells, a destructive phase (catagen) is initiated which leads to apoptotic cell death of the lower two-thirds of hair follicle followed by bulge formation, and a resting phase (telogen). Postnatally, the resting phase is followed by a spontaneous mesenchymal –epithelial cross talk that leads to a new hair cycle initiation.

Molecular Mechanisms Involved In Hair Follicle Formation and Regeneration

The signaling communication between epidermis and the underlying mesenchyme initiates hair follicle morphogenesis. These interactions depend on the signaling interplay of secreted molecules of Wnt/wingless family, the hedgehog family, members of TGF- β /BMP (Transforming growth factor- β/ bone morphogenetic protein), FGF (Fibroblast growth factor) and TNF (Tumor necrosis factor) families [67-69]. Different combinations of these signals may dictate the outcome – tooth, scale, hair or feather formation [67-69]. The Wnt pathway plays an essential role during hair follicle induction, Shh (Sonic hedgehog) is involved in late stage differentiation and morphogenesis, Notch signaling determines stem cell fate and BMP is involved in cellular differentiation. Wnt signaling proceeds through EDA/EDAR/NF-ϰB

(Ectodermal dysplasia/receptor/ nuclear factor-kappa beta) signaling where NF- ϰB regulates the Wnt pathway and acts as a signal mediator by up regulating Shh ligand expression. Dermal Shh and PDGF (Platelet derived growth factor) signaling up-regulates dermal noggin expression, which counteracts BMP mediated β-catenin inhibition [70].

Hair follicle induction

In mice Wnt and BMP are essential for development of skin epithelium (from ectoderm), whereas, Wnt/β-catenin signaling alone decides dermal fate. Mesenchymal cells from diverse origins populate the dermis and start interacting with overlying epidermis to induce the growth of regularly interspaced hair placodes. Specific cues from dermis are thought to induce overlying epidermal keratinocytes to assume an upright position and start proliferating. The hair follicle hosts two stem cell populations – one in the bulge and the other in hair germ, and their growth is governed by the epithelial mesenchymal interactions [71-73]. Canonical Wnt/ β-catenin signaling acts as the primary switch for hair follicle fate as absence of β-catenin or the inhibition of β-catenin by ectopic epithelial expression of the secreted Wnt inhibitor Dkk1 results in the absence of hair follicle induction [74, 75]. Conversely forced expression of a stable form of β-catenin causes strong enhanced placode formation due to the epidermal keratinocytes globally adopting a hair follicle fate [76, 77]. Edar signaling has also been implicated in hair follicle induction, by inhibiting BMP and refining β-catenin signaling by promoting Shh signaling[78].

Wnt signaling is mediated by the stabilization and translocation of the key signal transducer β-catenin, which is known to be necessary for hair follicle formation and regeneration. Inactive β-catenin is degraded in the cytoplasm by the GSK3 kinases that causes phosphorylation of β-catenin's N terminus and targets its cytoplasmic pool for ubiquitin-mediated degradation [79, 80]. Activation by *Wnt/Wingless* inhibits GSK 3 kinases, thus leading

to β-catenin accumulation in the cytoplasm further translocating to the nucleus where β-catenin interacts with Lef-1/Tcfs to generate a functional transcription factor complex thereby, activating the downstream target genes [81, 82]. Expression of activated β-catenin throughout the basal epidermis induces *de novo* hair follicle formation within the epidermis [83, 84]. Hair follicle initiation also requires down regulation of keratinocyte growth factor (KGF) and epidermal growth factor (EGF) signaling.

Hair follicle morphogenesis and organogenesis

Epithelial placode cells signal the underlying mesenchyme to form the dermal condensate that gives rise to the dermal papilla. Shh plays a pivotal role in dermal papilla maturation and growth [85, 86]. The dermal condensate then signals the epidermis to allow placode growth into the underlying mesenchyme and thus reciprocal epithelial-mesenchymal signaling leads to the maturation and formation of different hair follicle lineages [87]. Local gradient of hair follicle activators and inhibitors determines epidermal keratinocyte and follicular keratinocyte fate.

BMPs are secreted signaling molecules of the TGF-β superfamily that exert a biological activity via interaction with specific BMP receptors. Interactions of exogenous BMPs with its receptor BMPRIA, phosphorylates SMAD 1, 5 and 8, which function in complexes with SMAD 4. BMPs interact with a variety of growth factors like Wnt, Shh, TGF- β, EGF, FGF and Notch to a control a variety of cellular functions like cell proliferation, differentiation, apoptosis during skin and its appendage development [88-91]. The mesenchyme expresses Noggin, an extracellular BMP antagonist that induces hair follicle morphogenesis in the embryo and promotes new hair follicle growth postnatally [92, 93]. After the embryonic hair follicles have been initiated, BMP4 is expressed suggesting a negative feedback loop to prevent further new

hair follicle formation, but help with differentiation of cells into Inner root sheath (IRS) and hair shaft [94].

Shh signaling in skin controls the growth and morphogenesis of hair follicle epithelium through the Gli transcription factors [95]. It is crucial for hair follicle development and cycling as the deregulated members of Shh signaling cascade alter hair follicle formation and generates epidermal neoplasia [96]. Shh signaling controls the hair follicle morphogenesis and the initiation of primary and secondary hair follicles [86, 97]. In anagen skin, Shh is expressed in high levels in follicle matrix and acts as a mitogen to drive anagen regeneration [85, 98]. TGF-β2 signaling is essential for transient induction of transcription factor Snail and activation of MAPK pathway which in turn regulates cell proliferation and cell adhesion, precisely governing epithelial proliferation, junctional remodeling and bud formation which helps in proper progression of hair morphogenesis [99].

Hair follicle regeneration

The hair cycle undergoes three phases, which includes growth phase (anagen), regression phase (catagen) and telogen [71, 100]. During regeneration, hair germ stem cells are activated followed by the bulge stem cells [71]. In anagen, the dermal papilla limits the newly formed hair bulb and stimulates the undifferentiated bulge cell progeny, which are present along the outer root sheath (ORS) to proliferate. This leads to the formation of transiently amplified matrix cells in contact with dermal papilla to terminally differentiate to form hair and inner root sheath. During anagen to catagen transition, matrix cells undergo apoptosis and dermal papilla retracts upward. The result of growth factor signaling depends upon the cell type, the signal received and the receptor because, EGF and EGFR promote catagen, while IGF-1, FGF and PDGF promotes anagen. At the onset of telogen, BMP signals from surrounding dermal tissue impose a

threshold that needs to be overcome to initiate the next hair cycle or the dermal papilla is dislodged from the niche to maintain quiescence [92, 101-103]. TGF-β2 is an important factor for regeneration of hair follicle as it activates Smad2/3 pathway, which activates the target gene Tmeff1 that lowers the threshold of BMP in the niche promoting stem cell transition from telogen to anagen [104] .

Engineering hair follicles in vitro

Reynolds and Jahoda *et al*. demonstrated that dermal stem cells and dermal papilla cell isolation and expansion *in vitro [73, 105, 106]*, which lead to revolutionizing concepts in engineering hair follicle *in vitro* and *in vivo*. The extraction of hair follicles require microdissection and enzymatic dissociation using collagenase, dispases or a combination of both, where enzymatic damage to isolated cells and cell surface proteins could be an issue. Also, freshly isolated dermal papilla cells retain a high tendency to aggregate, but this characteristic gradually disappears with extended culture. Horne *et al*. observed that dermal papilla cells cultured beyond 6 passages could not form cell aggregates or induce hair follicles, although supplementation with 10 ng/ml fibroblast growth factor 2 resulted in rescuing the lost inductive capacity [73]. To effectively engineer hair follicles *in vitro,* the replication of dermal papilla - epithelial cell interactions is essential. This has been achieved by combining different cell populations like dermal papilla cells, keratinocytes, follicle outer root sheath cells in collagen gels, matrigel or a sandwiched mixture of both [107, 108]. Epidermoid cyst like spheroids and spike-like structures has been formed by encapsulation of keratinocytes in hydrogel, keratinocytes or outer root sheath cells from human hair follicles in collagen gel or matrigel [109]. Wu *et al*. cultured dermal papilla cells and dermal sheath cells in a collagen gel and showed the formation of hair follicle like concentric structures [107]. In a model developed by

Havlickova, a pseudo dermis composed of collagen I was mixed with interfollicular dermal fibroblasts and topped with stacked layers of matrigel/dermal papilla cells and matrigel/outer root sheath keratinocytes or a single layer of mixed dermal papilla cells and outer toot sheath keratinocytes in the matrigel. In both the systems, outer root sheath keratinocytes formed spheroid aggregates and retained their characteristic keratin expression patterns, with mixed cultures resulting in better proliferation. Qiao *et al*. cultured a mixture of embryonic mouse follicular dermal and epidermal cells using a hanging – drop method in methylcellulose and demonstrated the formation of proto-hair confirming the necessity of mesenchymal-epidermal interactions in folliculogenesis [110] .

In vivo induction of hair follicles

In an approach by Yoo *et al*., dermal papilla-like tissue was developed from umbilical cord MSCs following exposure to a dermal papilla forming medium [111]. This papilla when transplanted into athymic mice produced new hair follicles. Cohen *et al*. showed the formation of new whiskers by implanting isolated rat and guniea pig vibrissa trichogenic papilla to the rat ear [112] while Oliver *et al*. attempted to regenerate partial or complete hair follicles and showed that root sheath cells could regenerate dermal papilla and that the regeneration of dermal papilla was a prerequisite for hair follicle formation [113]. Three major models have been developed to evaluate the regeneration of hair follicles in immunodeficient mice, namely the silicon chamber model [114], the patch implantation model [65] and the subcutaneous cell injection model [115]. In the silicon chamber model, a bell shaped silicon chamber covers the murine full-thickness wound and a mixture of neonatal mice epidermal and dermal cells could lead to hair formation after 3 weeks [114, 116]. Kishimoto and Ehama *et al*. assessed the trichogenic efficiency of dissociated dermal papilla cells and confirmed that only versican positive dermal papilla cells

could result in new hair follicle formation [117]. The subcutaneous injection model was convenient and rapid and used by Jahoda *et al*. to culture papilla cells and demonstrates hair growth after injection into follicles of a nude mice ear [73]. However, this model repaired the injured hair follicles but could not regenerate new follicles due to the absence of epidermal-mesenchymal interactions. This model was also used by Zheng *et al*. to show that subcutaneously injecting a hair bud of epidermal cell aggregates and dermal papilla cells produced new hair, but the follicles grew outward from the aggregates and hair shaft projecting inwards into the aggregate [118]. Using this model, Wu *et al*. demonstrated that subcutaneous injection of mixture of dermal sheath cells and outer root sheath cells from human hair follicles within a customized cabin or as a cyst induced hair follicle-like structures indicating the need for *cell aggregation* [107]. Due to the associated limitations such as difficulties in controlling the injection location and cell confinement and guiding hair to grow outward, Jahoda *et al*. used the patch implantation model and demonstrated that both pelage and vibrissa dermal papilla cells retained their trichogenic capacity after introducing these cells between enzymatically separated epidermis and dermis of embryonic rat foot pads and then transplanting the combination into the rat dorsum [106, 119].

Thus, to overcome the limitations associated with the current models, we have developed a novel three-dimensional model to aid with skin regeneration along with its associated hair follicle like structures. This model is composed of Wharton's jelly mesenchymal stem cells cultured on a novel decellularized Wharton's jelly matrix and supplied with appropriate cues to favor ectodermal differentiation.

Ectodermal Differentiation of Wharton's jellyMesenchymal Stem Cells for Tissue Engineering and Regenerative Medicine Applications [1]

Wharton's jelly (WJ) is a mucoid, porous connective tissue that surrounds umbilical cord vessels and is derived from the extra embryonic mesoderm and partly from the embryonic mesoderm [120, 121]**) (**Figure 3**)**. It protects umbilical cord vessels against damage from the compression of vessels and supports the cord in maintaining blood flow during fetal gasping, normal movements, and forces of labor [122, 123]. The extracellular matrix (ECM) components of WJ are also known to be associated with a large number of growth factors like the insulin growth factor, fibroblast growth factor (FGF), and transforming growth factor-b, which control cellular proliferation, differentiation, synthesis, and remodeling of the ECM [124-127]. This mucoid connective tissue hosts some mesenchymal stem cells (MSCs) immersed in a ground substance called Wharton's jelly mesenchymal stem cells (WJMSCs) or umbilical cord MSCs [120, 121].

WJMSCs isolation, optimization, characterization, and scale-up have been extensively studied and described by several researchers [128-130] and therefore only discussed briefly here. WJMSCs can be extracted from three relatively indistinct regions of WJ called the perivascular, intervascular, and subamniotic region [131]. Significant differences *in vitro* have been noted between MSCs isolated from these three different regions structurally, by immunohistochemistry, and functional analysis [132, 133]. WJMSCs are like fibroblasts or

---

[1] Published as Jadalannagari S, Aljitawi OS, Ectodermal differentiation of Wharton's jelly mesenchymal stem cells for tissue engineering and regenerative medicine applications, Tissue engineering Part B: Reviews, 2015 June; 21(3): 314-22

myofibroblasts [128, 129, 134] in appearance, are known to display MSC surface markers, and adhere to the plastic along with the capacity to self-renew and differentiate into various lineages like bone, cartilage, and adipose [128, 129]. A single donor can provide 4–5 X 10^9 cells in five to six passages [128]. Because they have a high *ex vivo* proliferation index and low population doubling times, they can undergo a 300-fold expansion within six to seven passages without developing an abnormal karyotype [128, 131, 132, 135, 136]. These cells also have the capacity to expand in a complete xeno-free and serum-free media along with exhibiting superior growth kinetics and functional angiogenesis [137]. WJMSCs are known to have higher colony forming unit-fibroblast (CFU-F)[138] and produce some cytokines like the granulocyte-macrophage colony stimulation factor and granulocyte colony stimulating factor [139]. WJMSCs can be cryopreserved in 90% fetal bovine serum (FBS), 10% dimethyl sulfoxide for future applications, with 80% cell viability after a freeze thaw cycle as demonstrated by Puranik *et al*. [129].

The WJMSCs do not form teratomas, express a high percentage of tumor suppressor genes and secrete hematopoietic cytokines as compared to the other classes of MSC [140]. WJMSCs are also known to provide a stromal supportive niche for several primitive stem cell populations like hematopoietic stem cells and spermatogonial stem cells among others [141, 142]. Saito *et al*. also demonstrated that WJMSCs can support the growth of embryonic stem cells [143].

As described previously, MSCs obtained from WJ are multipotent and can successfully differentiate into diverse mature tissues favoring their use for regenerative medicine applications. WJMSCs share the same osteogenic differentiation pathway like the MSCs derived from bone marrow, but exhibit less mineralization in comparison to fetal bone marrow MSCs [144]. In comparison, WJMSCs also show higher collagen production and better compatibility with

decreased expression of collagen II. They also express prochondrogenic markers like Sox9 and Runx2 when co-cultured in the presence of microsphere-based scaffolds and polyglycolic acid scaffolds [145]. In addition, WJMSCs exhibit the potential to differentiate into cells of the adipogenic lineage as shown by the robust oil droplet formation when stained with oil O red staining following exposure to proper inductive stimuli and incubation times [132]. Due to their unique developmental position, these cells have an active growth potential, exhibit a specific phenotype, possess a fetal karyotype, express embryonic stem cell markers like Sox 2, Nanog, Oct 3/4A, MSC markers like CD73, CD90, CD105, and are also known to be hypoimmunogenic as they express molecules that can modulate natural killer cells and expand regulatory T-cell populations [146, 147].

The ectoderm is one of the three primary germ layers that can differentiate into structures of various shapes and sizes like the nervous system (peripheral nerves, brain, and spine), which develops from the neuroectoderm, and surface ectoderm that develops into the epidermis (skin and skin appendages), the lining of the mouth, anus, and nostrils, and exocrine glands (mammary, salivary, sweat, and lacrimal glands)(Figure 4). The organogenesis of these organs and parts is initiated during the embryonic periods, while the morphogenesis continues postnatally. These organs also have limited ability for regeneration like the cyclical growth of hair and feathers, continuous growth of nails and the rodent incisor, and growth of the mammary gland during puberty and pregnancy [148]. Despite the diversity in form and function, all these organs originate from adjacent layers of the epithelial (ectodermal) and mesenchymal (mesodermal or neural crest derived tissues). The development of these organs begins with the local thickening of the epithelial layers to form an ectodermal placode and is followed by a condensation of mesenchymal cells under the placode, which then buds into or out of the

mesenchyme. Continued folding and branching of the epithelium follow growth of these epithelial and mesenchymal components, which result in the final shape and size of the organ. There has been a growing interest in studying the potential applications of WJMSC differentiation into cells of ectodermal origin.

Surface Ectoderm-Related Regenerative Medicine Applications

Skin is composed of epithelium and along with its associated underlying connective tissue plays a role as the primary defensive barrier to maintain the physiological homeostasis [149]. Numerous diseases associated with trauma, cancer, burns, and infections among others affect the normal architecture of skin. Keratinocytes form the major population of the epithelial layer, are tightly attached to each other by cell–cell junctions, and are arranged into a number of distinctive layers. The surgery site problems associated with autologous biopsies to collect keratinocytes and long keratinocyte doubling times *in vitro* necessitate the need for an effective alternative to these areas affected by diseases [150].

Skin cells are continuously renewed by cells from the underlying epidermis, hair bulb, the melanocyte layer, and dermis [151]. Wound healing is characterized by complex biological and molecular events, which include inflammation, proliferation, and remodeling as described above [152, 153]. The major problems associated with prognosis of wound healing are scar formation, loss of normal function, and lack of formation of skin appendages, and the hurdles with healing and repair of wounds are ischemia to the affected areas, patient mobility, advanced age, and related diseases [154] .

Currently, stem cell-based therapies are attractive candidates in regenerative medicine for treating skin injuries. For example, Arno *et al*. showed that wound healing of an excisional full-thickness skin murine model was enhanced by WJMSC by promoting normal skin fibroblast

proliferation and migration [155]. In another example, Tam *et al*. used a nano scaffold of polycaprolactone with aloe vera as an antibacterial agent, impregnated with green, fluorescent protein-labeled WJMSCs in its conditioned medium, and studied healing of excisional and diabetic wounds in rats. Using scratch wound assays, they found that skin fibroblasts migrated faster from scratches into vacant areas accompanied by an increased expression of collagen I and III, elastin, fibronectin, superoxide dismutase, and metalloproteinase-1 compared to their controls [156]. These scaffolds with WJMSCs also showed rapid wound closure, re-epithelization, increased number of sebaceous glands and hair follicles along with positive keratinocyte markers like cytokeratin, involucrin, filaggrin, and elevated expression of intercellular adhesion molecule-1 (ICAM-1), tissue inhibitor of metalloproteinase-1, and vascular endothelial growth factor-A when applied to excisional wounds in rats for 28 days [156].

Zhang *et al*. studied the potential of a mixture of human umbilical cord MSCs, WJ pieces, and skin micro particles (composed of remnant tissue surrounding wounds made of cutaneous cells, transudate, inflammatory cytokines, inflammatory cell infiltration, fragments of hair follicles, sebaceous glands, sweat glands, and subcutaneous tissues) after transplantation into 10-mm, full-thickness, mid-dorsal, excisional skin wounds in mice. The transplanted MSCs and the other components demonstrated the development of new born skin and its appendages along with newly generated layers of the epidermis, sebaceous glands, hair follicles, and sweat glands after 7 days [134]. It is, therefore, possible that WJMSCs in combination with a three-dimensional (3D) scaffold mimicking the natural dermis and several paracrine and immunomodulatory factors could all act synergistically as wound dressings for slow healing and hard-to-heal chronic wounds [134, 156]. These experiments show that WJMSCs can be a novel cell source for human

oral mucosa and skin by forming epithelial keratinocytes [150]. However, these grafts have limited self-regeneration capacity and lack many skin appendages such as hair follicles, sebaceous glands, sweat glands and neural elements in the newly healed wounds [56, 157].

Therefore, this dissertation describes a novel model using WJMSCs cultured on DWJM to assist in skin regeneration along with its associated hair follicle structures and sebaceous glans. DWJM is characterized and established as a 3D scaffold material for tissue engineering applications. WJMSCs and BMMSCs are cultured on this matrix and the biocompatibility and chemo-attraction capabilities are demonstrated. WJMSCs on DWJM in osteogenic differentiation media are shown to generate CK19 positive cells with hair like structures on DWJM. The underlying molecular mechanisms are studied here, along with the translatability of these structures to a suitable mice model to promote wound healing and complete skin regeneration along with its associate structures such hair follicles and sebaceous glands.

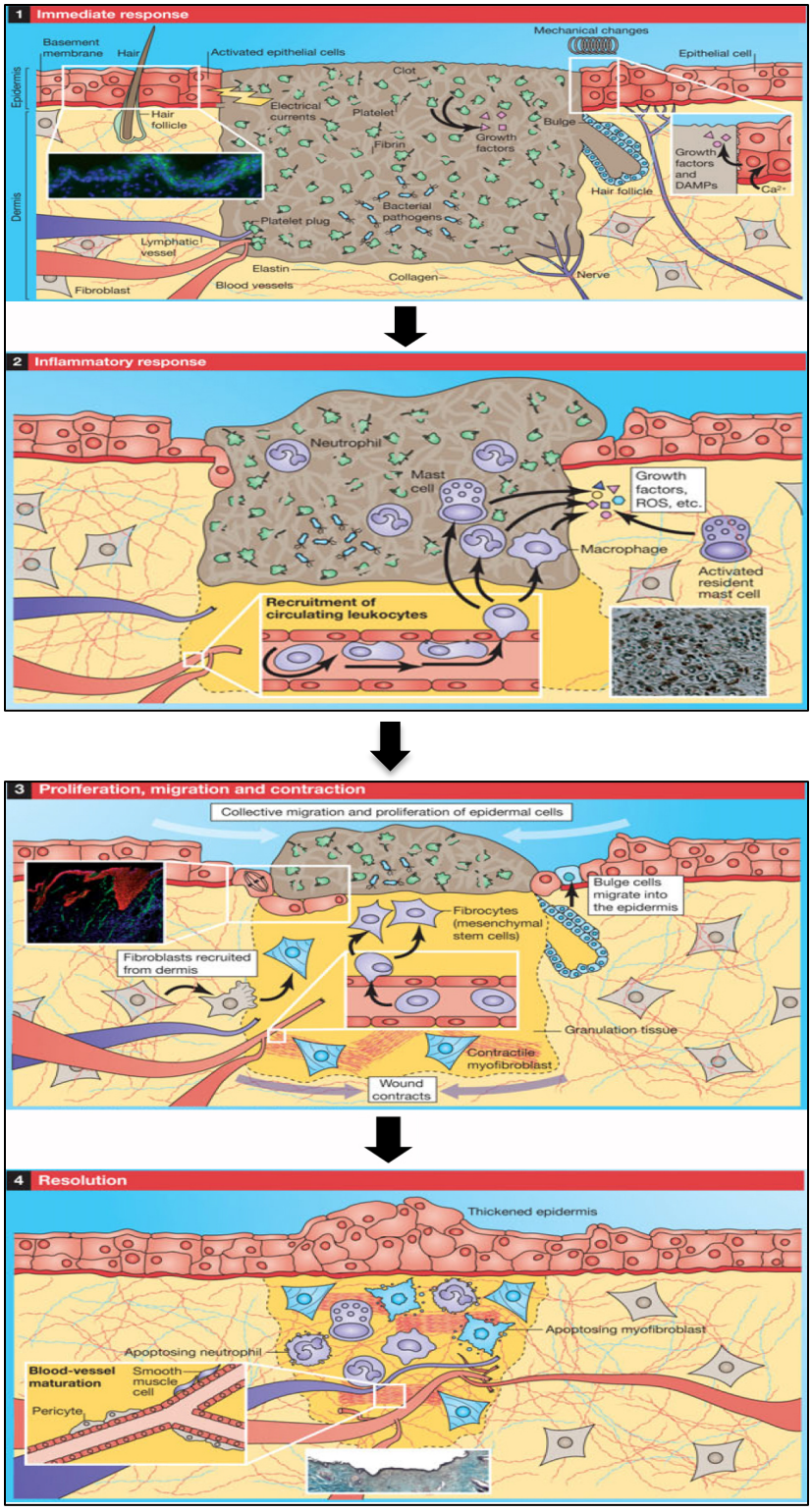

Figure 1- Schematic representation of the stages in Wound healing

Figure 1-1 demonstrates the immediate response after a wound. (The inset micrograph - JNK signaling pathway, green immunofluorescence - phospho JNK); Figure 1-2 represents the inflammatory response, (inset micrograph – immunohistochemistry for macrophages on a mouse skin wound 3 days post-injury (F4/80, brown staining, methyl green counterstain)). Figure 1-3 depicts the proliferation and migration of various cell types such as bulge cells and fibroblasts to the wound –edge epithelium (Inset micrograph is a mouse skin 5 days post injury representing thickened proliferative migratory repairing epithelium overlying fibrin clot and granulation tissue with angiogenesis (Red immunofluorescence is CK 14, while green immunofluorescence is CD31-endothelial cell marker)). Figure 1-4 shows the developing scar with altered matrix composition. (Inset – Masson's trichrome stain of a developing scar of mice skin 14 days post surgery).

Adapted from J of Cell Science, 2009 (122, pg. 3209-3213)

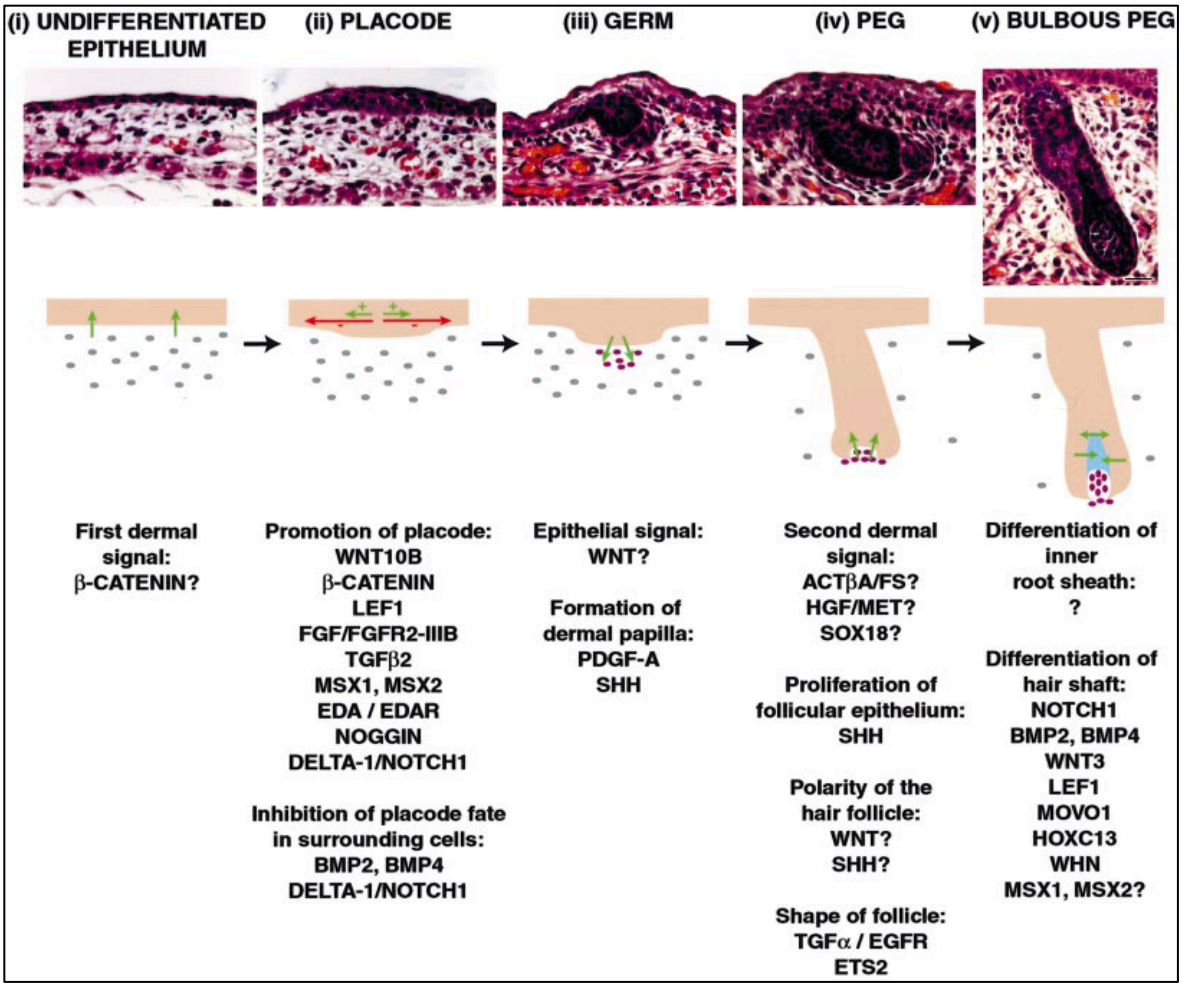

Figure 2 – Molecular mechanisms and stages involved in hair regeneration

(Adapted from Millar *et al.*,J of Investigative dermatology, 118(2), Feb 2002)

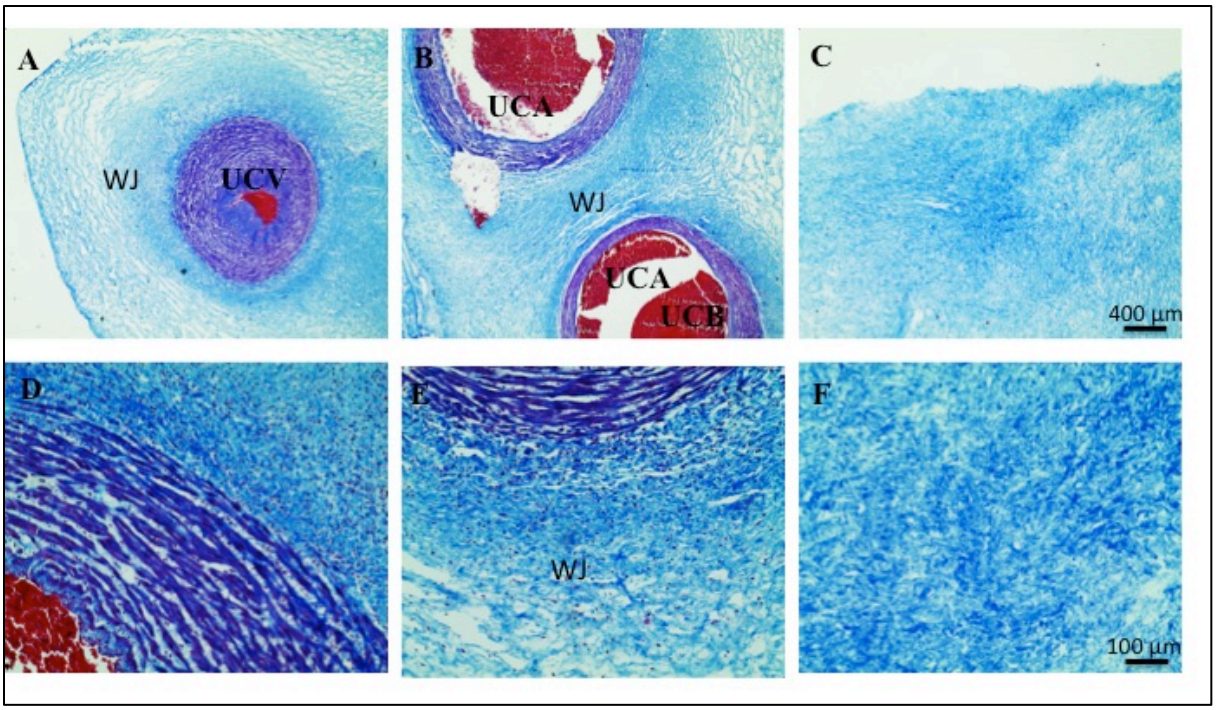

Figure 3 – Native umbilical cord and Decellularized Wharton's jelly matrix

Trichrome staining of human umbilical cord and decellularized Wharton's jelly. Images A, B, D, E represent human umbilical cord, while images C and F show decellularized Wharton's jelly matrix (DWJM) completely devoid of cells, but rich in collagen. Abbreviations – WJ – Wharton's jelly, UCA – Umbilical cord artery, UCV – Umbilical cord vein, UCB – Umbilical cord blood. Blue color represents collagen, Blue-black – nuclei of cells.

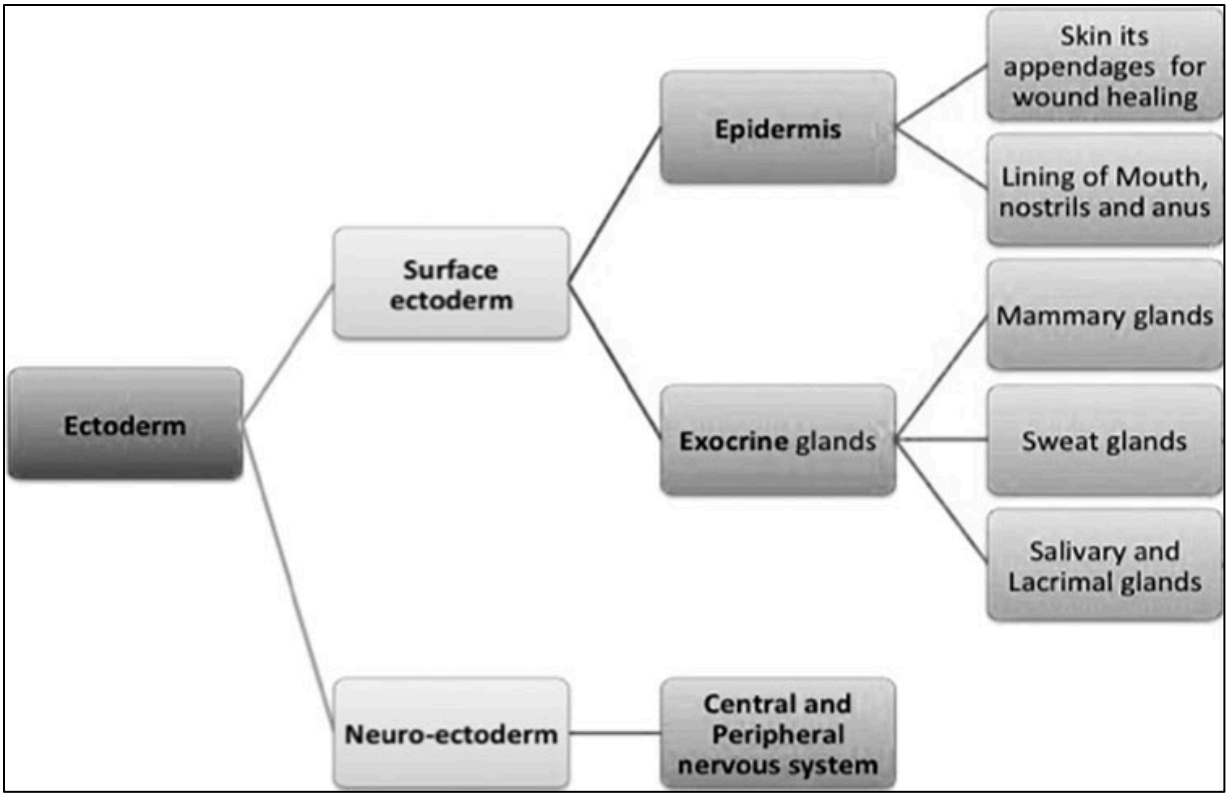

Figure 4 - Ectodermal differentiation and development.

(Jadalannagari *et al.*, Tissue Engineering Part B, 21(3), 2015.)

Table 1 - WJMSCs as candidates for epithelial differentiation

(Jadalannagari et al., Tissue engineering Part B, 21(3), 2015.)

Epithelial organ	*Cell source and culture conditions*	*Potential application*	*Authors*
Skin repair and wound healing	WJMSC with skin microparticles from skin injury site	For wound healing	Zhang *et al.*[4,15,27,61]
	WJMSC on Aloe vera, PCL scaffolds	For wound healing	Tam *et al.*[39]
Hair	WJMSC with and without decelled Wharton's jelly matrix	Ectodermal differentiation for hair follicle	Aljitawi *et al.*[41]
Sweat glands	WJMSC	Sweat-gland restoration after skin injury for cutaneous regeneration	Xu *et al.*[42]
Cornea	WJMSC injected into cornea of mucopolysaccharide VII mice	Keratinocyte and endothelial cell morphology was restored	Coulson-Thomas *et al.*[45]
	WJMSC on fibrin agarose scaffolds	Corneal epithelial cells were formed	Garzon *et al.*[33]

PCL, polycaprolactone; WJMSC, Wharton's jelly mesenchymal stem cell.

Chapter 2: Decellularized Wharton's Jelly from Human Umbilical Cord as a Novel 3D Scaffolding Material for Tissue Engineering Applications[2]

Introduction

Disease or trauma to the human body leads to damage and degeneration of tissues, thereby requiring their repair, replacement or regeneration. Tissue regeneration requires a combination of cells, scaffolds and appropriate media and growth factors. The properties of an ideal scaffold for tissue regeneration are high porosity, biocompatibility, biodegradability and suitable mechanical properties consistent with the location of implant [158]. Current treatment options for tissue regeneration involve the use of autografts or allografts. Nevertheless, autografts can be difficult to obtain due to expensive and painful procedures while allografts pose the risk of infections and immune rejections. Over the years, several types of scaffolds from natural or synthetic sources (polymers, ceramics, and composites) have been developed for regenerating tissues [158]. However, these scaffolds are associated with material specific limitations therefore creating interest in alternative biocompatible and bioactive natural or synthetic materials[159-165].

Wharton's jelly (WJ), a firm mucoid connective tissue that surrounds umbilical cord vessels [166], has multiple unique biochemical characteristics that are desired in a scaffold. WJ is home to mesenchymal stem cells (MSCs) which are immersed in a ground substance that is rich in collagen and hyaluronan and contains numerous sulfated glycosaminoglycans [166]. MSCs widely express the archetypal hyaluronan receptor, CD44, which is also expressed on

[2] Under Review as Jadalannagari S, Converse G, McFall C, Buse E, Filla M, Villar MT,Artigues A, Mellot AJ,Wang J,Detamore MS,Hopkins RA, Aljitawi OA, "Decellularized Wharton's jelly from human umbilical cord as novel 3D scaffolding material for tissue engineering application ", PLOS ONE, 2016.

osteocytes, chondrocytes, and hematopoietic marrow cells [167] **(**Figure 4**)**. WJ is also a rich source of peptide growth factors, notably insulin like growth factor-1 (IGF-1) and to a lesser extent platelet derived growth factor (PDGF), [127] which are both linked to controlling cell proliferation, differentiation, synthesis and remodeling of the extracellular matrix [168].

This work is predicated on the hypothesis that WJ could be effectively decellularized using customized procedures to produce a bioactive decellularized WJ matrix (DWJM). We also hypothesized that DWJM would provide a 3D environment well suited to specifically support undifferentiated mesenchymal cell culture. This paper examines in detail the decellularization processes used to obtain this matrix, its characterization along with the analysis of its contents. Here, we also show that WJ and BM (bone marrow) MSCs can be seeded on this matrix and cultured *in vitro.* Furthermore, we studied the gene expression profiles of these MSCs when seeded on our 3D scaffold and also assessed the biocompatibility of our matrix *in vivo* in a mice model.

Materials and Methods

Human umbilical cord collection, WJMSCs and WJ tissue harvest followed by decellularization were performed according to the IRB protocol # HSC 12129 of the university of Kansas Medical Center. Umbilical cords were immediately collected from consented donor mothers with full-term pregnancy after normal vaginal delivery. The umbilical cord was placed in a transport solution made of Lactated Ringer's solution supplemented with penicillin 800 U/ml (Sigma-Aldrich, St. Louis, MO), streptomycin 9.1 mg/ml (Sigma-Aldrich), and amphotericin 0.25 mg/ml (Sigma-Aldrich) and immediately refrigerated at 4°C. The decellularization process was initiated within 72 hours of umbilical cord collection.

Decellularization process

The decellularization procedure was recently described in our earlier publication [169]. Briefly, fresh human umbilical cords were transported from delivery room in a transport solution at 4°C. Umbilical cords were dissected in a laminar flow safety cabinet, by separating the matrix into large oval pieces from the surrounding membranes and vascular structures. Following this, they were subjected to two cycles of osmotic shock, by alternating with a hypertonic salt solution containing sodium chloride, mannitol, magnesium chloride, and KCl with an osmolarity of approximately 1,275 mOsm/L and 0.005% Triton X-100 in ddH_2O at 5,000 rpm in centrifuge at 4° C.

After two cycles of osmotic shock, the tissues were subjected to an anionic detergent (Sodium lauryl) and, sodium succinate (Sigma L5777), alternating with a recombinant nucleic acid enzyme, (Benzonase™) in buffered (Tris Hcl) water for 16 hours. Following this, an organic solvent extraction with 40% ethyl alcohol was performed for 10 minutes at 5,000 rpm in the centrifuge at 4° C. All of the detergent and other processing residuals were then removed

utilizing ion exchange beads (IWT-TMD (Sigma), XAD-16 Amberlite beads (Sigma), and Dowel Monosphere 550A UPW beads (Supelco)) in a reciprocating flow-through glass system for 30 hours at room temperature in ddH_2O. The decellularized matrix was cryopreserved using 10% human recombinant albumin (Novozymes) and 10% DMSO (Sigma) solution in standard RPMI media, employing a material specific computer controlled freezing profile that was developed to freeze at -1°C/minute to -180°C[170].

Assessment of DWJM scaffold

DNA Quantification.

The DNA was isolated using DNeasy Blood and Tissue Kit from Qiagen (Duesseldorf, Germany) per manufacturer's instructions. Pico Green dye (Molecular Probes, Eugene, OR) was used and the extracted DNA was quantified fluorometrically using Quant-it dsDNA Kit HS from Invitrogen (Carlsbad, California). The amount of extractable DNA was calculated per wet weight of tissue and expressed as a percent reduction in extractable DNA relative to non- decellularized tissues. All analyses were run in triplicate.

Glycosaminoglycans (GAGs) content analysis.

The Blyscan assay (Bio color, UK) was used for analysis of sulfated glycosaminoglycans according to the manufacturer's recommendations. Tissue samples from native umbilical cord WJ and DWJM were analyzed and the results were reported in μg/mg of glycosaminoglycan per wet tissue weight.

Hyaluronic acid immunohistochemistry.

After deparaffinization DWJM samples were blocked in 3% hydrogen peroxide for 10 minutes, rinsed and blocked in strepatividin/biotin (Vector Laboratories, Burlingame, CA.). The samples were rinsed and stained with hyaluronic acid binding protein (RMD Millipore, Danvers,

MA.) at 1:200 dilutions for 60 minutes at room temperature followed by a 15-minute incubation with LSAB+ strepatvidin-HRP (Dako, Carpinteria, CA). DAB+ chromagen (DAkp, Carpinteria, CA) was applied for 5 minutes and slides were counterstained with hematoxylin.

Protein estimation by mass spectrometry

DWJM samples from two different umbilical cord samples were analyzed following two methods of protein extraction. For the first method DWJM was snap-frozen using liquid nitrogen, homogenized using tissue homogenizer, and suspended in WJMSC culture medium described below. In the other method Ready Prep Protein Extraction Kit (Bio-Rad Laboratories, Inc., Hercules, CA) with zwitterion detergent ASB-14 as a solubilizing agent was used. This step was followed by a cleanup step using Ready Prep 2-D Cleanup Kit (Bio-Rad Laboratories, Inc., Hercules, CA). The protein pool present in the extracts were denatured in 6M guanidine hydrochloride, reduced, alkylated, and subsequently digested for 18 h with sequencing grade trypsin (12 ng/L, Promega, Madison, WI) at 37°C. Following enzymatic digestion, the extracted peptides were concentrated on a centrivac concentrator (Labconco, Kansas city, MO) to a final volume of 50 µl. The peptide extracts were analyzed by reversed phase chromatography using 2D NanoLC (Eksigent Technologies, Dublin, CA) coupled to a LTQ FT mass spectrometer (Thermo Fisher Scientific, Waltham, MA). The mass spectrometer was controlled by the Xcalibur software to perform continuous mass scan on the FT in the range of 400-1900 m/z at 50,000 resolutions, followed by MS/MS scans on the ion trap of the six most intense ions. All tandem ma scans were searched using Proteome Discoverer (version 5.3, Thermo Fisher) against a human protein database using trypsin cleavage specificity, with a maximum of 2 missed cleavages. The following variable modifications were selected: oxidation of M, deamidation of N

and Q and carboxymethylation of C was selected as a fixed modification, and a maximum of 4 modifications/peptides were allowed.

Mechanical testing

DWJM tissue sample was placed on a glass slide and the diameter was measured with a micrometer under a stereomicroscope. Tissue specimen was then loaded in an RSA-III dynamic mechanical analyzer (TA Instruments, New Castle, DE) and tested under unconfined uniaxial compression rate of 0.005mm/s to generate the stress-strain curve. Matrix height was measured directly using the RSA-III.

Isolation, expansion, and WJMSCs seeding onto DWJM

Preparation of DWJM for WJMSC seeding.

Freshly obtained fragments of DWJM were transferred to a large petri dish and covered with phosphate buffered saline (PBS). DWJM pieces (5-7mm in diameter) were obtained using a sterile 5-7 mm skin punch biopsy kit. The resulting DWJM pieces were cylindrical in shape with non-uniform heights, which varied between 2-3 mm. The volume of the obtained DWJM scaffolds' was ~72 mm^3. From this point on, these pieces of DWJM will be referred to as DWJM scaffolds. DWJM scaffolds were transferred using sterile forceps to a large petri dish and washed with PBS twice. At the time of seeding, the DWJM scaffolds were transferred to non-tissue culture treated plates.

MSC isolation and expansion

a. WJMSCs - WJMSCs were isolated and expanded according to the procedures described by Wang *et al.* [171]. Briefly, the outer layer of the cord was carefully removed and the cord was cut into smaller segments. The blood vessels were dissected from these cord segments and then cut into smaller pieces and digested with Collagenases (Worthington Biochemical Corporation,

Lakewood, NJ) in low glucose DMEM (Sigma-Aldrich) with 10% FBS (Atlanta Biologics, Atlanta, GA) and 1% Penicillin/Streptomycin (Sigma-Aldrich) overnight at 37°C to obtain WJMSCs. The WJMSCs were passaged and maintained in low glucose DMEM with 10% FBS and 1% Penicillin/Streptomycin. WJMSCs from passages 4 - 9 were used for the experiments.

b. BMMSCs - BMMSCs were isolated from bone marrow aspirates of healthy consented donors at University of Kansas Medical Center (HSC # 5929). The cells are isolated following standard ficoll density gradient separation method (Lymphoprep, Stem cell technologies, Vancouver, BC). The isolated cells were maintained in high glucose DMEM (Sigma-Aldrich), 20% FBS (Atlanta Biologics) and 1% Penicillin/Streptomycin (Sigma-Aldrich) at 37°C, 5% CO_2 and 90% humidity.

MSC characterization and phenotyping

MACS Miltenyi Biotec MSC human phenotyping kit was used for the characterization of expanded WJMSCs and BMMSCs. Flow cytometry analysis was performed using BD Flow cytometer LSR2. MSCs isolated from human umbilical cord and bone marrows were stained for CD14, CD20, CD34, CD45, CD73, CD90 and CD105.

MSC seeding onto DWJM

For each set of seeding experiments, single-donor (n=1) WJMSCs/BMMSCs was used. 1 x 10^6 MSCs were suspended in 50 µl culture medium and seeded on each DWJM scaffold (average seeding density was 1.4X$10^4$4 x 10^4/mm^3 DWJM scaffold) in a 48-well plate. 1 ml of medium/well was added to the cells on the scaffolds. For the gene expression studies, 0.25 x 10^6 – 1 x 10^6 WJMSCs/BMMSCs of passage 4-9 were seeded on DWJM in a 24-well non tissue culture treated plate (Corning Inc., Corning, NY) for 4-7 days and cultured in their respective media.

Evaluating seeded WJMSC adherence to and penetration of DWJM scaffolds

a. Confocal microscopy - To assess WJMSCs attachment to DWJM scaffolds, 1 x 10^6 WJMSCs were seeded on each DWJM scaffold in a 24-well culture plate. After 2 hours of cell seeding and culture, these scaffolds were transferred to a viewing chamber for confocal microscopy examination using Fluoview scanning laser confocal microscope (Olympus, Center Valley, PA). Prior to viewing, seeded DWJM scaffolds were rinsed twice with PBS and incubated with culture medium containing 2 μg Calcein stain (Molecular Probes, Eugene, OR) added to each seeded DWJM scaffold. Calcein is a cell-permeant dye that is converted to green-fluorescent Calcein in live cells. Using this stain, we tracked live WJMSCs seeded onto DWJM scaffold for 24 and 48 hours after cell seeding.

b. Dual beam electron microscopy – MSCs were seeded on DWJM as described in 2.3.4 and cultured in their appropriate media for 7 days. The matrix with cells was collected after 24 hours and day 7 and was fixed overnight in 4% paraformaldehyde (VWR, Randor, PA) in PBS at 4°C. Tissue Specimens were washed three times in PBS. Following this, specimens were stained for 24 hours with 2% Osmium Tetroxide (OT) to label lipids, as OT gives off a strong electron backscatter signal. OT stained samples were washed three times for 10 minutes in PBS. All samples were gradually dehydrated with ethanol and cleared in xylene, before being embedded in paraffin. Samples were sectioned to thicknesses of 10 μm or 20 μm using a microtome (Leica, Buffalo Grove, IL) and mounted on Super Frost glass slides (Thermo Fisher, Waltham, MA). OT-stained samples were deparaffinized in two washes of xylene for 3 minutes each. Further, OT samples were critical point dried in 100% ethanol using an Autosamdri 815B (Tousimis, Rockville, MD). Samples were sputter-coated with 5 nm of copper using a Q150T Turbo-

Pumped Sputter Coater (Quorum Technologies, West Sussex, and United Kingdom). Samples were imaged using a Versa 3D Dual Beam electron microscope (FEI, Hillsboro, OR) at a voltage of 30 kV. The Everhart-Thornley detector (ETD) and circular backscatter (CBS) detectors were used to detect secondary electrons and backscatter electrons, respectively.

c. Scanning electron microscopy (SEM*)* - DWJM scaffolds were fixed in 2 % glutaraldehyde for SEM processing. The fixed samples were washed with PBS for 10 minutes, placed into buffered 1% osmium tetroxide for 1 hour, and then washed 3 times 10 minutes each in distilled water. Further, the samples were dehydrated through a graded series of ethanol from 30%, 70%, 80%, 95%, and 100% for 15 minutes each. Following this, the samples were critical point dried in CO_2 in a model EMS 850 dryer, then they were mounted onto aluminum mounts and sputter coated with gold in a Pelco SC-6 sputter coater. Finally samples were viewed using a Hitachi S-2700 scanning electron microscope.

d. Transmission electron microscopy (TEM) - For TEM, scaffolds was rinsed in a buffer prior to fixing in 1% to 2% osmium tetroxide for 1 hour. After osmication, the scaffolds were dehydrated for 10-15 minutes in 30%, 70%, 80%, 95%, and 100% ethanol series before placing them in propylene oxide (PO) for 10 minutes twice. The scaffolds were then placed in equal mix of resin and PO overnight to allow tissue infiltration. At this point, the half/half mix was removed from the tissue and fresh 100% resin mixture was added to the sample and was allowed to sit on a platform rocker for at least 30 min. Subsequently, the samples were covered in resin. Finally, the samples were placed in 60°C oven overnight to cure the resin. Samples were then sectioned using a Leica UCT ultra microtome at 80 nm in thickness and contrasted with 4% uranyl acetate and Sato's Lead Citrate and viewed at 80 KV with a JEOL JEM-1400 TEM.

e. Live cell Imaging –DWJM scaffolds of 30µ thickness were placed on the base of a 12 well plate and the matrix was blocked with 3% BSA for 2 hours and incubated with 3 µl anti-fibronectin antibody [F1] (Alexa Fluor® 488) (Abcam, Cambridge, MA) at 4°C in dark for 12-15 hours. WJMSCs of passage 4 - 5 were cultured in a 12 well plate and labeled with cellVue® burgundy labeling kit (Affymetrix eBioscience, Santa Clara, CA) as per the manufacturer's instructions, immediately prior to seeding on the scaffolds. Briefly, 2.5 – 5 X 10^5 WJMSCs were seeded on the labeled matrix and cultured for 24 hours at 37°C and imaged using a Leica 10X HC PL Fluotar 506505 objective on a semi-automated Leica DMIRE2 inverted epifluorescent microscope outfitted with a Ludl Bioprecision motorized stage, Sutter Instruments Xenon Lamphouse with shutters and a Retiga SRV CCD camera controlled by custom TiLa KU (Time Lapse KU) acquisition and image processing software. Regions were imaged in Bright field, GFP (Chroma 41001 HQ480/40 excitation HQ535/50 Emission) and CY5 (Chroma 49006 ET620/60 excitation, ET700/75 emission). DWJM with WJMSCs was imaged for 18 hours, at every 15-minute interval.

f. Histology and Immunohistochemistry - DWJM scaffolds were fixed in either 10% formalin or 4% paraformaldehyde, embedded in paraffin, sectioned, and stained with H&E. Slides were reviewed using Olympus BX40 microscope and pictures were acquired using DP72 digital camera.

Tissue specimens from animal study were decalcified in a routine matter (using Rapid bone decalcifier solution from American MasterTech for 5-10 minutes), paraffin embedded, sectioned vertically, and stained with H&E. GFP immunohistochemistry staining was done by incubating slides with rabbit monoclonal GFP primary antibody from CST in 1:100 dilution for

45 minutes, followed by mach 2 rabbit secondary antibody for 45 minutes using a Clinical intellipath FLX automated slide stainer.

Evaluating seeded WJMSC proliferation

To assess WJMSC's viability and proliferative response following their seeding on DWJM, AlamarBlue® (AB) cell viability assay (ThermoFisher Scientific, Waltham, USA) was utilized. AB is a fluorometric assay that correlates with cell metabolic activity. DWJM scaffold pieces (7 mm in diameter and 2-3 mm in height) were seeded with expanded human WJMSCs. 1 x 10^6 cells were seeded on each DWJM scaffold. For controls, WJMSCs 1 x 10^6 were cultured as a monolayer in each well of a 24-well plate. AB was assessed 24 and 48 hours as well as 1 week following WJMSC seeding. These experiments were done in triplicate.

Evaluating WJMSC migration toward DWJM using migration Assays

3 - 7 x 10^5 WJMSCs were loaded to the upper chamber of Trans well set (Costar, Corning Inc.) and minced DWJM tissue was added to the lower chamber in low glucose DMEM with 10% FBS and 1% Penicillin/Streptomycin. After 4 hours, Trans-wells were removed and the migrated cells were counted using a Vi-cell (Beckman-Coulter). All the experiments were conducted in triplicate.

Molecular studies

RNA extraction from cells

WJMSCs and BMMSCs were cultured as a monolayer (2D) or on DWJM (3D) as described above for 7 days. The cells were collected at day 0 (monolayer prior seeding DWJM), day 4 and day 7 after seeding onto the matrix. WJMSCs were harvested from the scaffolds following overnight digestion with Collagenase II. The MSCs were washed twice with PBS and centrifuged at 13000 rpm, 4°C for 20 minutes to obtain a cell pellet. The cell pellet was

suspended in 1 ml of Trizol (Life technologies) and stored at -80°C until further processing. Once all the samples were collected, RNA was extracted using the standard procedure as described by the manufacturer (Life technologies, Carlsbad, CA). Briefly, aqueous phase containing RNA was separated using 0.2 ml chloroform, 0.7 volumes of isopropanol was added and centrifuged to precipitate RNA. The RNA pellet was washed twice with 75% ethanol and dissolved in 30-50µl of nuclease free water. RNA was quantified using Nano drop spectrophotometer 8000. 1.5µg of RNA was treated with DNA-*free*™ DNase treatment and removal kit (Life Technologies). High capacity cDNA reverse transcription kit (Applied Biosystems) was used to generate cDNA from the extracted total RNA samples using Bio-Rad T100 thermal cycler.

Quantitative real-time PCR analysis

The quantitative real-time PCR (qPCR) reactions (20 µl) were performed with TaqMan gene expression master mix (Life Technologies), and TaqMan array 96 well plates (Applied Biosystems, Foster City, CA) using StepOnePlus™ real-time PCR system (Applied Biosystems). The primers used are described in Table 2. The qPCR reactions were performed in triplicate. StepOnePlus™ real-time PCR system (Applied Biosystems) was used for the qPCR. GAPDH was used as an internal control to normalize the samples to obtain ΔC_t. $2^{-\Delta\Delta Ct}$ was used to analyze the relative gene expression levels.

Animal studies

DWJM scaffolds were washed twice in PBS and pre-incubated in low glucose DMEM (Sigma-Aldrich) with 10% FBS (Atlanta Biologics) and 1% Penicillin/streptomycin (Sigma-Aldrich) for 24 hours at 37°C, 5% CO_2 and 90% relative humidity. After incubation, the scaffolds were washed multiple times in PBS to remove the media before transplantation in the

mice. All the animal experiments were performed according to the University of Kansas Medical Center IACUC protocol # 2013.2158. All the animal studies were performed on transgenic 10kB DMP1 - Cre floxed mice (6-8 week old) expressing osteocyte specific green fluorescent protein (GFP)[172]. Mice were anesthetized with intraperitoneal injection (IP) of ketamine (90-150 mg/kg) (Vedco) and xylazine (7.5-16 mg/kg). Buprenorphine SR (0.15-0.5 mg/kg) (Zoopharm pharmacy) was given intraperitoneally pre-op. One midline skin incision of approximately 1cm in length was made on the dorsal surface of the cranium, followed by the separation of skin and periosteum. A 5 mm cranial defect was made with a trephine bur (Fine Science Tools, Foster City, CA) attached to an electric Dremell hand piece (Ideal micro drill, Harvard apparatus, Holliston, MA). A full-thickness parietal bone defect was created with minimal invasion of the dura matter. The defect was left empty (n = 4) or filled with the decellularized matrix (n = 4) and the skin was sutured with 5-0 coated Vicryl (polygalactin 910) (Ethicon™, Johnson and Johnson Co., New Brunswick, NJ). Animals that had cranial defects, but received no implant served as sham-operated controls. Craniotomy defects in mice were either left unfilled (control) or filled with DWJM to study the cellular migration and localization by observing GFP expression.

IVIS Imaging

The mice were imaged using IVIS imaging station (PerkinEmler) 24 and 48 hours post-surgery. Mice were anaesthetized with isofluorane gas prior to imaging. The animals were euthanized after imaging according to the protocol and cranial samples with the matrix were collected in 10% phosphate buffered formalin (Newcomen supply) for 24 hours.

Statistical analysis

All data were expressed as means ± standard error of mean (SEM) and analyzed using, student's t-test, two-way analysis of variance (ANOVA) with Bonferroni post-test, or Man-Whitney U test. A threshold of $p \leq 0.05$ determined statistical significance. The statistical analyses were performed utilizing Graph Pad Prism software version 6 (Graph Pad Software, Inc.).

Results

Characterization of DWJM Scaffolds

The isolated DWJM scaffolds (Figure 5A) were tested for the success of decellularization process. Histologically, the decellularized Wharton's jelly matrix was porous and devoid of any intact cells, nuclei or other cellular components (Figure 5B). The DWJM matrix was also found to have abundant hyaluronan glycosaminoglycan as observed in the immunohistochemistry images (Figure 5C). Scanning electron microscopy pictures indicated that DWJM had open spaces resembling lacunae, with sizes ranging from 20-100 μm (Figure 5D). Transmission electron microscopy also demonstrated absence of intact cells in the examined DWJM scaffold (Figure 5E).

DWJM scaffold biochemical and biomechanical characteristics

DNA quantification studies

DNA was isolated from the native WJ matrix and from DWJM and quantified as described above. The amount of mean dsDNA content per DWJM sample wet weight was 1.7×10^{-3} μg/mg (range: $1.4 \times 10^{-3} – 2 \times 10^{-3}$ μg/mg) with standard deviation of 0.2×10^{-3} μg/mg while the mean dsDNA per WJ matrix wet weight sample was 5.1×10^{-2}μg/mg (range: $3.17 \times 10^{-2} – 7.33 \times 10^{-2}$ μg/mg) with standard deviation of 1.9×10^{-2} μg/mg (Figure 6A). Therefore, for all the analyzed scaffolds, 96.6% ± 0.4% of dsDNA was removed.

Protein content analysis

Mass spectrometry revealed that examined DWJM matrix pieces were composed of several structural proteins, including collagen I, III, VI, and XII. Transforming growth factor beta was also observed, in addition to matrix proteins like fibronectin-I (binds to extracellular matrix components such as collagen, heparin sulfate), tenascin and lumican. A full list of the

proteins identified on mass spectrometry evaluation of DWJM, prepared by both methods, as shown in Table 3.

Glycosaminoglycan content analysis

GAGs are glycoproteins with a protein core and polysaccharide branches with carboxylic and or sulfate ester groups and that form bridges and link collagens to construct an interpenetrating network of extracellular matrix to maintain and define shape of connective tissues and organs [173, 174]. Glycosaminoglycan analysis indicated that DWJM contained sulfated GAGs (mean = 0.661 ± 0.107 μg/mg), which was significantly less than the native umbilical cord Wharton's jelly tissue (3.0 ± 0.355 ug/mg, $<p = 0.05$) (Figure 6B).

Mechanical testing

After decellularization, the DWJM matrix under unconfined uniaxial compression demonstrated a curve characteristic of elastomeric scaffolds (Figure 6C), thus indicating DWJM as a suitable scaffolding biomaterial [175].

DWJM scaffold seeding with WJ and BM MSCs

MSC characterization by flow cytometry

The isolated WJMSCs (Figure 7A) and BMMSCs (Figure 7B) were plastic adherent and stained positive for MSC markers such as CD 73, CD 90, and CD 105 by flow cytometry. WJ and BM MSCs were negative for hematopoietic cells markers like CD45, CD34, CD14 or CD11b, CD79α or CD19.

Assessment of MSC adherence to and penetration of DWJM

A green Calcein AM stain was used to study WJMSC seeded onto DWJM scaffolds. Within 2 hours of seeding, clusters of round cells were observed on the surface of DWJM scaffolds (Figure 8A-B). Histological examination of the DWJM matrix after seeding WJMSCs for 6

weeks also showed the presence of elongated and spindle shaped cells covering the outer surface of the matrix (Figure 8C). Similar observations were made when the matrix with WJMSCs was observed under a scanning electron microscope, which also revealed the presence of spindle shaped and round cells (Figure 8D). Thus, WJMSCs cultured on DWJM adhere to the matrix but acquire different cellular morphologies.

Dual beam imaging - WJMSCs and BMMSCs were seeded onto separate DWJM scaffolds and cultured for 7 days in appropriate media. Samples were collected at 0, 1 and 7 days after seeding the scaffolds and imaged using a FEI Versa 3D dual beam microscope. DWJM was composed of fibers of varying thickness (Figure 9A*) while in DWJM seeded with cells; several clusters of circular lipid structures were identified (Figure 9B*- E*). WJMSCs were positively identified 1 mm medially from the outer edge of DWJM at day 1 and day 7 (Figure 9G#, H# respectively), whereas, BMMSCs were identified approximately 800 μm from the outer edge at day 1 (Figure 9I#) and 1 mm medially from the outer edge at day 7 (Figure 9J#). Thus, these images demonstrate that WJMSCs and BMMSCs not only attached on the surface, but also penetrated into the matrix.

Live cell Imaging – DWJM is composed of fibronectin, which was labeled using alexaflour 488-conjugated anti-fibronectin antibody. This staining revealed fibrous network of fibronectin within DWJM (Figure 10). WJMSCs labeled in burgundy color were visualized on the surface of DWJM, inside the matrix and outside the matrix. Time-lapse imaging over 18 hours demonstrated migration of WJMSCs in and out of DWJM. In addition, WJMSCs successfully populated DWJM matrix (Figure 10 and videos 1-2).

Proliferation of WJMSCs seeded onto DWJM scaffolds

Alamar blue cell viability assay was performed to assess the proliferation of WJMSCs seeded onto DWJM. For these experiments, WJMSCs were cultured as a monolayer (2D) or seeded over DWJM scaffolds (3D). The viability of the cells was calculated as fluorescence readout in the assay. Increased fluorescence reading directly correlates to proliferation and viability of the cells. After 1 week WJMSCs cultured in 3D had lower fluorescence compared to WJMSCs cultured in 2D, indicating that the cell-matrix interactions allowed the cells to proliferate but not as much as WJMSCs cultured in 2D (Figure 11A).

Cell migration Assay

In 4 hours, a significantly higher number of WJMSCs migrated across the Trans well when DWJM was present (Figure 11B) potentially indicating that DWJM matrix acts as a chemo attractant. This chemo attractant quality of the matrix was further investigated in our animal model.

Gene expression studies

A) Cell adhesion genes (Figure 12A, Figure 13A) **–** Expression levels of cell adhesion genes CD 44, Endoglin (CD105), ITGB1 (CD29), Thy1 (CD90), ALCAM (CD166) and VCAM1 were tested in WJMSCs and BMMSCs after culturing in DWJM for 7 days. There was no significant change in the expression of ITGB1, while ENG, THY1, ALCAM and VCAM1 remained below baseline levels in WJMSCS cultured in DWJM. On the other hand, after 4 days, BMMSCs cultured in DWJM showed 0.5 fold reductions in the expression of ENG, ITGB1, THY1, ALCAM and VCAM1 genes. However, by day 7 we observed an increase in expression of these genes restoring their expression to baseline levels in the case of ENG, ITGB1, and ALCAM.

B) Chondrogenic genes (Figure 12B**,** Figure 13**B) –** The expression of prechondrocyte marker SOX9 and chondrocyte markers aggrecan (ACAN) and COL2A1 were examined in WJMSCs and BMMSCs cultured in DWJM. ACAN and COL2A1 were undetected in WJMSCs cultured in DWJM, while in BMMSCs; ACAN was down regulated over time. SOX9 expression was up regulated in WJMSCs and BMMSCs compared to baseline with BMMSCs showing 4-fold increase at day 4 and 15 fold increase at day 7. HAS2 expression was increased 3 fold at day 4 and 1 fold at day 7 for WJMSCs cultured in DWJM, while BMMSCs showed a decrease in HAS2 expression.

C) Adipogenic genes (Figure 12C, Figure 13C) **–** WJMSCs and BMMSCs demonstrated expression of the adipogenic differentiation genes - fatty acid binding protein (FABP4) and Peroxisome proliferator- activation receptor – γ (PPARγ). WJMSCs cultured in DWJM demonstrated a decrease in the expression of FABP4 and PPARγ, while BMMSCs demonstrated increased expression of both genes at one week compared to baseline. Though these differences were statistically significant, their biological significance is unclear given the magnitude of change is small in both cases.

D) Myogenic genes (Figure 12D, Figure 13D) **-** The expression of vimentin (VIM), byglycan (BGN), desmin (DES), actin alpha 2 (ACTA 2) and collagenase 6 (COL6A1) were studied in WJMSCs and BMMSCs cultured DWJM. At day 7 of culture, DES was down regulated in WJMSCs, while BMMSCs demonstrated no significant change from baseline. However, the decrease in ACTA2 expression in both the cell lines was noteworthy.

E) Osteogenic genes (Figure 12E,

Figure 13E) – The expression of RUNX2, a key transcription factor associated with osteoblastic differentiation was evaluated in WJMSCs and BMMSCs cultured in DWJM. In WJMSCs the expression of RUNX2 was increased 4 folds above baseline value at day 4 followed by significant decrease at day 7. However, in case of BMMSCs expression of RUNX2 increased by 0.5 fold and 1.5 fold over baseline values, at day 4 and 7, respectively. The expression of other osteogenic lineage markers Alkaline Phosphatases (ALPL) and COL1A1 was assessed over time and it was observed that COL1A1 was down regulated in both cell types, while there was no significant difference in ALPL levels in BMMSCs. WJMSCs exhibited transient increase in SPP1 expression (8 fold increase) at day 4, while WJMSCs and BMMSCs demonstrated no significant change in SPP1 expression at day 7 compared to baseline.

F) Apoptosis, Proliferation, and other differentiation genes (Figure 12F, Figure 13F) – WJMSCs and BMMSCs cultured in DWJM showed no significant change in the expression of BAX (apoptotic regulator) at day 7, while proliferation marker (MKI67) exhibited significant decrease in gene expression when compared to the respective baseline values. WJMSCs demonstrated a significant, albeit small, decrease in the expression of PCNA at week 7.

Animal studies

Mice that had the 5 mm defect alone (Figure 14A) served as our control group, while the animals that received DWJM were the treatment group (Figure 14B). All the animals survived surgeries and were imaged under anesthesia at 24 hours and 2 weeks post surgery (Figure 14D) and were euthanized as per the protocol. Structural integrity of DWJM was evaluated by visual inspection after removing the skin and exposing the defect at the end of the experiment (Figure 14C). The matrix appeared intact 14 days after surgery (Figure 14C) and histological examination revealed the presence of cells (Figure 14E, H, I), some of which were also GFP

positive (Figure 14F, J). The cells migrated into the matrix as early as 24 hours thereby validating it as a chemo attractant and biocompatible matrix.

Discussion

This chapter demonstrates that DWJM is a novel 3D scaffold that is biocompatible and allows cellular penetration and has suitable mechanical properties for cellular growth and proliferation. Although a wide variety of scaffolds – synthetic and natural are already available for tissue engineering, natural polymers like collagen, gelatin, silk, chitosan, and elastin pose some difficulties with processing, purity and protein denaturation, while, metal alloys and osteoconductive ceramics are difficult to handle and shape and also lack biodegradability [159, 160, 176]. Though polymers like poly (lactic-acid) (PLLA), poly (glycolic acid) (PGA), polycaprolactone (PCL), poly (lactic acid-co-glycolic acid) (PLGA) fit the properties of an ideal scaffold, they are synthetic in origin and lack biological properties, thus, arising the necessity/need for developing an ideal natural scaffold material [159-164, 177].

In the current study, we establish DWJM as a novel 3D matrix, completely devoid of cells and dsDNA. In contrast to the methods published by Chan *et al.* [178] , we demonstrate a method to decellularize the WJ matrix tissue after the removal of vascular tissues, allantoic duct, and amniotic epithelium, thereby eliminating any potential contamination and residual components. Our method results in an acellular matrix, with the innate properties of WJ as evidenced by histology and electron microscopy. Additionally, we demonstrated that this decellularization process results in a matrix material with negligible DNA content, consistent with current recommendations for qualifying as decellularized tissue [179].

Mass spectrometry analysis demonstrated a presence of various proteins like collagen, fibronectin, lumican, and tenascin, which are important extracellular matrix proteins desirable in a scaffolding material for tissue engineering. Fibronectin has been shown to enhance the quality of scaffolding material used for osteogenic differentiation [180]. Lumican is a matrix protein that

has been correlated with *in vivo* bone formation by osteospheroids prepared *in vitro* from human mesenchymal stem cells[181]. Tenascin was found to be overexpressed when fibroblast cells were cultured in porous poly-caprolactone-based scaffolds and under torsion in a bioreactor [182]. TGF-β was identified in these scaffolds, which also happens to be an important factor in chondrogenic differentiation of MSCs as it enhances COL2A1 expression at the expense of COL1A1[183]. The impact of TGF-β on MSC differentiation is not limited to chondrogenic differentiation as it also plays a role in regulating osteogenic differentiation [184]. DWJM also contains sulfated GAGs, which are reported to enhance mesenchymal stem cell osteogenic differentiation in addition to improving cell-matrix interactions [185]. Similarly, GAGs were found to promote chondrogenic differentiation of human mesenchymal stem cells[186]. GAGs like chondroitin sulfate were also found to enhance the biological activity of collagen I scaffolds in supporting chondrocytes [187].

When the WJMSCs were cultured on DWJM, there was immediate attachment and penetration of the seeded cells into deeper parts of DWJM scaffolds. Despite the uniform distribution of WJMSCs within DWJM scaffolds while seeding, some surface areas of DWJM attracted WJMSCs in clusters while some areas had cells growing in layers. In contrast, mesenchymal cell condensation has been reported to occur early in process of chondrogenesis, where mesenchymal cells produce matrix proteins including collagen I and fibronectin while extracellular matrix proteins (e.g., tenascin) interact with cell adhesion molecules and initiate the transition to committed chondrocytes [188] TGF-βI has a role in inducing pre-cartilage condensation [189] and the DWJM matrix has retained TGF-β and other matrix proteins like collagen, fibronectin, and tenascin I. Therefore, we postulate that these proteins might have provided critical cues resulting in the WJMSCs developing areas of cell condensation. We also

hypothesize that further tuning of the preparation process to yield symmetrical surfaces might allow for equal cell penetration or enhance cell condensation for specific tissue regenerative purposes.

Our results show differences in the rate of proliferation between cells cultured in three dimensions (3D) versus 2 dimensions (2D). WJMSCs cultured in 2D grow horizontally to confluence while; WJMSCS on 3D grow in clusters, attach and penetrate into DWJM. Cells in 3D also demonstrated a decrease in expression of the Ki-67 gene, a marker of proliferation, thereby indicating that the MSC proliferation slows down as cells interact with DWJM scaffolds. Therefore, we show that WJMSCs and BMMSCs can be seeded on DWJM and cultured, although they have a slower proliferative rate compared to the monolayer cultures. This similar impact of culture condition (2D versus 3D) on the rate of cell proliferation was examined previously with some studies showing that 3D culture conditions were found to slow down cell proliferation [190]

Wang *et al.* described that WJMSCs express matrix receptors like CD 44 and Endoglin (CD 105) [191]. Although BMMSCs physiologically do not express CD 44 in human or mice, Qian *et al.* demonstrated that *in vitro* culture of these MSCs could result in CD 44 expression. [192-194]. In our study, we observed increased expression of CD 44 gene in WJMSCs and BMMSCs cultured in DWJM over 7 days culture. CD 44 is a cell adhesion receptor involved in interacting with multiple ligands like hyaluronan, fibronectin and collagens [195]. The mass spectrometry analysis of DWJM identified fibronectin and collagen as components of the matrix while other researchers have also shown that hyaluronic acid is the most abundant component of the glycosaminoglycans in the Wharton's jelly matrix [196]. Similarly, the decellularization process adopted in this work also showed that DWJM matrix retained hyaluronic acid

abundantly. Thus, the induction of CD44 in both the MSCs cultured on DWJM could possibly be associated with anchoring of the cells to hyaluronic acid in the matrix. Cell surface markers like Thy1, Endoglin, ALCAM, CD44 and VCAM have been used to isolate homogeneous MSC population [192, 197, 198]. When BMMSCs were cultured over DWJM, no significant changes in gene expression were noticed for genes Endoglin, and cell adhesion molecules – Thy 1 and ALCAM, while WJMSCs showed decreased expression of these genes. These subtle differences in the expression of the adhesion genes between WJMSCs and BMMSCs could be attributed to WJMSCs being native to the Wharton's jelly matrix, while BMMSCs are being introduced into a new environment.

RUNX2 is the most studied transcription factor expressed in MSCs upon their commitment to osteogenic differentiation [199, 200] while, SOX9 inhibits RUNX2, thus blocking the osteoblastic maturation during chondroprogenitor fate determination [201]. Loebel *et al.* has shown that SOX9 is an early indicator during *in vitro* osteogenic differentiation of MSCs and that the RUNX2/SOX9 ratio can be used to screen for osteogenesis [202]. In WJMSCs cultured over DWJM, we observed an increase in the expression of SOX9, while the RUNX2 expression was decreased. However, BMMSCs exhibited an increase in SOX9 and RUNX2 expression. Despite these differences, the ratio of RUNX2/SOX9 showed the same decreasing trend for WJMSCs and BMMSCs cultured over DWJM (WJMSCs: 3.26 at day 4 to 0.62 at day 7; BMMSCs: 0.34 at day 4 to 0.16 at day 7) thereby indicating non-commitment to osteogenic lineage. Several researchers have already demonstrated the potential of WJMSCs differentiation into myogenic lineage *in vitro* and *in vivo* [203, 204]. BGN, a critical protein for collagen fibril assembly and muscle regeneration and ACTA 2, a protein essential for maintaining cell motility, structure and integrity were significantly down regulated in both the

MSCs over time. Using gene expression studies, we conclude that WJMSCs and BMMSCs cultured in DWJM show no lineage specific differentiation towards osteogenic, chondrogenic, myogenic or adipogenic genes, thereby demonstrating that DWJM facilitated the cells to remain undifferentiated.

We also transplanted the DWJM scaffold in a 5 mm cranial defect in mice with GFP labeled osteocytes and showed the migration of cells into the matrix as early as 24 hours by immunohistochemistry, and at 2 weeks by *in vivo* live imaging. Thus, DWJM was a biocompatible matrix that attracted cells from the surrounding tissues. Therefore, we corroborate that DWJM scaffolds are biocompatible and have favorable surgical characteristics like porosity, elasticity, and compressibility, which make it easy to configure in irregular or curved shapes. Based on these characteristics, we envision DWJM scaffolds will have several potential applications related to tissue engineering.

Conclusions

In this chapter we have demonstrated the successful isolation and decellularization of human WJ matrix and characterized this matrix as a potential candidate for use as a scaffolding material for future tissue engineering applications. We show that this naturally obtained matrix can be made completely devoid of cells but comprised of glycosaminoglycans especially rich in hyaluronic acid and several other key extracellular matrix proteins. We also demonstrate that DWJM is a biocompatible matrix that allows cellular adherence, penetration, growth and proliferation with suitable mechanical properties *in vitro* and *in vivo*. Together, this chapter presents DWJM as a novel and natural 3D scaffold that can be evaluated for tissue engineering and regenerative medicine applications.

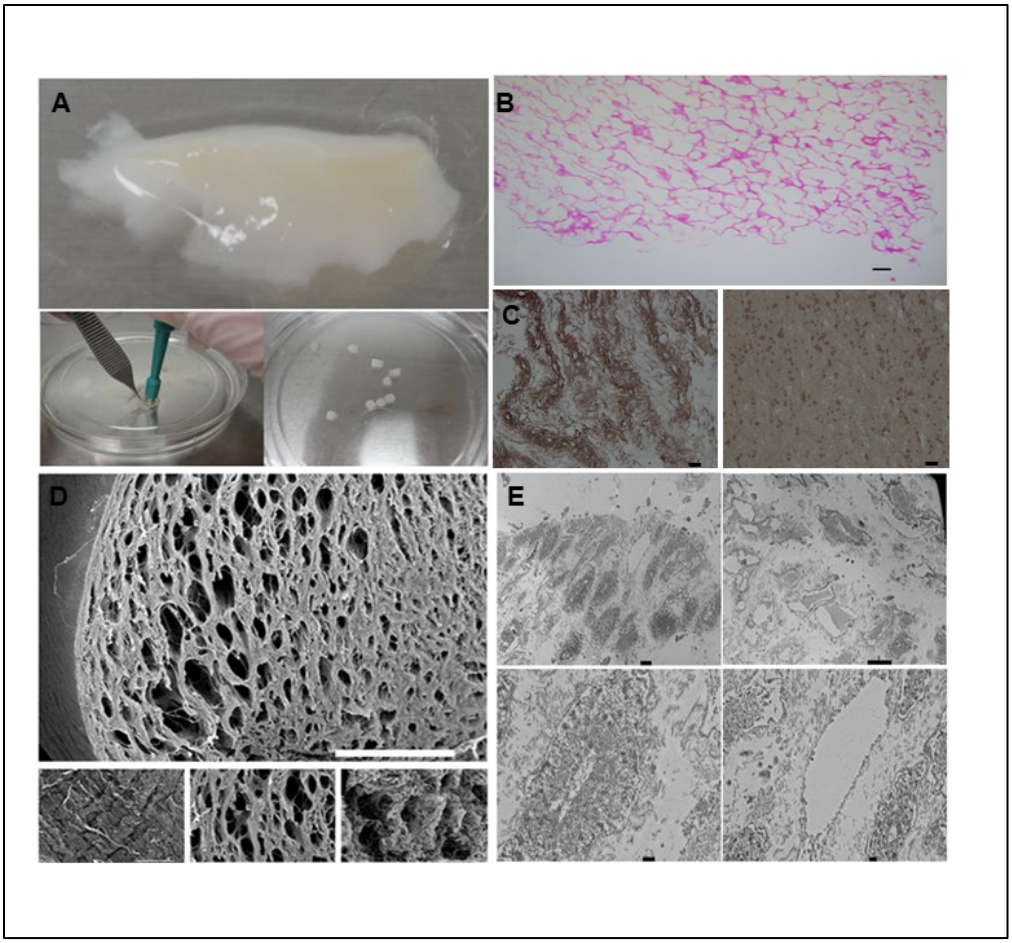

Figure 5 - Characteristics of decellularized Wharton's jelly matrix (DWJM).

A) A fragment of the isolated DWJM. 5-7 mm in diameter pieces were obtained using a 5-7 mm skin punch biopsy kit, (right lower corner image). B) H&E stained sections of the DWJM showing empty spaces. (Scale bar represents 0.1 mm). C) Hyaluronic acid immunohistochemistry images of DWJM indicating abundant hyaluronic acid expression at one region and less abundant at the other. (Scale bar represents 25μm). D) Scanning electron microscopy pictures of DWJM. One surface appeared flat with compact matrix (left lower image) while, less dense tissue with open spaces was identified in other areas (lower right and middle images). (Scale bar for the full picture was 600 μm). E) Transmission electron microscopy pictures of DWJM. More electron dense areas of DWJM (left upper image) and less electron dense areas (right upper image) were observed. No intact cells were observed in all the panels. (Scale bar for left upper image was 2 μm, for right upper image was 10 μm, and the two lower images was 500 nm.)

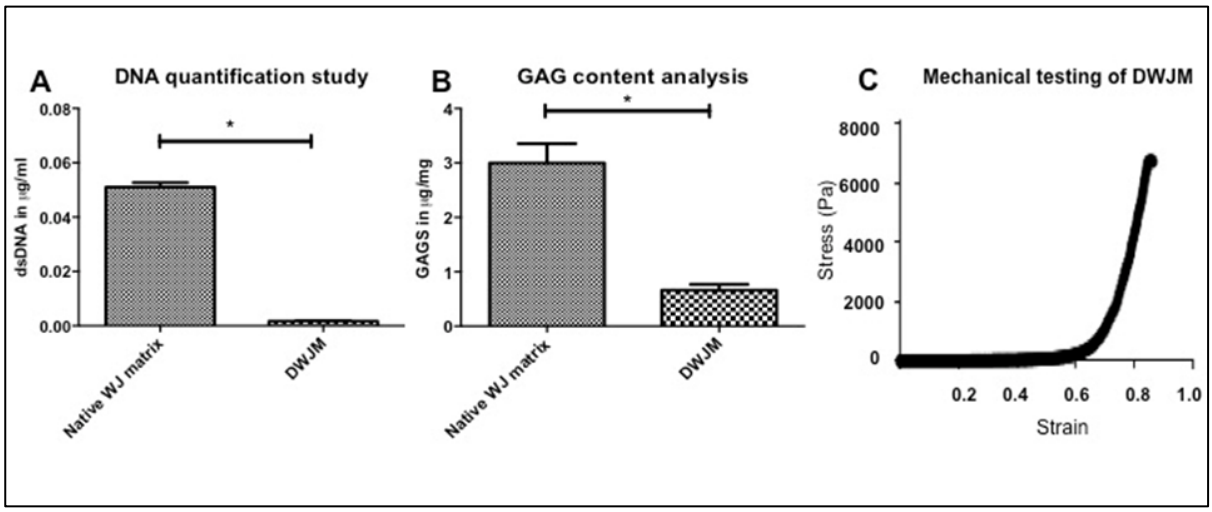

Figure 6 - Assessment of decellularized Wharton's jelly matrix.

A) DNA quantification study performed on the matrix before decellularization and after decellularization. DWJM showed a significantly lesser DNA compared to the native WJ matrix before decellularization. B) Glycosaminoglycan contest assessment of the matrix before and after decellularization, and C) Mechanical testing of DWJM. * Indicate statistical significance ($p < .05$)

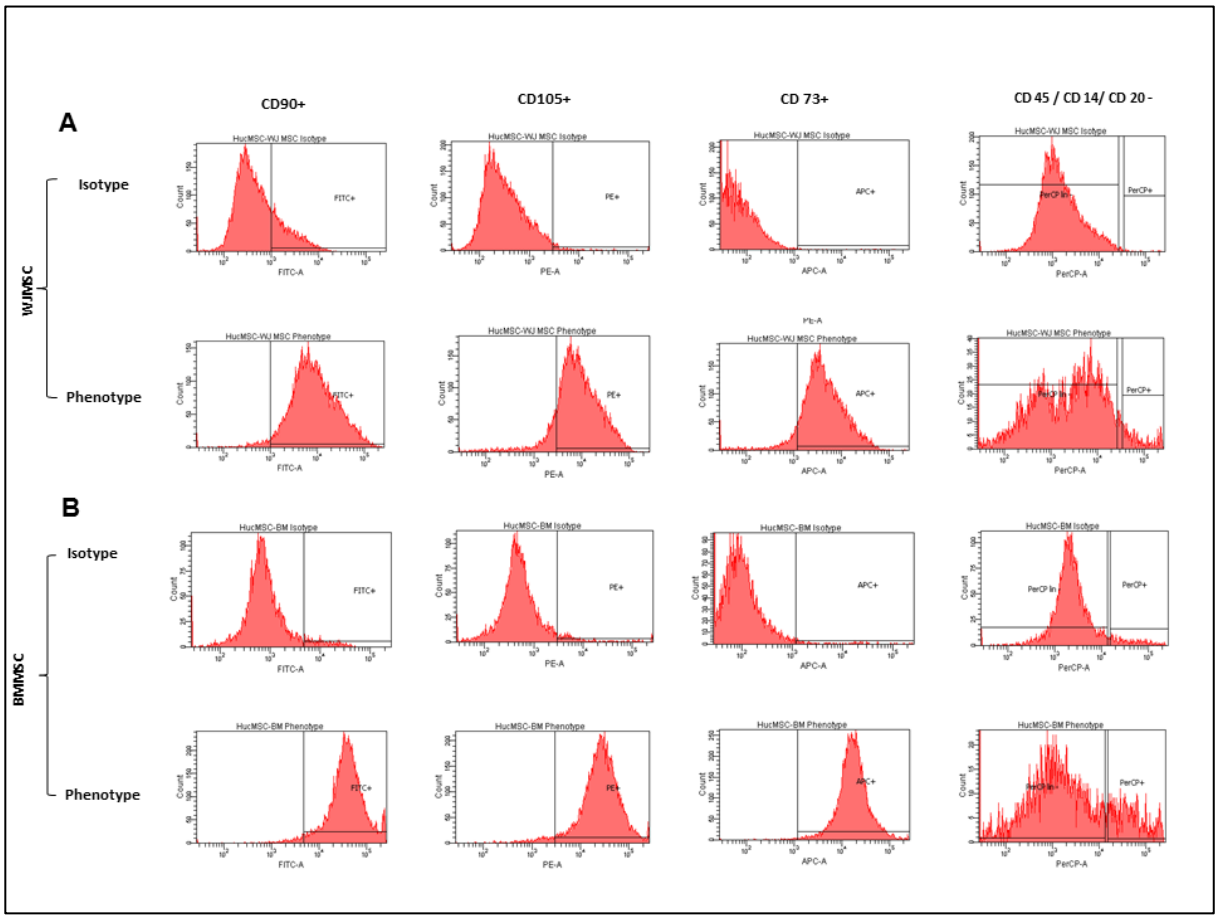

Figure 7 - MSC characterization by flow cytometry.

A) Wharton's jelly mesenchymal stem cell (WJMSCs) and, B) Bone marrow mesenchymal stem cell (BMMSCs). All the MSCs stained positive for CD 90 (FITC), CD 105 (PE) and CD 73 (APC), and were negative for CD 45(Per CP), CD 34(Per CP), CD 14 or CD 11b (Per CP) and CD 20 (Per CP).

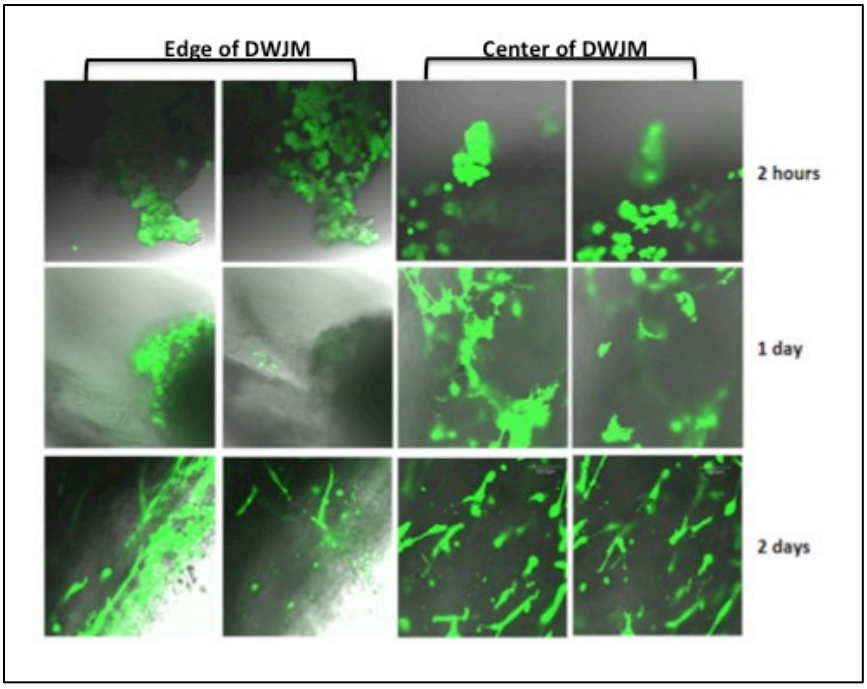

Figure 8 – WJMSCs and DWJM *in vitro* interactions.

Confocal microscopy images of WJMSCs on DWJM after 2 hours (upper panel), 1 day (center panel), and 2 days (lower panel) of cell seeding. Calecin AM was used to label the cells and excited using 488 nm laser. The live cells were stained in green.

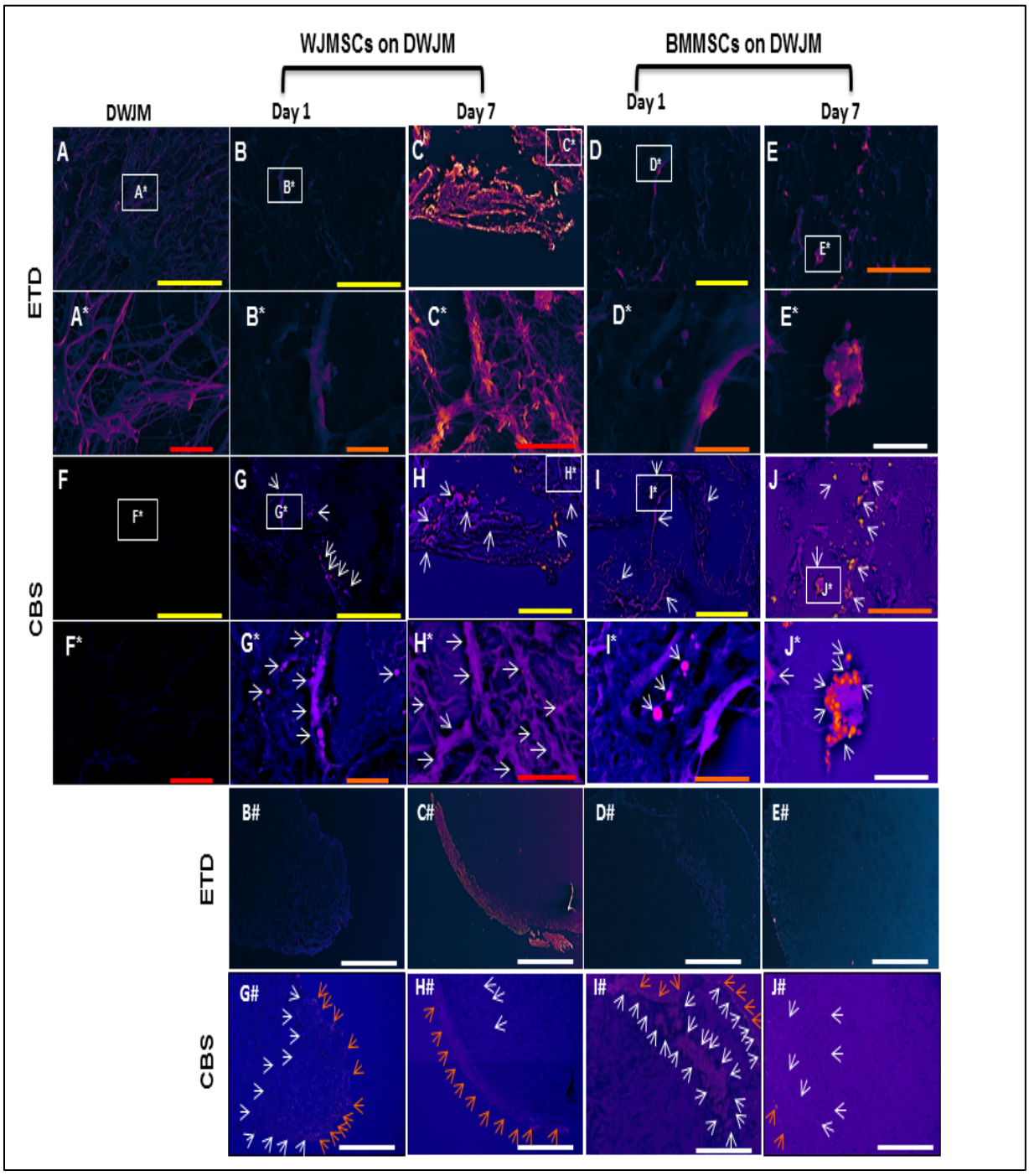

Figure 9 – MSCs and DWJM interactions.

Dual beam microscopy imaging of DWJM with and without MSCs.

Images A-E is on the ETD detector and F-J is using the CBS detector respectively. (A, F) DWJM with no cells seeded into the matrix. (B, G) DWJM with WJMSCs seeded for 1 day, (C, H) DWJM with WJMSCs seeded for 7 days, D, I) DWJM with BMMSCs seeded for 1 day, and E, J) DWJM with BMMSCs seeded for 7 days. A* and F*) 10X magnification of inset in panel A and F respectively; B* and G*) 5X magnification of inset in panel B and G respectively; C* and H*) 5X magnification of inset in panel C and H respectively; D* and I*) 5X magnification of inset in panel D and I respectively; E* and J*) 5X magnification of inset in panel E and J respectively. B#-E# and G#-J# are the low power magnification of images B-E depicting MSCs seeded on DWJM. The Everhart-Thornley detector (ETD) is a standard secondary electron detector used in scanning electron microscopy to study the topography, while the circular backscatter (CBS) is a backscatter detector that reveals lipid content when samples are stained with osmium Tetroxide (OT). Images have been pseudo-colored to enhance definition proportional to secondary electron signal for ETD and to identify backscatter signal for the CBS detector. Red coloring represents lipid content for samples imaged with the CBS detector. Orange Arrows correspond to the outer edge of the DWJM. White Arrows correspond to positive lipid staining. Yellow Scale Bar = 100 μm. Orange Scale Bar = 50 μm. Red Scale Bar = 20 μm. White Scale Bar = 10 μm.

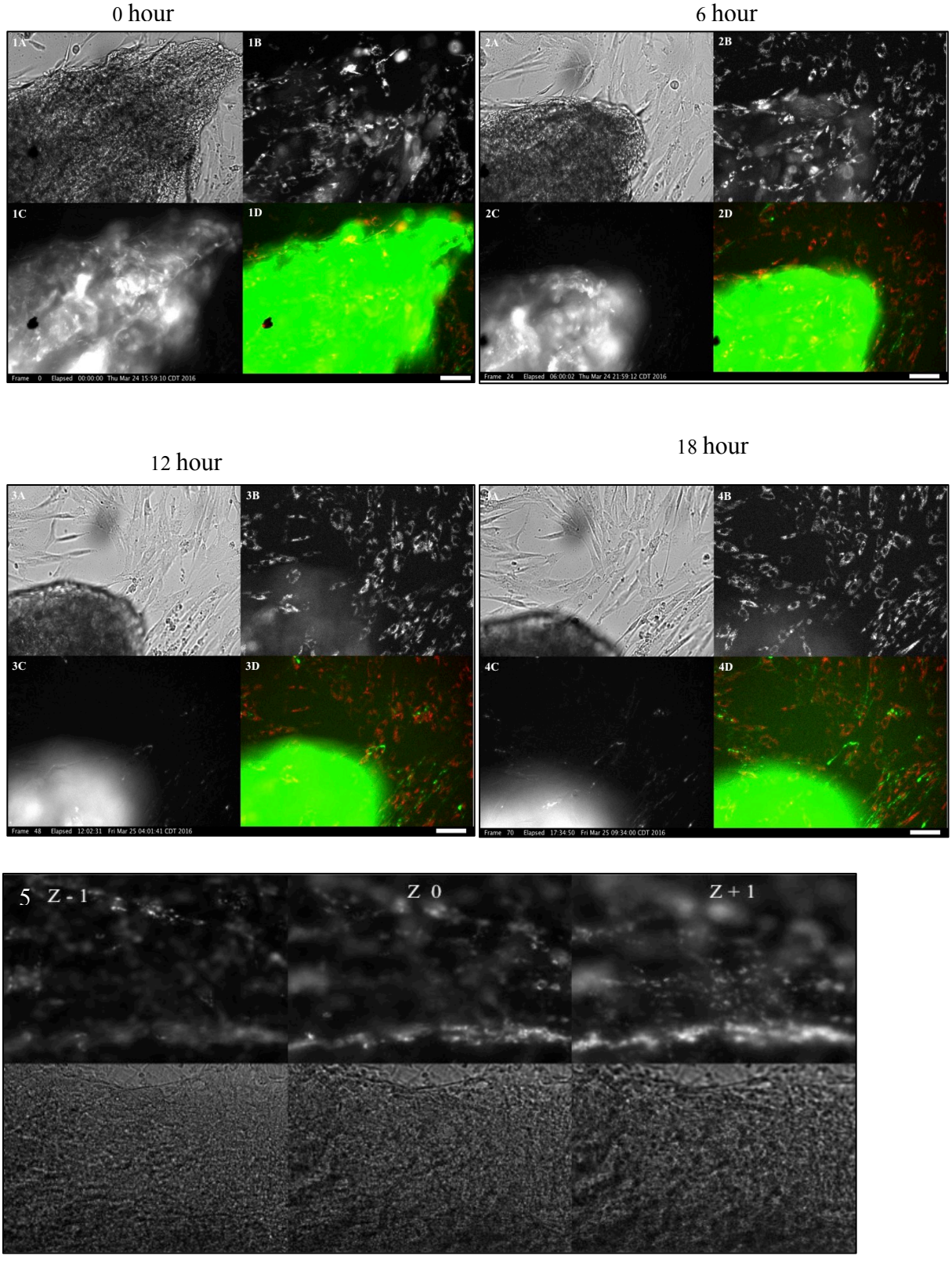

Figure 10 – WJMSCs and DWJM interactions. Time lapse imaging of WJMSCs seeded on DWJM.

Images 1-4 A represent bright field image of WJMSCs on DWJM, 1-4 B represents labeled WJMSCs, 1-4 C are labeled DWJM and 1-4 D shows labeled WJMSCs on DWJM. Figure 10-1A-1D, 2A-2D, 3A-3D, 4A-4D are WJMSCs on DWJM at time 0 hour, 6 hours, 12 hours and 18 hours, respectively. WJMSCs can be seen proliferating and migrating inside and outside the DWJM. Figure 10-5 represent WJMSCs at three different depths in the matrix as Z–1, Z 0, Z+1. The upper panel represents labeled WJMSCs on DWJM, while the lower panel demonstrates labeled DWJM. WJMSCs are labeled in burgundy color and DWJM is labeled in green. WJMSCs on DWJM are in yellow color. Scale bar = 100 μm.

(Cellular movement can be observed in the videos 1 and 2)

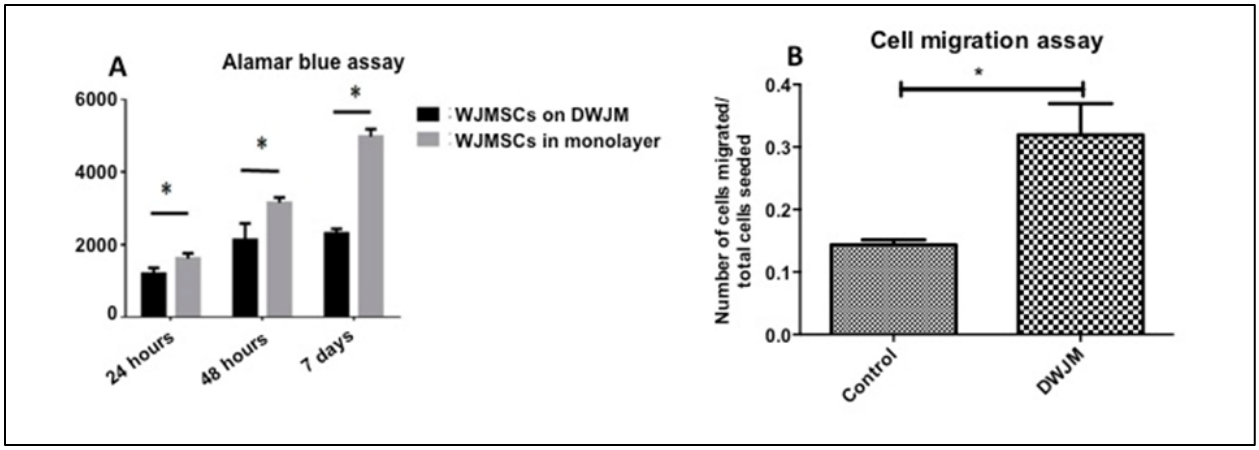

Figure 11 - WJMSC proliferation following seeding onto DWJM and transmigration toward DWJM.

A) Alamar Blue assay to assess the viability of cells seeded on the matrix and B) Cell migration assay performed using trans-wells with cells alone (control) and cells migrating towards DWJM (DWJM), n=3, * Indicates $p < 0.05$.

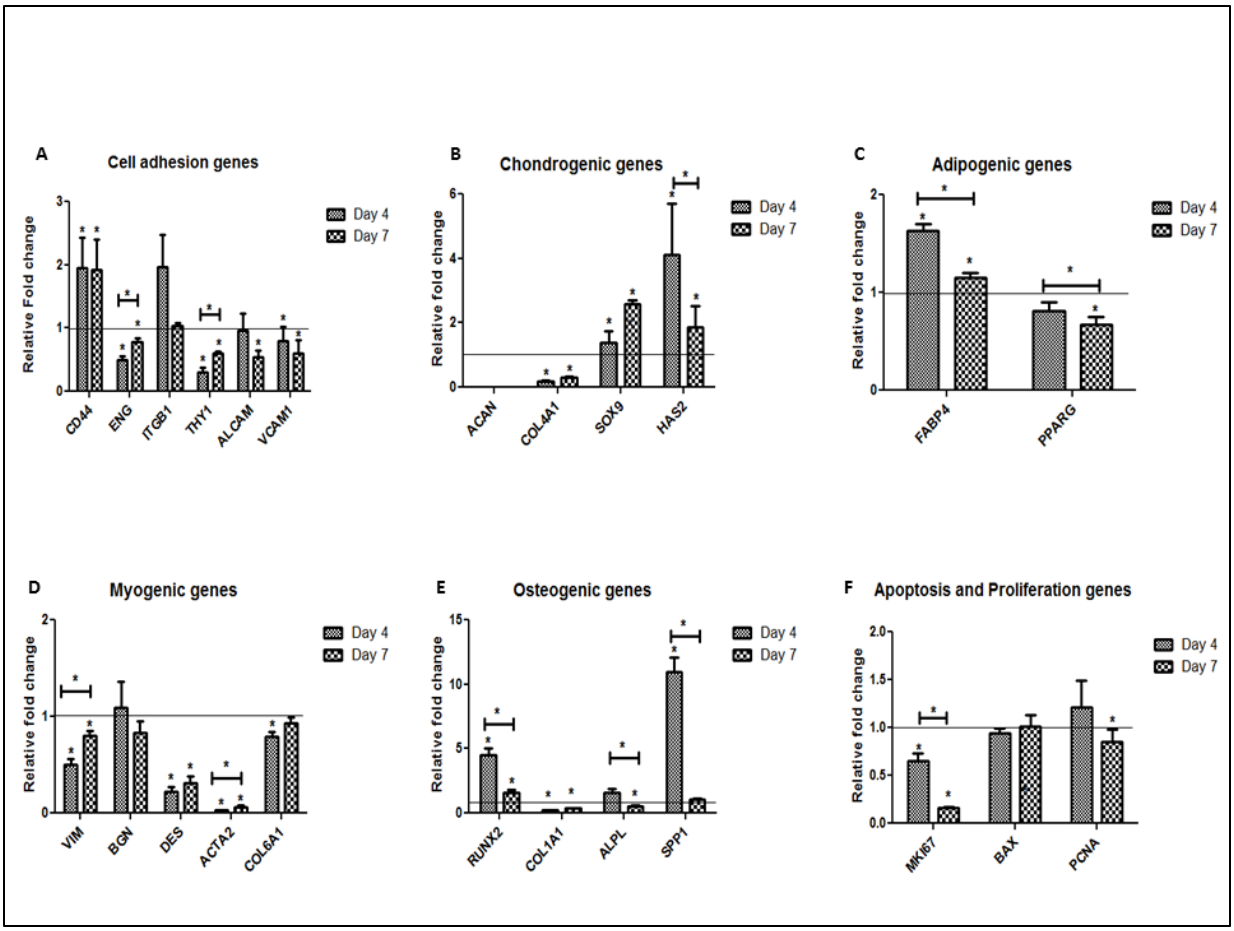

Figure 12 - Differentiation potential of WJMSCs seeded onto DWJM.

Panel A-F are relative gene expression of WJMSCs seeded on DWJM for A) Cell adhesion genes, B) Chondrogenic genes, C) Adipogenic genes, D) Myogenic genes E) Osteogenic genes, F) Apoptosis and proliferation genes. The relative fold change is represented on the y-axis and all the experiments were conducted in triplicates (n=3). The horizontal line represents the gene expression of cells before seeding at Day 0. * Represents $p<0.05$

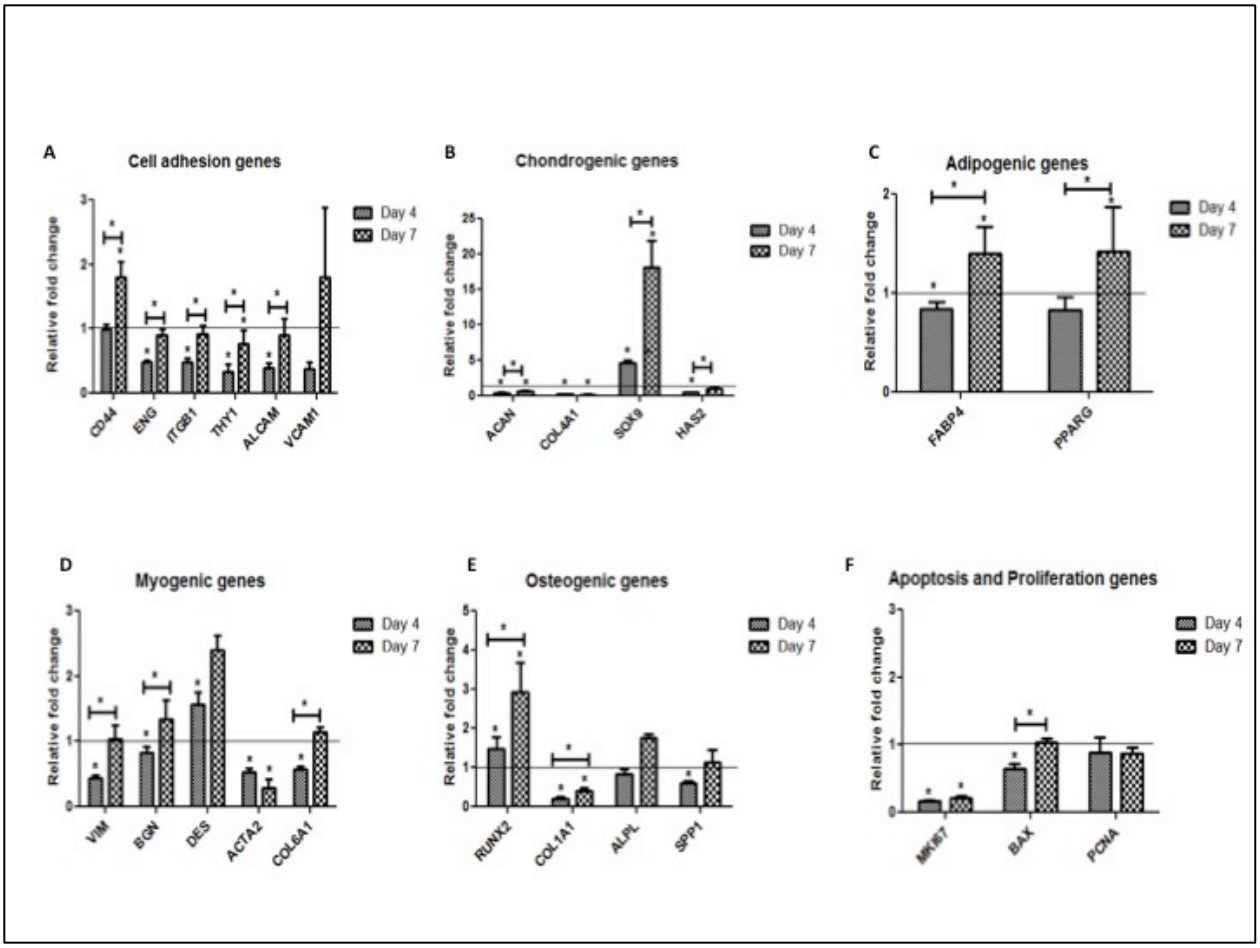

Figure 13 –Differentiation potential of BMMSCs seeded onto DWJM.

Panel A-F are relative gene expression profiles when BMMSCs are cultured on DWJM for A) Cell adhesion genes, B) Chondrogenic genes, C) Adipogenic genes, D) Myogenic genes E) Osteogenic genes, F) Apoptosis and proliferation genes. The relative fold change is represented on the y-axis and all the experiments were conducted in triplicates (n=3). The horizontal line represents the gene expression of cells before seeding at Day 0. * Represents $p<0.05$

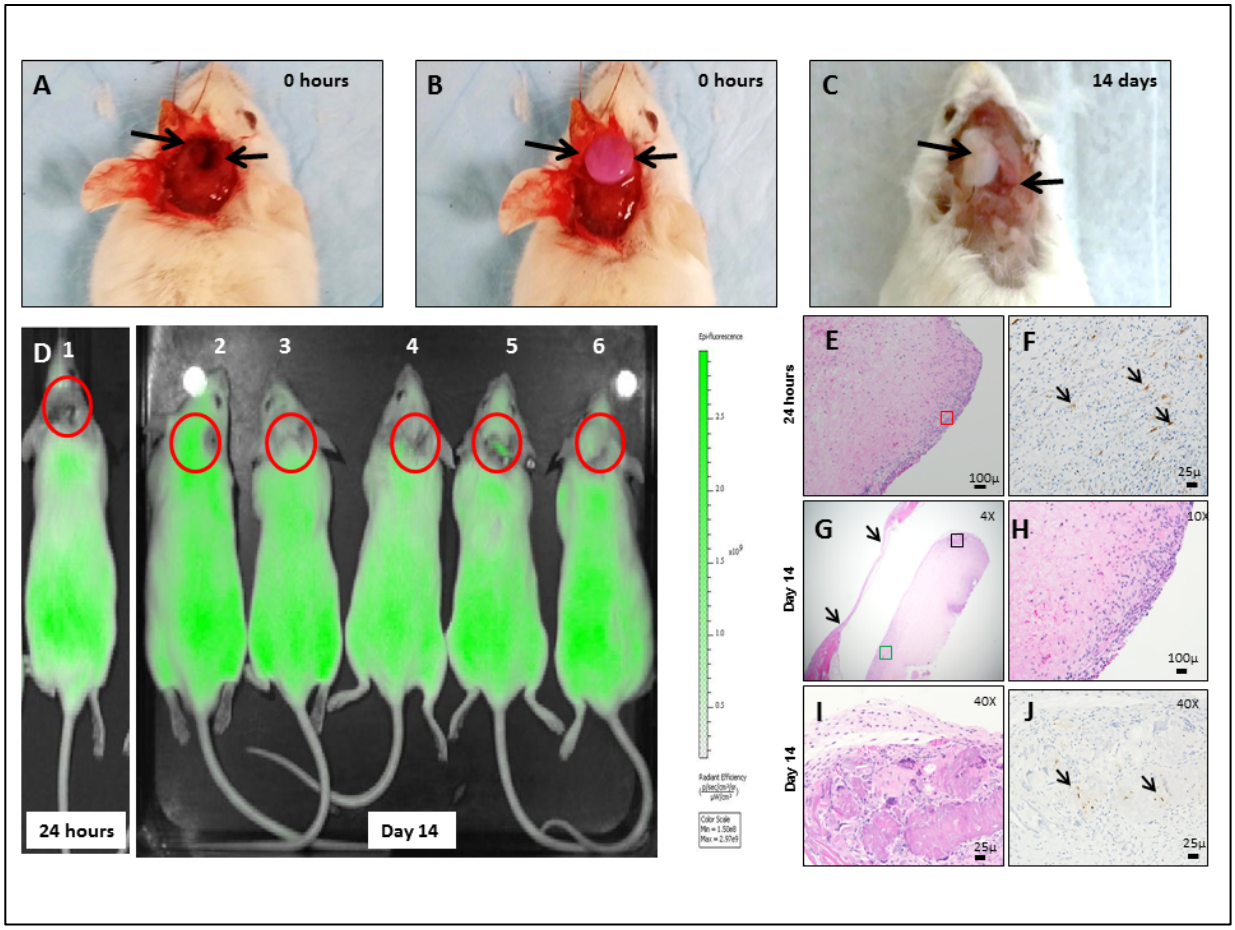

Figure 14 - DWJM transplantation in a cranial defect mouse model.

A) Mice with cranial defect, B) mice with defect and DWJM, C) mice with defect and DWJM 14 days post-surgery. Arrows in A represent the defect, B shows the DWJM and C is the defect and DWJM 14 days post-surgery. D) IVIS imaging of the mice post – surgery - 1) Mice with DWJM 24 hours post surgery; 2-6 designates mice 14 days after the surgeries. D2 is mice without any intervention, D3 and D4 are mice with the defect alone and D5 - D6 represents mice with defect and DWJM. The red circles indicate the defect sites. *The green fluorescence signal at the defect site signifies the migration of the GFP positive cells into the defect.* Images E-J represent the histology images of bone specimen with DWJM 14 days post surgery, with image E) H&E

section of DWJM tissue specimen 24 hours post surgery and image F depicts the GFP immunohistochemistry staining of the same. Images G-J represent DWJM sample 14 days post surgery respectively, at different magnifications as indicated. The arrows in image F, J represent GFP positive cells. The arrows in Image G indicate the beginning and end of defect while black box represents image H and green box is image I. All the experiments were repeated twice (n=2).

Table 2 - Real time PCR TaqMan primers and their description.

Gene symbol	Detector	Gene name
GAPDH	GAPDH-Hs99999905_m1	Glyceraldehyde-3-phosphate dehydrogenase
ACAN	ACAN-Hs00153936_m1	Aggrecan
SOX9	SOX9-Hs00165814_m1	SRY (sex determining region Y)-box 9
COL2A1	COL2A1-Hs00264051_m1	Collagen, type II, alpha 1
ALPL	ALPL-Hs01029144_m1	Alkaline phosphatase, liver/bone/kidney
RUNX2	RUNX2-Hs00231692_m1	Runt-related transcription factor 2
ITGB1	ITGB1-Hs00559595_m1	Integrin, beta 1 (fibronectin receptor, beta polypeptide, antigen CD29 includes MDF2, MSK12)
CD44	CD44-Hs01075861_m1	CD44 molecule (Indian blood group)
THY1	THY1-Hs00174816_m1	Thy-1 cell surface antigen
ENG	ENG-Hs00923996_m1	Endoglin
ALCAM	ALCAM-Hs00977641_m1	Activated leukocyte cell adhesion molecule
CD14	CD14-Hs00169122_g1	CD14 molecule
MKI67	MKI67-Hs01032443_m1	Antigen identified by monoclonal antibody Ki-67
BAX	BAX-Hs00180269_m1	BCL2-associated X protein
VIM	VIM-Hs00185584_m1	Vimentin
ACTA2	ACTA2-Hs00426835_g1	Actin, alpha 2, smooth muscle, aorta
SPP1	SPP1-Hs00959010_m1	Secreted phosphoprotein 1
COL1A	COL1A1-Hs00164004_m1	Collagen, type I, alpha 1
COL4A1	COL4A1-Hs00266237_m1	Collagen, type IV, alpha 1
COL6A1	COL6A1-Hs01095585_m1	Collagen, type VI, alpha 1
DES	DES-Hs00157258_m1	Desmin
HAS2	HAS2-Hs00193435_m1	Hyaluronan synthase 2
BGN	BGN-Hs00156076_m1	Biglycan
VCAM1	VCAM1-Hs01003372_m1	Vascular cell adhesion molecule 1

NOS3	NOS3-Hs01574659_m1	Nitric oxide synthase 3 (endothelial cell)
PCNA	PCNA-Hs00427214_g1	Proliferating cell nuclear antigen

Table 3 - Proteins identified in DWJM using mass spectrometry.

Protein name	Accession number (1)*	Sequence coverage	MW [kDa]	Theoretical. pI	Peptides number	Unique Peptides
Collagen alpha-3(VI)	219521324	13.70	278.0	8.15	18	18
Collagen type I alpha-1	110349772	6.01	138.8	5.80	7	2
Collagen type I alpha 1	180392	9.13	98.5	6.83	7	2
Collagen, type VI, alpha 1	119629727	12.06	108.5	5.43	8	8
Human Serum Albumin	55669910	16.78	65.2	5.80	7	7
Collagen type I alpha 2	825646	6.49	72.2	7.96	4	4
Collagen type VI alpha-2 isoform 2C2	115527062	13.74	108.5	6.21	8	8
Fibronectin 1	219518912	5.38	239.5	5.88	5	5
G-gamma-hemoglobin	183851	31.68	11.0	6.68	2	2
Protein kinase, DNA-activated, catalytic	119607089	0.47	458.5	7.08	1	1

polypeptide						
Tenascin C	156229767	4.93	210.4	4.98	4	4
TGFBI	221044656	19.25	55.7	6.84	4	4
Lumican	4505047	15.68	38.4	6.61	3	3
Collagen, type III, alpha 1	119631314	2.66	106.3	8.10	2	2
Osteoglycin	55957237	13.06	30.4	8.34	3	3
TGFBI	37589544	3.00	75.1	7.23	1	1
Actin, alpha	119612724	12.50	30.3	5.00	2	1
Beta actin, gamma 1	194375299	10.21	37.3	5.71	2	1
HCG2044004	119628289	46.88	3.6	9.32	1	1
Collagen, type XII, alpha 1, isoform CRA_c	119569135	2.22	333.0	5.53	3	3
Hemoglobin alpha 2	13958153	59.21	8.4	7.14	2	2
Immunoglobulin heavy chain variable region	145911949	33.33	9.6	6.52	1	1
Ig G1 H Nie	229601	3.57	49.2	8.54	1	1
Decorin	119617856	14.29	28.0	8.13	2	2
Unnamed protein product	40036688	17.72	17.8	8.38	1	1

N6AMT2	119628685	29.07	9.8	4.36	1	1
Dynein, axonemal, heavy chain 14	220732359	5.31	40.7	5.21	1	1
Chain D, Crystal Structure Of A Sparc-Collagen Complex	215261061	36.36	3.0	11.00	1	1
Golgin subfamily A member 3 (GOLGA3) protein	38174254	4.63	93.0	5.05	1	1
Glyceraldehyde 3-phosphate dehydrogenase	134254708	14.46	17.3	8.60	1	1
Triacylglycerol lipase (EC 3.1.1.3), hormone-sensitive - human	1082874	3.18	85.4	7.77	1	1
PLEKHG3 protein	120537866	3.32	80.8	5.40	1	1
OPK V NimA family	38502049	4.01	67.9	8.98	1	1

Plexin D1, isoform CRA_c	119599646	1.09	193.4	6.96	1	1
CDH24	28375477	10.79	26.3	5.43	1	1
Beta IV spectrin isoform sigma3	11602888	1.76	148.5	6.37	1	1
FBLN1	22761800	3.61	70.5	5.91	1	1
Unnamed protein product	40035675	3.16	68.9	9.32	1	1
Immunoglobulin heavy chain variable region	13171510	52.73	6.2	8.76	1	1
Periostin isoform thy8	166343771	3.19	80.3	8.19	1	1
Transferrin receptor protein 2	33589848	3.37	88.7	6.11	1	1
H2AFJ	194382012	17.12	12.1	10.40	1	1
Large tumor suppressor, homolog 2 variant	62089380	1.95	101.4	9.22	1	1
Truncated beta-globin	58201131	47.50	4.5	9.47	1	1
Dermatopontin	27151769	39.8	24	4.82	4	4
Serum albumin	4502027	36.29	69.3	6.28	17	17

preproprotein [Homo sapiens]						
Ig kappa chain C region	125145	32.08	11.6	5.87	2	2
Fibrinogen beta chain	399492	26.68	55.9	8.27	6	6
Fibrillin-1	311033452	17.69	312	4.93	25	25
Apolipoprotein A-I isoform X2 [Homo sapiens]	530398069	15.73	30.8	5.76	3	3
Ig gamma-1 chain C region	121039	15.5	36.1	8.19	3	3
Mimecan isoform X2 [Homo sapiens]	530391203	11.74	33.9	5.63	2	2
Fibrinogen gamma chain	20178280	9.05	51.5	5.6	2	2
Keratin, type I cytoskeletal 9	239938886	8.35	62	5.24	2	2
Fibronectin isoform 6 preproprotein [Homo sapiens]	47132549	6.8	239.5	5.88	9	9
Fibrinogen alpha chain isoform alpha	11761629	6.52	69.7	8.06	3	3

pre-protein						
Alpha-fetoprotein	120042	6.4	68.6	5.68	2	2
Keratin, type II cytoskeletal 1	238054406	5.59	66	8.12	3	3
Versican core protein	2506816	2.06	372.6	4.51	3	3
Fibrillin-2	238054385	1.03	314.6	4.86	2	2

Abbreviations: TGFBI: transforming growth factor, beta-induced**,** FBLN1: fibulin-1, H2AFJ: histone H2A.J.

*: Accession number refers to the accession number in the National Center for Biotechnology Information (NCBI) protein database.

Chapter 3: Decellularized Wharton's jelly matrix as a Three-Dimensional Scaffold for Ectodermal Differentiation of WJMSCs.[3]

Introduction

The mammalian hair follicle development begins towards the end of the first trimester of pregnancy and their number remains the same thereafter [205]. Hair regeneration occurs in three phases: anagen (the growth phase), telogen (the resting phase) and catagen (the regression phase). Loss of an adult hair follicle from head or body is considered permanent and a complete loss of hair follicles observed in cases of severe burn victims and baldness is associated with mental stress [111]. The therapeutic treatment for hair loss involves transplantation of natural hair from hair rich occipital areas to hair deficient sites, although this surgery is limited by the availability and the ability to transplant hair [206]. Currently researchers are trying to revive hair follicles by *in vitro* culturing of hair follicle cells and implanting them at the treatment area [207-209]. The local dermal-epidermal interaction control hair growth, while the dermal papilla, a condensation of cells at the base of the hair follicle actively promotes follicle induction and hair fiber growth [73, 210]. Hence, difficulties in obtaining good quality and sufficient number of dermal papilla cells along with maintaining the trichogenic ability of these cells poses to be the biggest challenge [62, 73, 209, 211]. WJMSCs are abundantly available in Wharton's jelly (the mucoid porous connective tissue of the human umbilical cord), can be easily obtained and are being increasingly recognized for their ectodermal differentiation potential [111, 212].

---

[3] Published as, Jadalannagari S, Berry AM, Hopkins RA, Bhavsar D, Aljitawi OS, " Potential mechanisms underlying ectodermal differentiation of Wharton's jelly mesenchymal stem cells", Biochemical and biophysical research communications, August 2016.

Aljitawi *et al.* previously demonstrated that WJMSC cultured on DWJM in osteogenic differentiation media differentiate into hair-like structures with CK19 positive cells [213]. Herein, we further examined WJMSC differentiation into hair-like structures and CK19 positive cells and explored the molecular mechanisms that potentially explain ectodermal differentiation in our model. It is well documented that communication between different pathways like the Wnt/ β-catenin, TGF- β and BMP4 pathways is critical for hair follicle development. β-catenin is an effector of intercellular adhesion and functions in Wnt signaling pathway along with Lef-1/Tcf DNA binding proteins, to form a transcription factor. Gat *et al.* reported that this pathway operates in keratinocytes and showed that mice expressing stable β-catenin undergo a process resembling *de novo* hair morphogenesis [214]. It is also shown that Wnt pathway is active in both epithelial and mesenchymal components of developing follicles [215]. Post natally, initiation of new hair growth phase requires neutralization of the inhibitory activity of bone morphogenetic protein 4 (BMP4) by the BMP antagonist noggin. During telogen, BMP4 mRNA predominates noggin in epithelium and mesenchyme with BMPR1A expressed in the follicular germ while, through anagen, BMP4 is down regulated, and noggin mRNA is increased. As a hair growth inducer, noggin increases Sonic Hedge Hog (SHH) mRNA in hair follicle, while BMP4 down regulates SHH [92, 216]. The morphogen SHH of the Hedge Hog family is generated in the hair follicle placode and is known for regulating hair follicle epithelial growth [100, 217]. Woo *et al.* demonstrated that SHH acts directly on the dermal condensate and helps in maintaining dermal condensate cell identity and maturation during hair follicle morphogenesis [218]. SHH and Noggin form a positive loop in hair development [92, 216], while Noggin and BMP6 (maintains dermal papilla hair inductive function) constitute part of a negative feedback loop regulating hair outgrowth [219].

Plikus *et al.* has demonstrated that at the start of telogen, intradermal BMP levels are high, which gradually decrease towards the onset of anagen. During telogen, the dermal papilla produces a high level of BMP inhibitors like noggin, to reduce BMP threshold and maintains stem cell quiescence [220]. Oshimori *et al.* has shown that TGF-β2 plays an important role in dampening BMP signaling thereby promoting hair follicle stem cell activation. They also proved that the stem cell activation is a result of a comprehensive niche in which TGF-β2 functions specifically at quiescence to activate the stem cells in a short – range, concentration – dependent fashion [104]. Smads are a group of signaling mediators and antagonists of TGF-β2, activin and BMPs [221]. It has been previously shown that TGF-β2 activates Smad 2/3 transiently in hair follicle stem cells during tissue regeneration [104]. Smad 4 affects hair follicle differentiation by mediating BMP signaling and Smad-7 significantly affects hair follicle development and differentiation by blocking TGF-β/Activin/BMP pathway along with inhibiting Wnt/ β-catenin signaling via ubiquitin-mediated β-catenin degradation [221]. Thus, in this chapter, I will be exploring the molecular mechanisms associated with differentiation of WJMSCs seeded on DWJM and cultured in osteogenic media into potential hair follicle precursor cells *in vitro*.

Materials and Methods

Human umbilical cord collection, WJMSCs isolation and harvesting of decellularized Wharton's jelly tissue were performed according to the IRB protocol # HSC 12129 of the University of Kansas Medical Center. Umbilical cords were collected immediately after normal vaginal delivery from consented donor mothers with full-term pregnancy. The umbilical cord was placed in a transport solution made of Lactated Ringer's solution supplemented with penicillin 800 U/ml (Sigma-Aldrich, St. Louis, MO), streptomycin 9.1 mg/ml (Sigma-Aldrich), and amphotericin 0.25 mg/ml (Sigma-Aldrich) and immediately refrigerated at 4°C. The decellularization process was initiated within 72 hours of umbilical cord collection.

Decellularization process

The decellularization procedure was carried out as described in our earlier publication [169]. Briefly, umbilical cords were dissected and were subjected to two cycles of osmotic shock, by alternating with a hypertonic salt solution containing sodium chloride, mannitol, magnesium chloride, and KCl. The tissues were further subjected to an anionic detergent (Sodium lauryl) and, sodium succinate (Sigma L5777), alternating with a recombinant nucleic acid enzyme, (Benzonase™) in buffered (Tris Hcl) water for 16 hours. Following this, an organic solvent extraction was done and all of the detergent and other processing residuals were then removed utilizing ion exchange beads. The decellularized matrix was cryopreserved using 10% human recombinant albumin (Novozymes) and 10% DMSO (Sigma) solution in standard RPMI media, employing a material specific computer controlled freezing profile that was developed to freeze at -1°C/minute to -180°C [222].

Isolation, expansion, and MSCs seeding onto scaffolds

Preparation of DWJM for seeding with MSCs

Freshly obtained fragments of DWJM were transferred to a large petri dish and covered with phosphate buffered saline (PBS). DWJM pieces (5-7mm in diameter) were obtained using a sterile 5-7 mm skin punch biopsy kit. The resulting DWJM pieces were cylindrical in shape with non-uniform heights, which varied between 2-3 mm. The volume of the obtained DWJM scaffolds' was ~72 mm^3. From this point on, these pieces of DWJM will be referred to as DWJM scaffolds. DWJM scaffolds were transferred using sterile forceps to a large petri dish and washed with PBS twice. At the time of seeding, the DWJM scaffolds were transferred to non-tissue culture treated plates.

Preparation of Dermal graft for cell seeding

The Alloderm® dermal grafts (DG) were purchased from Life cell Inc. (Bridgewater, NJ). 7 mm scaffolds 150-250 μm in thickness were obtained using a sterile 5-7 mm skin punch biopsy kit. These scaffolds were soaked in sterile PBS solution before using for rehydrating the tissue *in vitro* and *in vivo*.

MSC isolation and expansion

a. WJMSCs

WJMSCs were isolated and expanded according to the procedures described by Wang *et al.* [171]. Briefly, the outer layer of the cord was carefully removed and the cord was cut into smaller segments. The blood vessels were dissected from these cord segments and then cut into smaller pieces and digested with Collagenases (Worthington Biochemical Corporation, Lakewood, NJ) in low glucose DMEM (Sigma-Aldrich) with 10% FBS (Atlanta Biologics, Atlanta, GA) and 1% Penicillin/Streptomycin (Sigma-Aldrich) overnight at 37° C to obtain

WJMSCs. The WJMSCs were passaged and maintained in low glucose DMEM with 10% FBS and 1% Penicillin/Streptomycin (also called as regular media (RM)). WJMSCs from passages 4 - 9 were used for the experiments. The WJMSCs were also cultured in hair follicle derma papilla cell growth media (HFDPM) (Cell Applications Inc., San Diego, CA) with 10% FBS and 1% Penicillin/Streptomycin for 2 weeks.

b. BMMSCs

BMMSCs were isolated from bone marrow aspirates of healthy consented donors at University of Kansas Medical Center (HSC # 5929). The cells are isolated following standard ficoll density gradient separation method (Lymphoprep, Stem cell technologies, Vancouver, BC). The isolated cells were counted and plated to select for MSCs based on adherence to plastic in culture flasks. The adherent cells were maintained in high glucose DMEM (Sigma-Aldrich), 20% FBS (Atlanta Biologics) and 1% Penicillin/Streptomycin (Sigma-Aldrich) at 37°C, 5% CO_2 and 90% humidity.

MSC characterization and phenotyping

MACS Miltenyi Biotec MSC human phenotyping kit was used for the characterization of expanded WJMSCs and BMMSCs. Flow cytometry analysis was performed using BD Flow cytometer LSR2. MSCs isolated from human umbilical cord and bone marrows were stained for CD14, CD20, CD34, CD45, CD73, CD90 and CD105.

MSC seeding onto scaffolds

For each set of seeding experiments, single-donor (n=1) WJMSCs/BMMSCs was used. 1 x 10^6 MSCs were suspended in 100µl culture medium and seeded on each DWJM scaffold/dermal graft scaffold (average seeding density was 1.4 X 10^4 - 4 x 10^4/mm^3 DWJM scaffold) in a 24-well non tissue culture treated plate. 1 ml of medium/well was added to the cells

on the scaffolds. After 2 days, the media was changed to osteogenic differentiation media (OD) composed of the regular media with 100nM dexamethasone (Sigma-Aldrich, St. Louis, MO), 5mM β-glycerolphosphate (Sigma-Aldrich, St. Louis, MO), 10nM 1α 25 di-hydroxy vitamin D3 (Enzo life sciences, Farmingdale, NY), 50μg/ml ascorbic acid 2-phoshate (Sigma-Aldrich, St. Louis, MO) and the cells were cultured for 4 weeks. For the gene expression studies, 0.25 – 1.0 x 10^6 WJMSCs/BMMSCs of passage 4-7 were seeded on DWJM on a 24-well non tissue culture treated plate (Corning Inc., Corning, NY) for 2-4 weeks and cultured in their respective media. Samples were harvested at day 0, week 2 and week 4. Day 0 was used as the control for all the qPCR analysis **(**Figure 15**).**

Evaluating seeded WJMSC adherence to DWJM, proliferation and characterization of the hair-like structures

Confocal microscopy

To assess WJMSC attachment to DWJM scaffolds, 1 x 10^6 WJMSCs were seeded on each DWJM scaffold in a 24-well culture plate. After 4 weeks of cell culture, these scaffolds were viewed using Fluoview scanning laser confocal microscope (Olympus, Center Valley, PA). Prior to viewing, seeded DWJM scaffolds were rinsed twice with PBS and incubated with culture medium containing 2 μg Calcein AM stain (Molecular Probes, Eugene, OR). Calcein AM is a cell-permeant dye that is converted to green-fluorescent Calcein in live cells.

Scanning electron microscopy (SEM)

DWJM scaffolds were fixed in 2 % glutaraldehyde for SEM processing. The fixed samples were washed with PBS for 10 minutes, placed into buffered 1% osmium tetroxide for 1 hour, and then washed 3 times 10 minutes each in distilled water. Further, the samples were dehydrated through a graded series of ethanol from 30%, 70%, 80%, 95%, and 100% for 15

minutes each. Following this, the samples were critical point dried in CO_2 in a model EMS 850 dryer, then they were mounted onto aluminum mounts and sputter coated with gold in a Pelco SC-6 sputter coater. Finally samples were viewed using a Hitachi S-2700 scanning electron microscope.

Histology and Immunohistochemistry

DWJM/Dermal graft scaffolds were fixed in 10% formalin or 4% paraformaldehyde for 24hours, embedded in paraffin, sectioned with an average thickness of 40 μm, and stained with H&E. Slides were reviewed using Olympus BX40 microscope and pictures were acquired using DP72 digital camera.

Immunohistochemistry staining was performed using IntelliPATH FLX™ automated stainer (Biocare Medical, Concord, CA) at room temperatures. Briefly, after deparaffinization and rehydration, tissue sections were separately incubated with primary antibodies against Cytokeratin 19 (1:50 dilution; Biocare Medical, Concord, CA), collagen 1 (Abcam, Cambridge, MA), and Smooth muscle actin (SMA) (1:500 dilution, Dako, Carpinteria, CA) for 30 minutes are room temperature respectively. After rinsing, CK19 and SMA sections were incubated with anti-mouse HRP-labeled polymer (EnVision™ + system, Dako, Carpinteria, CA) while collagen 1 sections were incubated with MACH 2™ rabbit HRP-polymer (Biocare Medical, Concord, CA). Finally, the staining was visualized by DAB (Dako, Carpinteria, CA) and nuclei were counterstained with hematoxylin. B-catenin immunohistochemistry was done using mouse anti-human antibody (CST, Danvers, MA) and an anti-mouse secondary antibody.

Molecular studies

RNA extraction from cells

WJMSCs and BMMSCs were cultured as a monolayer (2D) or on DWJM/dermal graft (3D) as described above. WJMSCs were harvested from the scaffolds following overnight digestion with Collagenase II. The MSCs were washed twice with PBS and centrifuged at 13000 rpm, 4°C for 20 minutes to obtain a cell pellet. The cell pellet was suspended in 1 ml of Trizol (Life technologies) and stored at -80°C until further processing. Once all the samples were collected, RNA was extracted using the standard procedure as described by the manufacturer (Life technologies, Carlsbad, CA). Briefly, aqueous phase containing RNA was separated using 0.2 ml chloroform, 0.7 volumes of isopropanol was added and centrifuged to precipitate RNA. The RNA pellet was washed twice with 75% ethanol and dissolved in 30-50µl of nuclease free water. RNA was quantified using Nano drop spectrophotometer 8000. 1.5µg of RNA was treated with DNA-*free*™ DNase treatment and removal kit (Life Technologies). High capacity cDNA reverse transcription kit (Applied Biosystems) was used to generate cDNA from the extracted total RNA samples using Bio-Rad T100 thermal cycler.

Quantitative real-time PCR analysis

The quantitative real-time PCR (qPCR) reactions (20 µl) were performed with TaqMan gene expression master mix (Life Technologies), and TaqMan array 96 well plates (Applied Biosystems, Foster City, CA) using StepOnePlus™ real-time PCR system (Applied Biosystems). The primers used are described below in (Table 4). The qPCR reactions were performed in triplicate. StepOnePlus™ real-time PCR system (Applied Biosystems) was used for the qPCR. GAPDH was used as an internal control to normalize the samples to obtain ΔC_t. $2^{-\Delta\Delta Ct}$ was used to analyze the relative gene expression levels.

Immunoblot analysis

For immunoblot analysis of β-catenin, BMP4, SMAD, WJMSCs and BMMSCs were cultured with or without DWJM and with or without osteogenic differentiation media for 4 weeks. Immunoblot for each condition was performed in experimental triplicates. Following the differentiation, DWJM was digested with collagenase (Worthington Biochemicals, Lakewood, NJ) over night at 37°C and the obtained cells were washed twice with 1× PBS. Protein was harvested using ice-cold RIPA buffer containing protease and phosphatase inhibitor cocktail following three freeze thaw cycles at -196°C and 37°C respectively. Cell lysates were collected and the protein concentrations were determined using DC Protein assay kit (Bio-Rad, Hercules, CA). 20 µg of cell lysate was resolved on a 4-12% Bis-Tris gel (Invitrogen, Carlsbad, CA) and then transferred onto a 0.22µ nitrocellulose membrane (Maine manufacturing). Novex XCell II™ Blot Module was used for the semi-wet transfer (Life technologies, Carlsbad, CA). The membranes were blocked with Odyssey® blocking buffer (Li-Cor, Lincoln, NE) washed with 1× TBS containing 0.1% tween 20 (TBST). Immunoblotting was performed using anti-β-catenin rabbit monoclonal antibody (dilution of 1:1000) (8480, Cell signaling technology, Danvers, MA), anti-BMP4 rabbit monoclonal antibody (dilution of 1:1000) (ab124715, Abcam, Cambridge, MA), and anti-Smad polyclonal goat antibody (AF3797, R&D systems, Minneapolis, MN) at 1:1000 dilutions in blocking buffer. After multiple TBST washes, IRDye® 800CW goat anti-rabbit IgG (Li-Cor, Lincoln, NE) and Pierce™ donkey anti-goat IgG (Thermo-Scientific, Rockford, IL) (dilution 1:10000) were used respectively. Further, the blot was washed with TBST three times and imaged using Li-Cor Odyssey imaging system and ImageStudio software.

The membrane was stripped using Restore fluorescent stripping buffer (Thermo scientific, Rockford, IL) and re-probed for β-actin using rabbit anti β-actin antibody (dilution of 1:1000) (Cell signaling technologies, Danvers, MA) and IRDye® 800CW goat anti-rabbit IgG secondary antibody (Li-Cor, Lincoln, NE). Densitometry analysis was performed on all (n=6) images using ImageStudio software. The intensities of proteins were normalized to their corresponding β-actin intensities.

Statistical analysis

All data were expressed as means ± standard error of mean (SEM) and analyzed using student's t-test, two-way analysis of variance (ANOVA) with Bonferroni post-test. A threshold of $p \leq 0.05$ was used to determine statistical significance. The statistical analyses were performed utilizing Graph Pad Prism software version 6 (Graph Pad Software, Inc.).

Results

Regeneration of hair like structures

Decellularized Wharton's jelly matrix was used to culture WJMSCs in RM (Figure 16A) and OD (Figure 16B-D). WJMSCs cultured in OD, demonstrated some structures reproducibly protruding through the outer layers of DWJM. These structures were 10 - 30μ in length at week 2 that increased to about 100μ at week 4 (Figure 16C-D). Also, some of these structures were coiled underneath the outer layer (Figure 16B) and others were around 30μ - 100μ in width (Figure 16D) at week 4. These structures were similar in diameter (11μ -100μ) to human hair follicles observed among various ethnic groups [223]. WJMSCs cultured on DWJM in media without the osteogenic components did not demonstrate these structures (Figure 16A). WJMSCs cultured on Alloderm, also appeared to grow on the Alloderm, and cellular condensations were observed between the edges of dermal graft, causing them to roll, but no hair like structures were noticed.

After 4 weeks of culture, matrix without cells was observed under scanning electron microscope, and appeared like a randomly woven fibrous mesh (Figure 17A) while, WJMSCs cultured on DWJM in regular media appeared to attach and grow in the pores and on the surface of DWJM (Figure 17B). Two types of cells were observed - spherical and round in shape (Figure 17B). WJMSCs cultured in osteogenic media also attached on the matrix and had a smooth appearance. Cells were undistinguishable and structures of sizes 30-100μ were observed protruding from the matrix (Figure 17C-D).

When DWJM with differentiated cells was observed under a confocal microscope using calcein AM dye, cells aligned on the surface of DWJM and some cells were observed inside the matrix (Figure 18A-D). Staining of dermal grafts seeded with cells also demonstrated presence

of live cells on the surface (Figure 18E-H). WJMSCs cultured on DWJM in osteogenic media also showed cells aligned on the surface and revealed that these structures were associated with live cells (Figure 18I-L).

Evaluation of histology sections of the DWJM seeded with WJMSCs in RM and OD demonstrated that WJMSCs were present on the outer surface in multiple layers while in some areas they were more abundant and formed cellular condensations (

Figure 19A-F). Cells were also observed inside the pores of the matrix (

Figure 19C, F). Staining of DWJM without cells was negative for CK19 (marker of hair follicle stem cells and epithelial progenitors [224]) and smooth muscle actin (marker for hair follicle dermis [225]). Interestingly, WJMSCs cultured on DWJM for four weeks were CK19 positive (Figure 20A-D) indicating the possible ectodermal differentiation similar to keratinized hair. Aljitawi *et al.*, also demonstrated that CK19 protein expression was increased over time when WJMSCs were cultured in OD. Staining of sections of DWJM seeded with WJMSCs for Smooth muscle actin (SMA), a marker for hair follicle dermis [225] revealed positive labeling for SMA suggesting enrichment of hair follicle dermis cells (Figure 20E-H). Staining with collagen revealed the matrix was rich in collagen and that the cells on the surface and inside the pores were also positive for collagen I (Figure 20I-L). Finally, WJMSCs cultured on dermal graft also stained strongly for CK19 and SMA, suggesting potential ectodermal differentiation (Figure 20I-P).

Hair-like structure development on DWJM is a unique feature of WJMSCs alone

When BMMSCs were seeded on DWJM and cultured similarly, they appeared to attach and occupied the matrix, although no hair like structures were observed. Similarly, when WJMSCs were cultured on dermal graft scaffolds, they occupied the matrix and proliferated, but

no hair like structures were observed. Thus, the hair like structures on DWJM appears to be a result of WJMSCs interaction with DWJM alone (Figure 22A-D).

Hair-like structure is an attribute of osteogenic media

WJMSCs cultured on DWJM in OD media developed the hair like structures, while commercially available hair inducing media did not have the potential for this differentiation (Figure 23). To further our understanding of the relative contribution of various osteogenic media components in ectodermal differentiation, we cultured WJMSCs on DWJM in osteogenic media eliminating a single component of the osteogenic media at a time. We observed that media without dexamethasone did result in hair like structures, while media lacking vitamin D3, ascorbic acid or β-glycerolphosphate did not (Figure 24). These results suggest that dexamethasone might not be a critical component in inducing ectodermal differentiation of WJMSCs.

Exploring key factors in WJMSC-DWJM interactions

The communication between the epidermis and the underlying mesenchyme initiates hair follicle morphogenesis. These interactions depend on the interplay of secreted molecules from Wnt/wingless family, the hedgehog family, members of TGF-β /BMP (Transforming growth factor-β/ bone morphogenetic protein), FGF (Fibroblast growth factor) and TNF (Tumor necrosis factor) families [67-69].

β-Catenin

Canonical Wnt/ β-catenin signaling acts as the primary switch for hair follicle fate. Absence or the inhibition of β-catenin by ectopic epithelial expression of the secreted Wnt inhibitor DKK1 results in lack of hair follicle induction [74, 75]. Conversely, forced expression of a stable form of β-catenin causes strong enhanced placode formation due to epidermal

keratinocytes globally adopting a hair follicle fate [76, 77]. β-catenin expression was studied by immunohistochemistry at week 2,4 and it was observed that WJMSCs on DWJM in OD stained positive for β-catenin while WJMSCs on DWJM and RM did not express β-catenin. The differentiated cells on the surface and inside the matrix stained positively for β-catenin implicating β-catenin in ectodermal differentiation of WJMSC towards hair follicle when cultured in DWJM (Figure 21A-F).

From gene expression studies, we observed that WJMSCs cultured on DWJM in regular media decreased the expression of *β-catenin* mRNA at week 2 by 0.5 fold; while, osteogenic media increased the expression by 0.5 fold. At week 4, there was a decrease in the expression of *β-catenin* mRNA, regardless of culture conditions, indicating that β-catenin is an early signal that that might contribute to the formation of hair-like structures in our model (Figure 25A).

Immunoblot analysis of total β-catenin protein level was performed using whole cell lysate from WJMSCs cultured in the presence and absence of DWJM with RM/OD media. Densitometry analysis revealed significant increase in β-catenin expression at week 2 (4 fold for OD media), followed by a decrease at week 4 (0.25 fold for OD media) in 3D cultures, when compared to the control (2D culture) (Figure 26). Similar trend in modulation of β-catenin expression was observed for cells cultured in RM. However, the magnitude of alteration observed was much lower (week 2:1.2 fold increase and week 4: 0.75 fold decrease) as compared to OD media (Figure 26). This suggests that osteogenic media along with DWJM has a synergistic effect on expression of β-catenin.

Noggin and BMP4

The mesenchyme expresses noggin, an extracellular BMP antagonist that induces hair follicle morphogenesis in the embryo and promotes new hair follicle growth post-natally [92,

93]. After the initiation of embryonic hair follicles is completed, BMP4 is expressed, activating a negative feedback loop to prevent further new hair follicle formation and help with differentiation of cells into IRS and hair shaft [94].

WJMSCs cultured as a monolayer in OD media displayed increased mRNA levels for *noggin* at week 2 as compared to cells cultured with RM. Also, *noggin* levels returned to basal levels in both media conditions by week 4 (Figure 25B). Further, mRNA levels of *noggin* increased significantly (2 fold increase) after two weeks of 3D culture on DWJM in OD media and returned to basal levels by week 4 (Figure 25B). Induction of *noggin* mRNA levels was highest when WJMSCs were cultured on DWJM in the presence of OD media. The expression of BMP4 mRNA was almost negligible in WJMSCs cultured with or without DWJM (Data not shown).

TGF-β and SMAD

TGF-β2 activates SMAD 2/3 in the hair follicle stem cells and lowers the level of BMP in the niche thereby, promoting stem cell transition from telogen to anagen [104] . In the absence of TGF-β2, hair follicle stem cells exhibit significant delays in hair regeneration. TGF- β1 has also been proposed to play an important role in catagen regulation by inhibiting keratinocyte proliferation and inducing keratinocyte apoptosis [226] . Jian *et al.* showed that TGF-β1 induces rapid nuclear translocation of β-catenin in MSCs in a SMAD dependent manner.

Hence, we evaluated the expression of *SMAD2* mRNA and observed that WJMSCs cultured on DWJM in OD demonstrated a 2-fold increase in *SMAD2* at week 2 returned to basal levels by week 4 as compared to WJMSCs at day 0 (Figure 25C). Similarly, the expression of *TGF-β* mRNA in WJMSCs and OD increased 0.5 fold at week 2 (Data not shown). Western blot analysis revealed induction of SMAD protein levels when WJMSCs were cultured as a

monolayer in the presence of OD as compared to RM at week 2 (Figure 26). By week 4 there was a sharp decline in SMAD levels suggesting tight regulation of total protein level in the cell. WJMSCs cultured on DWJM in both RM and OD media showed similar trend of diminishing expression level from week 2 to week 4. However, there was lower amount of SMAD protein when WJMSCs were cultured in the presence of DWJM.

Versican

Versican is a proteoglycan involved in extracellular matrix assembly and cellular adhesion. Kishimoto *et al.* demonstrated that *versican* expression is essential for hair inductive properties [117]. Also, human hair follicles express versican in the dermal papilla during anagen, thereby suggesting its role in anagen induction and maintenance of anagen [227]. Willert *et al.* demonstrated that *versican* is a target of Wnt signaling through the β-catenin pathway and plays an essential role in maintaining dermal papilla cells in the state of anagen [228].

WJMSCs cultured in the presence of OD media showed a strong induction of *versican* mRNA levels at week 2 (6 fold) as compared to RM (3 fold). *versican* mRNA levels at week 4 were back to the basal levels, similarly, there was an up-regulation of *versican* mRNA levels when WJMSCs were cultured on DWJM in RM (8 fold) and OD media (5 fold) at week 2 and lowered levels at week 4 (Figure 25D).

Exploring key factors in BMMSC-DWJM interactions

BMMSCs cultured in both 2D and 3D conditions (on DWJM) using RM and OD media, displayed poor induction of *β-catenin* (Figure 27 A). Further, BMMSCs showed a consistent increase in mRNA expression level of *noggin* from week 2 to week 4 irrespective of the culture conditions. Also, BMMSCs cultured in 3D environment on DWJM in the presence of OD media displayed the highest induction of *noggin* mRNA level (90 fold) (Figure 27 B). In contrast, when

BMP4 was studied at the protein level, a significant protein band was found at 47KDa for all the samples in both the cell lines. However, BMMSCs cultured in both 2D and 3D conditions (on DWJM) using RM and OD media displayed no significant change in the mRNA levels of *SMAD* (Figure 27 C) and a significant decrease in *versican* (Figure 27 D).

Investigating WJMSC-dermal graft interactions

When WJMSCs were cultured on Alloderm, a 4-fold increase in versican gene expression was observed when cultured in RM, while there was a 2-fold increase in OD at week 2. At week 4, there was a decrease in expression of versican in both the media treatments when compared to week 2. There was a 1-fold rise in β-catenin expression at week 2 in RM, while there were no variations noted in the other conditions or time points. Noggin, SMAD and TGF-β2 expression were significantly down regulated when WJMSCs were cultured on Alloderm. Thus no noteworthy differences in gene expression were noted when WJMSCs were cultured on Alloderm® in regular media or osteogenic differentiation media (Figure 28).

Studying hair follicle dermal papilla induction media in our model

When WJMSCs were cultured in 2D or on DWJM in a hair follicle dermal papilla induction media, there was a significant decrease noted in TGF-β, SMAD2 and β-catenin. Although there was a decrease in BMP4 gene expression, noggin mRNA was undetected. This potentially demonstrates that this media in our model is not promoting ectodermal differentiation (Figure 29).

Discussion

A series of interactions between the dermal mesenchyme and the epithelial-derived epidermis lead to skin appendages development. During hair follicle formation, the mesenchymal cells that form the dermal component are first visible as a cell agglomeration below the primary epidermal thickening [100, 157]. Our observation of cell condensations on the DWJM could be suggestive of similar agglomerations. Hair follicles are complex organs with the hair shaft made of epidermal tissues, but supported by basement membrane, dermal tissues, appendages and several other cells for their development, nutrition, movement, differentiation, growth, physical stability and coloring [229]. Reynolds and Jahoda *et al.* observed the expression of smooth muscle actin in hair follicles *in situ* and in hair follicle dermal cells *in vitro*. They showed that smooth muscle actin was present in the two dermal components – the dermal papilla and dermal sheath components of rat vibrissa, rat pelage and human hair follicles *in vitro* [225]. Morioka *et al*. also demonstrated that dermal sheath of skin and outer root sheath of hair follicle strongly stained for smooth muscle actin (SMA) [229]. Similarly, we stained DWJM seeded with differentiated cells and observed the cells to be positive for SMA. It was demonstrated by Stasiak *et al.* that keratin 19 distributions was observed in epidermal basal cells, in a defined region of the hair follicle and in the nipple epidermis [230]. Michel *et al.* evaluated keratin 19 as a biochemical marker for skin stem cells of hair follicles and demonstrated that CK19 expressing cells were localized in a well-defined zone of hair follicles below the sebaceous glands and bulge area. CK19 expression was detected throughout the phases of hair follicle cycling although the expression varied with hair size [224]. Similarly, we show that WJMSCs cultured on DWJM in OD media generated CK 19 positive cells on the edges and as cellular condensations.

Several researchers have demonstrated the central role of Wnt/β-catenin signaling in hair follicle morphogenesis and differentiation [100, 231, 232]. Van Mater *et al.,* showed that Wnt/β-catenin signal in hair follicle precursor cells is an important signal for telogen-anagen transition [233] . Wnt signaling is also involved in patterning of skin as mice with constitutive overexpression of an inhibitor of Wnt signaling in skin [74] or with skin-specific deletion of β-catenin fail to develop hair follicles [75] . Conversely mice expressing constitutively active form of β-catenin in their skin display new hair follicle morphogenesis in the inter-follicular epithelium [84]. Thus, we studied β-catenin expression in the cells seeded onto DWJM and observed that the cells in the area of cellular condensation and the cells on the surface of DWJM stained strongly positive for β-catenin, thereby favoring differentiation of hair follicles.

My work has identified ascorbic acid 2-phosphate and vitamin D3 to be important in the development of hair-like structures *in vitro* in our model. Others have reported similar findings such as, Kim *et al*. has shown that ascorbic acid 2-phosphate, a derivative of L-ascorbic acid (Vitamin C), stimulates the growth of human dermal papilla cells, promotes the elongation of hair shafts in hair follicles in culture and induces early conversion from telogen to anagen in mice. They have also demonstrated that ascorbic acid 2-phosphate induces the expression of versican in human dermal cells, which enhances the initiation and growth of hair follicles [227, 234]. Vegesna *et al*. has proved that vitamin D3 or an active form like 1, 25 di-hydroxyvitamin D3 has the potential to act on keratinocytes and initiate hair follicle cycling and stimulate hair growth in nude mice. It has also been shown that a mouse lacking the vitamin D3 receptor display defects leading to postnatal alopecia [235, 236]. In our model, the hair like structures were formed in osteogenic media without dexamethasone, while removing vitamins C, D3 or β-glycerophosphate from culture media did not produce any hair-like structures. Thus, we believe

that ascorbic acid and vitamin D3 are essential components for hair follicle formation when WJMSCs are cultured on DWJM.

The ectodermal differentiation potential of WJMSCs seeded on DWJM is a research area that has never been explored. The use of osteogenic media (OD) to culture WJMSCs while seeded on DWJM was initially utilized to promote osteogenic differentiation. To our surprise, evidence of hair type regeneration was detected. Interestingly, bone and hair regeneration follow similar processes like resorption by osteoclasts or catagen in hair, growth phase by osteoblasts or anagen and resting phase or telogen in hair. They also follow the similar molecular pathway of BMP-Wnt-Shh [237]. Botchkarev *et al*. showed that BMP4 is produced by dermal papilla fibroblasts and secondary germ keratinocytes and prevents onset of anagen by interactions of noggin. BMP2, BMP4 and BMPR-1A are expressed in epithelial and mesenchymal cells of developing hair bulb and in coordination with noggin, these BMPs induce anagen phase, while up regulating Shh[92, 216]. Shh is essential for hair follicle morphogenesis and hair cycle initiation. β-catenin promotes hair follicle morphogenesis and differentiation [101] while acting out-of phase with the BMPs [220]. In a study by Mundy *et al*., the peptide aldehyde proteasome inhibitor PSI that stimulates osteoblast differentiation and bone formation was studied in two separate clinical trials to treat male pattern baldness. In the phase I clinical study, 12 caucasian males with male pattern baldness who received the treatment showed a significant increase in linear hair growth, number of anagen hair, telogen hairs and anagen/telogen ratio. In another double blind phase II clinical study with 50 men with androgenetic alopecia, topical application of this protease inhibitor showed an increase in hair density, and cumulative hair thickness following 8 weeks of treatment [238]. These studies supplemented with research by Aljitawi *et al.* [213], help confirm the relatedness of osteogenic differentiation to ectodermal differentiation.

Ultimately, different combinations of the signals may dictate the outcome of cellular differentiation such as – a tooth, scale, hair or feather formation [67-69]. The Wnt pathway plays essential role during hair follicle induction, Shh (Sonig hedgehog) is involved in late stage differentiation and morphogenesis, and Notch signaling determines stem cell fate and BMP is involved in cellular differentiation.

To understand the molecular mechanisms behind this ectodermal differentiation and the formation of these hair like structures we extracted the undifferentiated and differentiated cells at different time points and performed molecular analysis at the transcript level and protein level for major key factors involved in WJMSC-DWJM interactions. We found that the up regulation of β-catenin, noggin, and versican during the early days of *in vitro* culture followed by a decrease in the BMP4, TGF-β and SMAD could be the primary factors in the ectodermal differentiation in our model. We did not find similar trends in BMMSCs cultured on DWJM or WJMSCs cultured in commercially available media thereby enabling us to conclude that these hair-like structures were the result of WJMSC interaction with DWJM alone.

Conclusion

In this chapter, we demonstrate that WJMSCs cultured in osteogenic media on DWJM, differentiated into CK19 and smooth muscle actin positive cells. WJMSCs cultured on DWJM also produced hair-like structures reproducibly protruding from DWJM. Other MSCs like BMMSCs did not have the potential for such differentiation. We also explored the individual components of osteogenic differentiation media and showed that dexamethasone is dispensable, but ascorbic acid 2-phosphate, β-glycerolphosphate and 1α, 25 di-hydroxy vitamin D3 are essential for hair-like structure formation. We investigated well-known pathways essential for this differentiation and showed that the up regulation of β-catenin gene and decreased expression of BMP4 gene are key players in our model. β-catenin is an early signal responsible for hair follicle formation and is accompanied by higher expression of noggin, a BMP inhibitor. In our model we show that, WJMSCs cultured on DWJM in osteogenic media exhibited β-catenin expression and an up regulation of noggin mRNA in addition to undetectable BMP4 mRNA expression. On the other hand, in BMMSCs, BMP4 mRNA was detected at significant levels, which we believe plays a role in their deficiency to form hair-like structures.

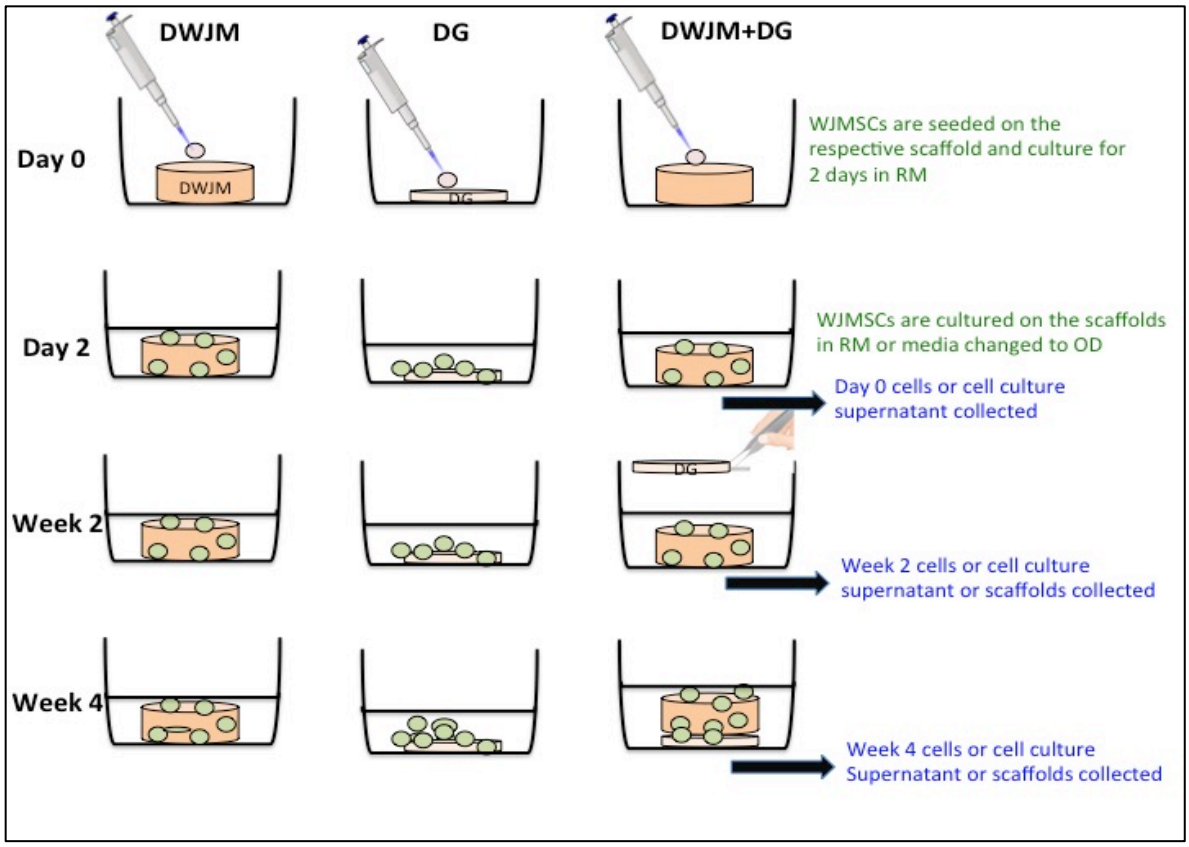

Figure 15 – Schematic representation of the experimental design.

WJMSCs were seeded on DWJM or DG and cultured in RM for 2 days. After 2 days they were grown in RM or the media was changed to OD. Samples from RM and OD media were collected after 2 weeks and 4 weeks and processed accordingly. The scaffolds were processed for histology and immunohistochemistry, the cell culture supernatant was used for ELISA and the cells were harvested and used for gene expression or immunoblot studies.

WJMSCs are represented as green circles, DWJM – 7mm diameter with 2-3mm thickness, DG – 7mm diameter with 200-500µ thicknesses. Abbreviations: WJMSCs – Wharton's jelly mesenchymal stem cells, DWJM – Decellularized Wharton's jelly matrix, DG - Alloderm dermal graft, RM – Regular media, OD - Osteogenic differentiation media.

Image not drawn to scale.

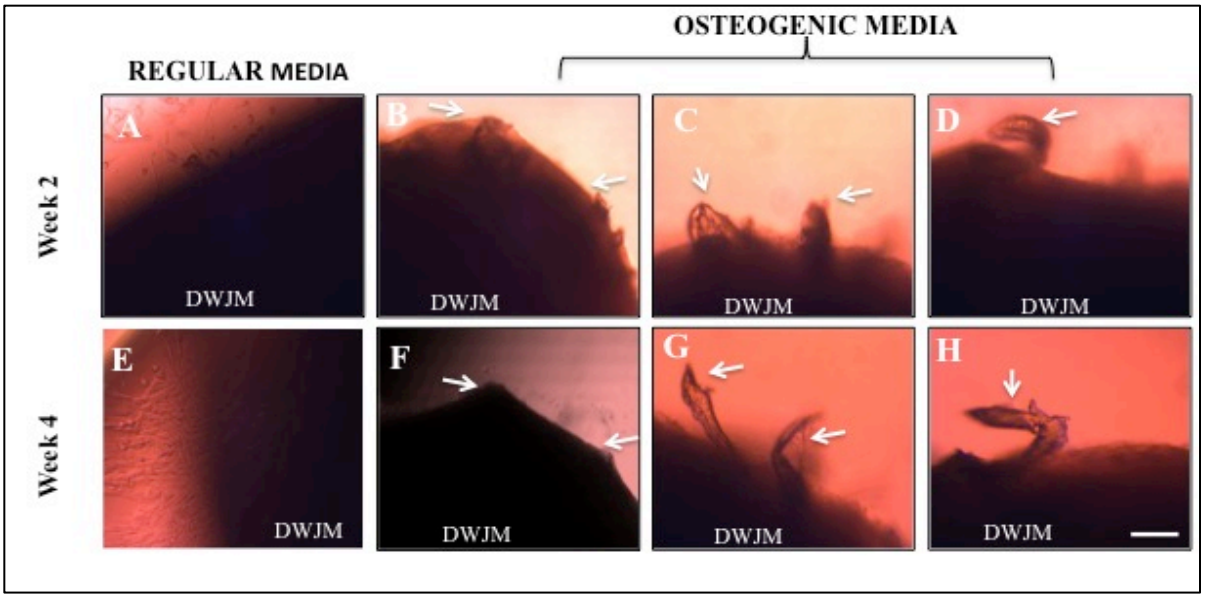

Figure 16 – Bright field microscopy images of hair-like structures according to different culture conditions.

The upper panel represents WJMSCs cultured on DWJM or 2 weeks, and the lower panel indicates WJMSCs cultured on DWJM for 4 weeks. The white arrows point to the coiled or protruding hair-like structures. Figure A demonstrates the smooth surface of DWJM when WJMSCs were cultured on DWJM in RM, while B represents some coiled and protruding hair – like structures. It can also be observed that these structures were growing in size over time. Scale bar represent 200µ.

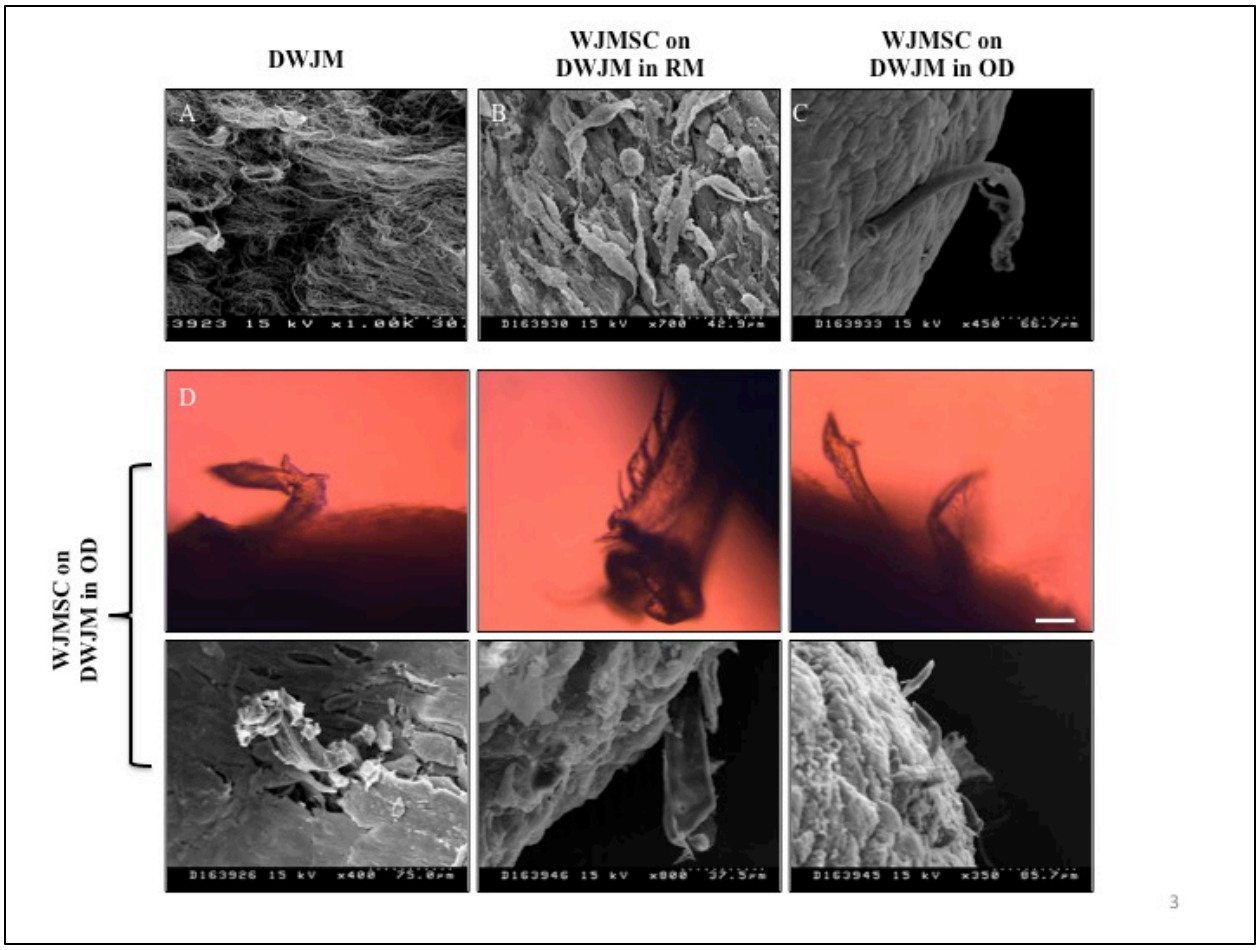

Figure 17 – Scanning electron micrograph images of hair – like structures according to different culture conditions.

The top and bottom panel show Scanning electron micrographs. The image A demonstrates DWJM, B is WJMSCs cultured on DWJM in RM and C is WJMSCs on DWJM cultured in OD for 4-6 weeks. The middle and bottom row represents hair-like structures on DWJM when WJMSCs were cultured on DWJM in OD media. The media row and bottom row represent similar structures in bright field microscope and under scanning electron microscope respectively. Scale bar represent 200µ.

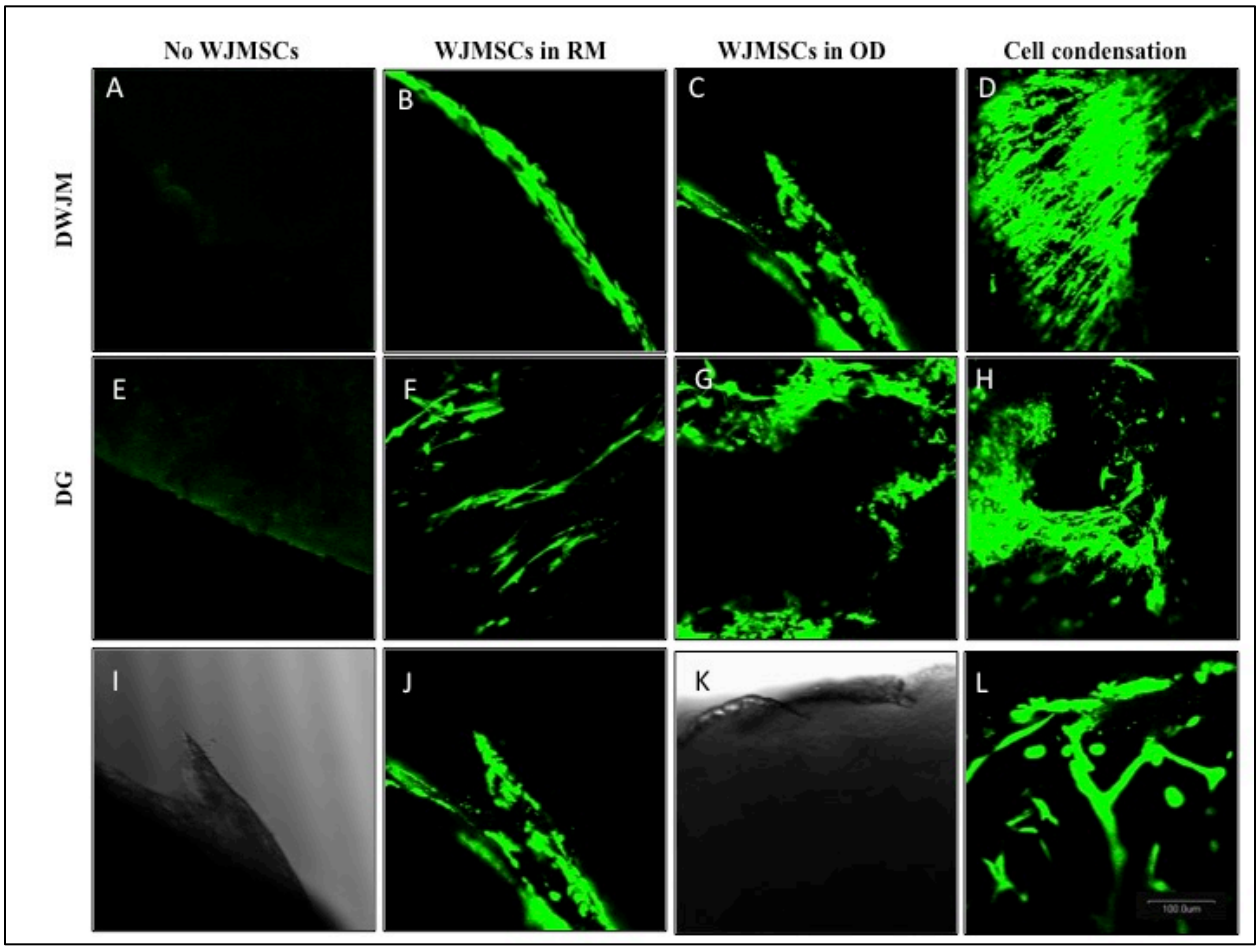

Figure 18 - Confocal microscopy images of WJMSCs seeded onto DWJM and DG.

Image A, E represent DWJM and DG respectively. Image B shows WJMSCs aligned on the surface of DWJM when cultured in RM, while Image D shows WJMSCs arranged randomly on DG in RM. Images C, D, represent WJMSCs on DWJM in OD. Image C shows hair-like structure made up of cells, while Image D represents cell condensations inside DWJM. G, H are WJMSCs cultured on DG in OD arranged in a randomly.

Images K and I show bright field images of the hair-like structures on DWJM, while J and L represent confocal microscopy of the same. *Calcein AM was used to stain the live cells; therefore living cells are stained in green.* The scale bars represent 100µ.

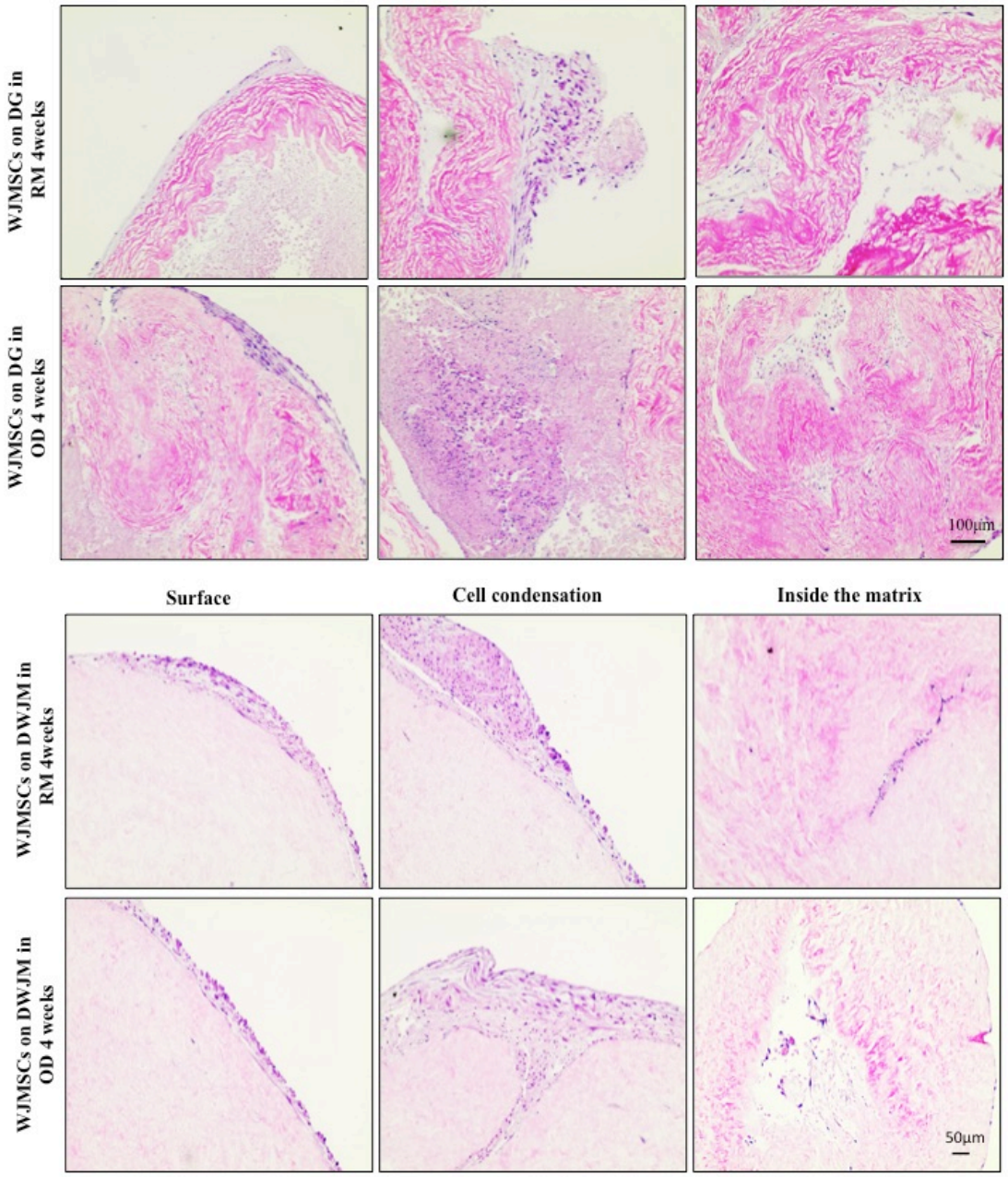

Figure 19 – Histological assessment of WJMSCs seeded onto DWJM and DG.

When WJMSCs were cultured on DWJM in RM or OD, cells were attached and growing on the surface, with cellular condensation observed in some areas. Cells were also observed growing inside the pores of DWJM. WJMSCs were also seen to be attached and growing on the dermal graft. Some cells were observed inside the matrix, while areas of cellular condensations were also observed.

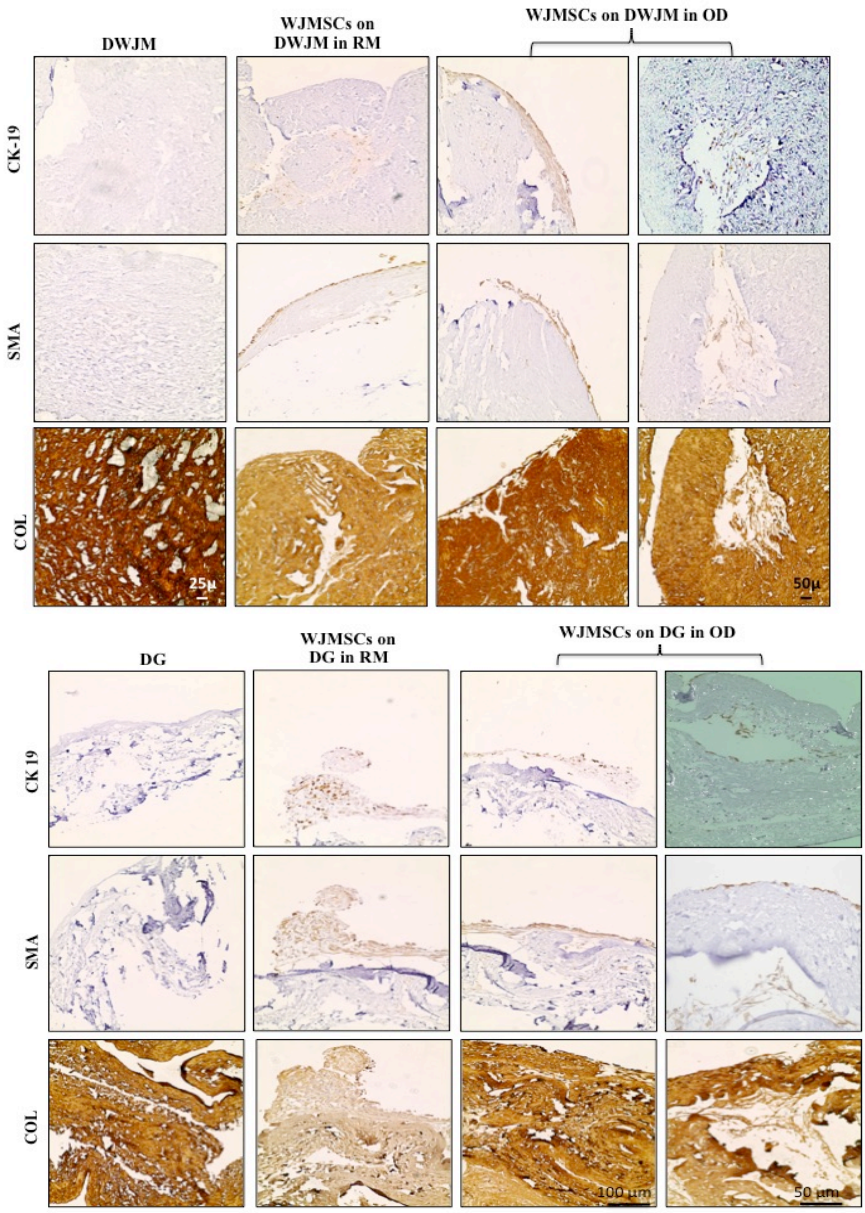

Figure 20 – Ectodermal differentiation of WJMSCs seeded onto DWJM and DG assessed by immunohistochemistry.

The scaffolds with/without cells were stained for α-smooth muscle actin (SMA), cytokeratin-19 (CK19) and Collagen. DWJM and DG stained negative for SMA and CK19, while both the grafts stained highly positive for collagen (COL). WJMSCs cultured on DWJM/DG in RM/OD stained the cells positive for all the markers tested, suggesting similar differentiation patterns.

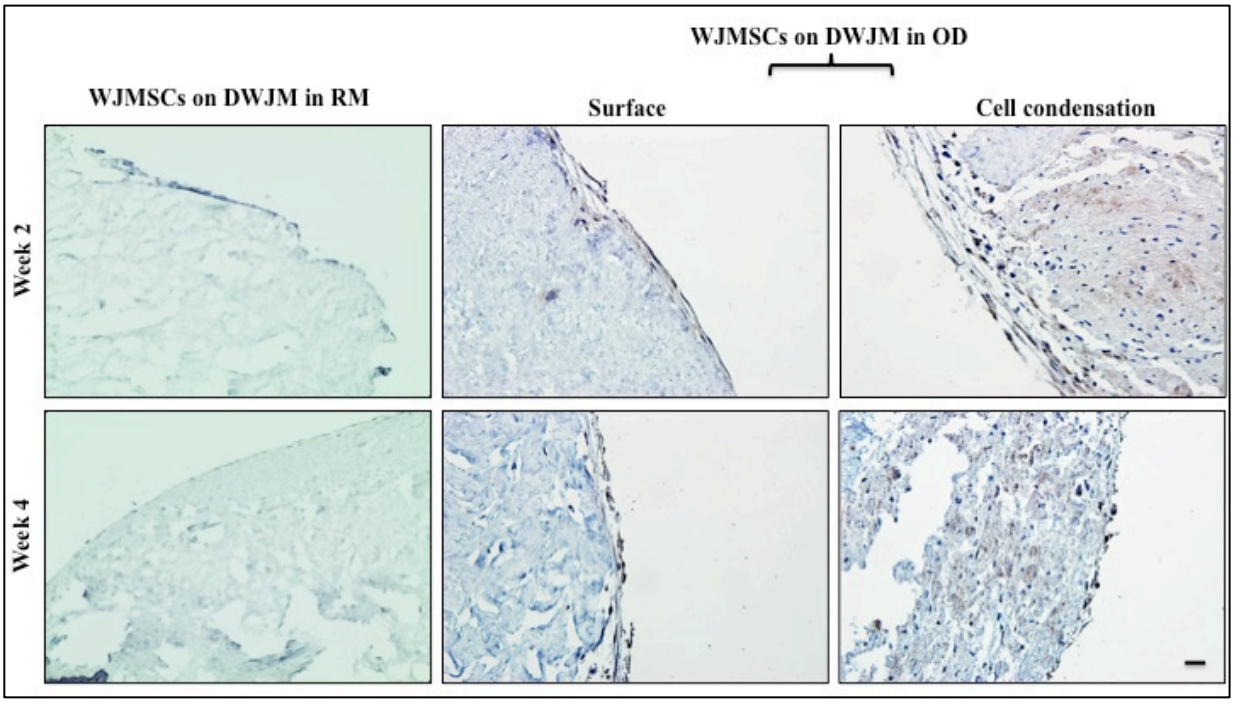

Figure 21 - β-catenin expression in WJMSCs seeded onto DWJM in RM and OD by immunohistochemistry.

WJMSCs cultured on DWJM in RM did not reveal any β-catenin positive cells, while WJMSCs cultured on DWJM in OD stained positive for β–catenin, on the surface as well as the cellular condensations. Scale bar represent 400μ.

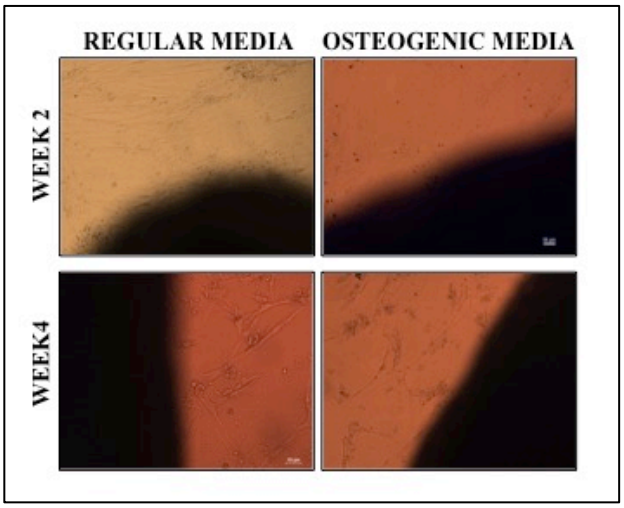

Figure 22 – Assessment of hair-like structures in BMMSCs seeded onto DWJM. BMMSCs were cultured on DWJM in RM and OD for 2-4 weeks and the surface of DWJM appeared smooth and no hair-like structures were observed. The scale bars represent 50μ.

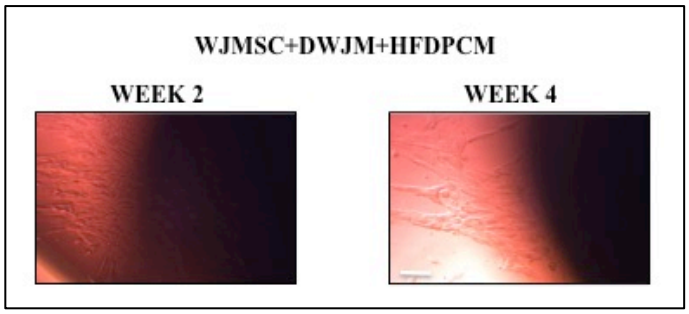

Figure 23 – The effects of hair follicle dermal papilla conditioning media on WJMSCs seeded onto DWJM.

When WJMSCs were cultured on DWJM in a hair follicle dermal papilla conditioning media, the surface of DWJM was smooth and no hair-like structures were observed. The scale bar represents 50μ.

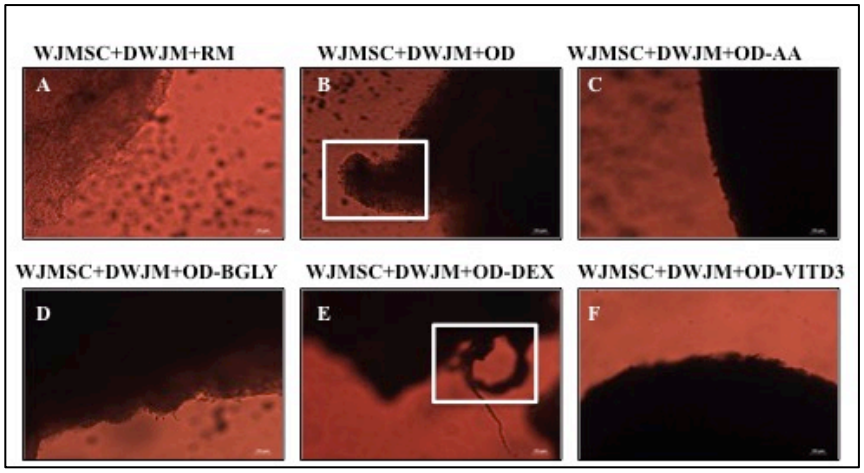

Figure 24 - The effect of various components of osteogenic differentiation media on hair-like structure development in our model.

To understand the components of OD responsible for the formation of hair-like structures, WJMSCs were cultured on DWJM in OD media by eliminating a single component every time. Image A, B represent WJMSCs cultured on DWJM in RM and OD respectively. Images C is WJMSCs on DWJM in OD without ascorbic acid (AA), Images D is WJMSCs on DWJM in OD without β-glycerolphosphate (BGLY), Images E is WJMSCs on DWJM in OD without Dexamethasone (DEX) and Images F is WJMSCs on DWJM in OD without Vitamin D3 (VITD3). The white box shows the hair-like structures protruding from DWJM. The scale bars represent 10μ.

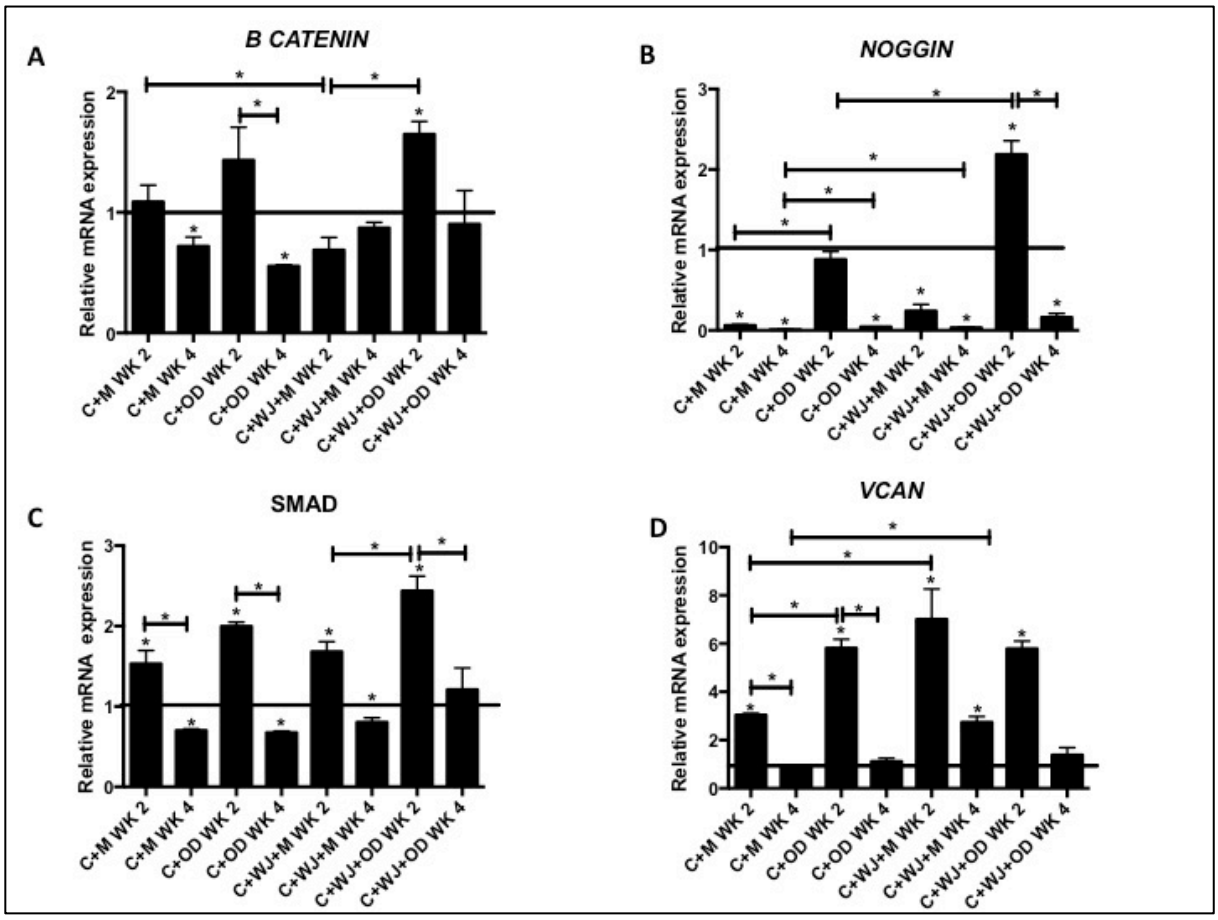

Figure 25 - Potential key players responsible for ectodermal differentiation in our model. Gene expression profiles of key genes potentially responsible for ectodermal differentiation of WJMSCs seeded onto DWJM according to different experimental conditions.

The relative gene expression values for B-catenin, noggin, SMAD AND versican (VCAN) genes is as demonstrated. The horizontal line represents the gene expression of WJMSCs cultured in RM at day 0. Values are represented as mean ± Standard error (SEM) and n=3. * Indicates $p < 0.05$.

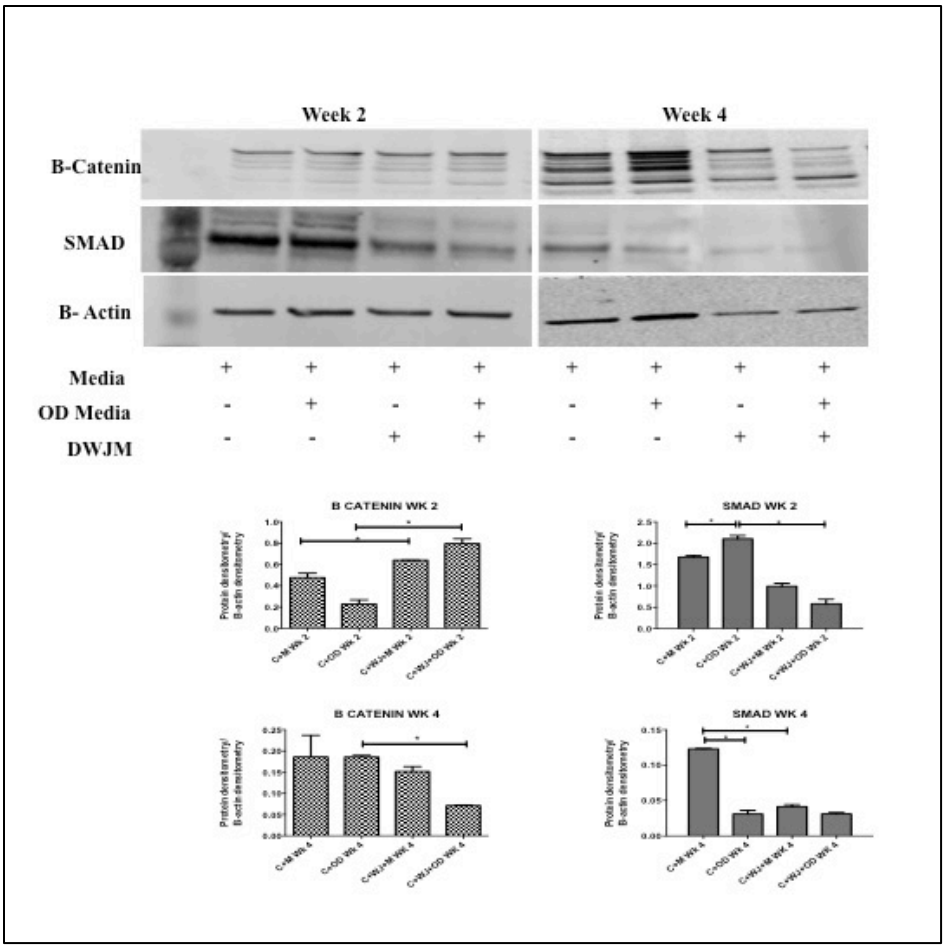

Figure 26 – Potential key proteins potentially responsible for ectodermal differentiation in our model.

B-Catenin and SMAD protein levels were tested by immunoblot analysis. β – actin was used as the control. Densitometry was performed with background subtraction and protein bands were normalized against the β-actin band of the same sample. Values are represented as mean ± Standard error (SEM) and n=3. * Indicates $p < 0.05$.

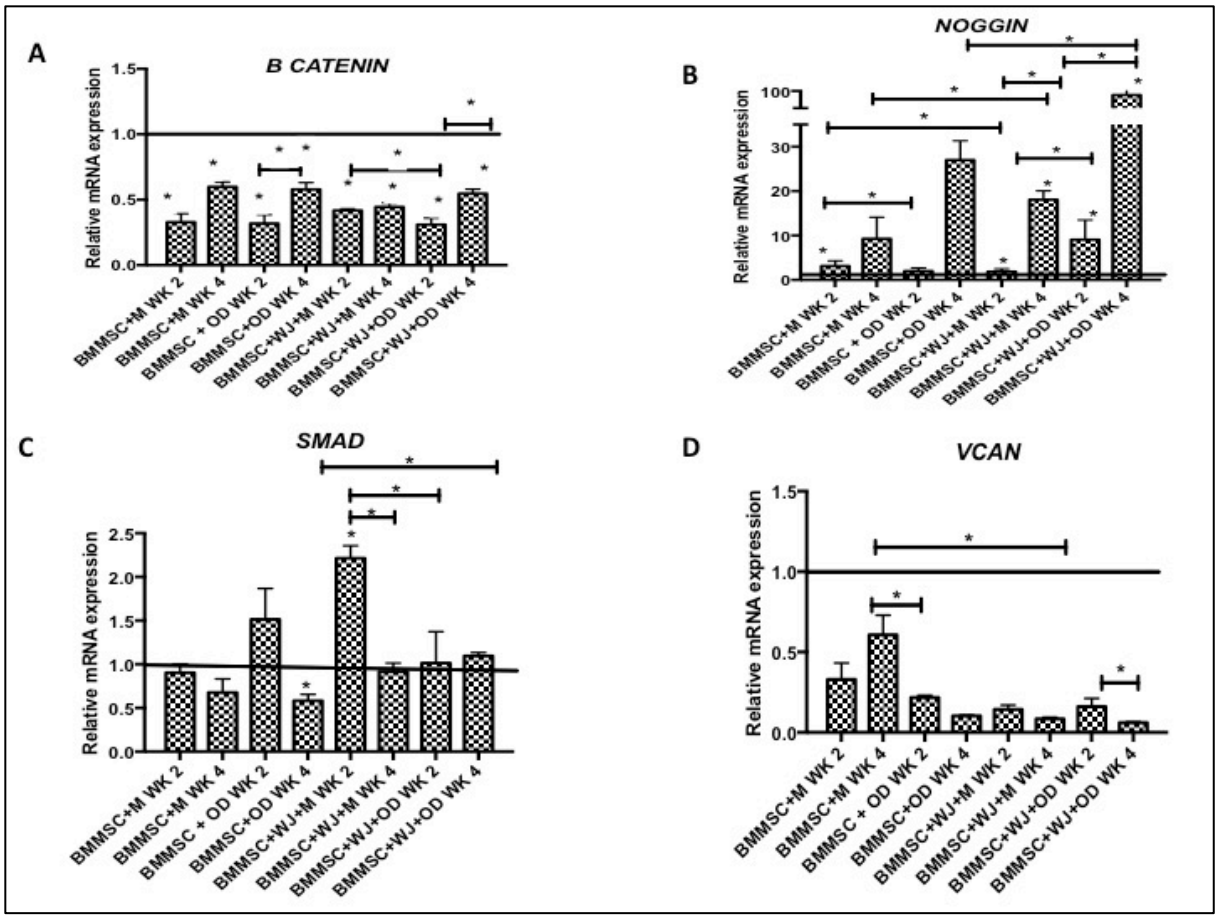

Figure 27 - Gene expression profile of key genes responsible for ectodermal differentiation in BMMSCs seeded onto DWJM.

The relative gene expression values for β-catenin, noggin, SMAD AND versican (VCAN) genes is as demonstrated. The horizontal line represents the gene expression of WJMSCs cultured in RM at day 0. Values are represented as mean ± Standard error (SEM) and n=3. * Indicates $p < 0.05$.

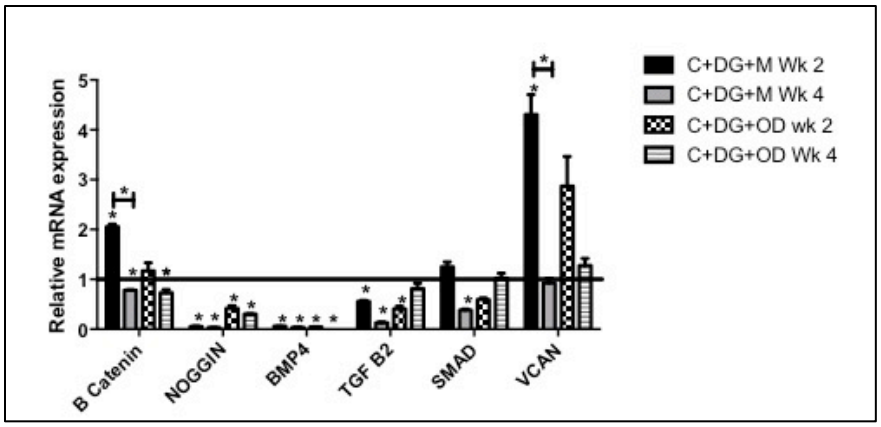

Figure 28 - Gene expression profile of key genes responsible for ectodermal differentiation in WJMSCs cultured on DG

The relative gene expression values for B-catenin, noggin, BMP4, TGF-β2, SMAD AND versican (VCAN) genes is as demonstrated. The horizontal line represents the gene expression of WJMSCs cultured in RM at day 0. Values are represented as mean ± Standard error (SEM) and n=3. * Indicates $p < 0.05$.

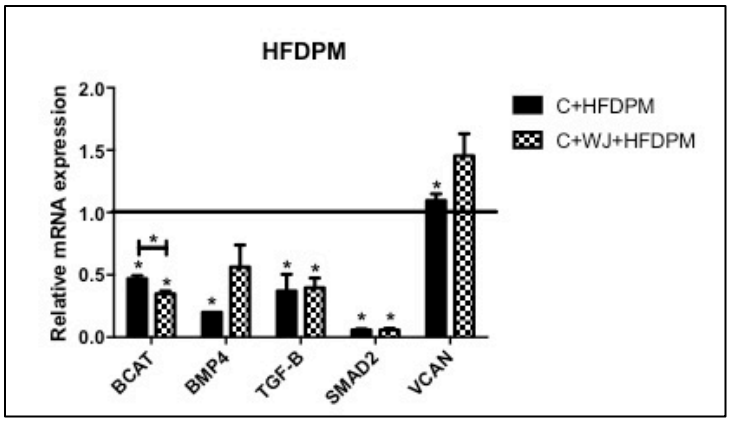

Figure 29 - Gene expression profile of key genes responsible for ectodermal differentiation of WJMSCs cultured in hair follicle dermal papilla media

The solid bar represents WJMSCs cultured in Hair follicle dermal papilla media (HFDPM), while the patterned bars represent WJMSCs cultured on DWJM in HFDPM. The relative gene expression values for B-catenin, noggin, BMP4, TGF-β2, SMAD AND versican (VCAN) genes is as demonstrated. The horizontal line represents the gene expression of WJMSCs cultured in RM at day 0. Values are represented as mean ± Standard error (SEM) and n=3. * Indicates $p < 0.05$.

Table 4 - Primers used in molecular experiments.

Gene symbol	Detector	Gene name
GAPDH	Hs02758991_g1	Glyceraldehyde-3-phosphate dehydrogenase
NOG	Hs00271352_s1	Noggin
BMP4	Hs03676628_s1	Bone morphogenetic protein- 4
CTNNB1	Hs00355049_m1	Catenin (cadherin-associated protein), beta1
TGFB2	Hs00234244	Transforming growth factor-beta 2
SMAD2	Hs00183425_m1	SMAD family member 2
VCAN	Hs00171642_m1	Versican

Table 5 – Abbreviations

C+M WK 2	WJMSCs cultured in 2D in regular media and sample collected at week 2
C+OD WK 2	WJMSCs cultured in osteogenic differentiation media 2D and sample collected at week 2
C+M WK 4	WJMSCs cultured in 2D in regular media and sample collected at week 4
C+OD WK 4	WJMSCs cultured in 2D in osteogenic differentiation media and sample collected at week 4
C+WJ+M WK 2	WJMSCs cultured on DWJM in regular media and sample collected at week 2
C+WJ+OD WK2	WJMSCs cultured on DWJM in osteogenic media and sample collected at week 2
C+WJ+M WK 4	WJMSCs cultured on DWJM in regular media and sample collected at week 4
C+WJ+OD WK4	WJMSCs cultured on DWJM in osteogenic media and sample collected at week 4

Chapter 4: Exploring the Potential of CK19 Positive Cells in Ectodermal Differentiation *in vivo*

Introduction

Wound healing is a well-orchestrated, complex process involving biological and molecular events such as cell migration and proliferation, extracellular matrix deposition, angiogenesis and remodeling [239]. In the repair and management of full thickness wounds, autologous grafts are considered the gold standard approach. But the limited availability and creation of morbidity at the donor site pose biggest challenges [21, 22]. Split thickness autologous graft is an alternative, but this is also associated with problems such as increased scarring and keloid formation [240, 241]. Therefore, tissue engineered skin grafts are a promising alternative for their ability to rapidly close wounds [157]. However, skin appendages such as hair follicles, sebaceous glands and sweat glands cannot be restored due to their limited self-regeneration abilities [242] .

Thus, several novel mesenchymal stem cells based therapies for skin regeneration and repair are being developed with the potential to regenerate skin with its associated appendages [243-247]. Stem cell aggregates from rat bone marrow MSCs (BMMSCs) were applied to rat cutaneous wound and showed that the aggregates presented better neo-vascularization and collagen deposition compared to intravenous or topical application [248]. Doi *et al.* injected two kinds of MSCs, one obtained from human umbilical cord blood (UCBMSCs) and the other from Wharton's jelly (WJMSCs) on a 5 mm full thickness skin defect in nude mice and showed that the umbilical cord blood derived MSCs are a favorable potential stem cell source for wound healing with less scarred tissue formation [243]. Luo *et al.* used UCBMSCs on cutaneous skin wounds and showed enhanced healing and keratinocyte differentiation at the wound site [249].

Mesenchymal stem cells obtained from Wharton's jelly of the human umbilical cord are, easily accessible, noncontroversial, and multipotent with ability of differentiating into bone, cartilage, muscle, adipose and neural cells [128]. Sabapathy *et al.* seeded WJMSCs on a decellularized amniotic membrane scaffold and transplanted on a mice model to demonstrate that this combination aids in reduced scar formation with hair growth and improved biomechanical properties [244]. Pratheesh *et al.* isolated caprine WJMSCs and transplanted on a full thickness skin wound in a rabbit model to show that these MSCs had better epithelialization and collagen deposition compared to the controls [245]. Arno *et al.* used human WJMSCs conditioned media on normal skin fibroblasts and proved that WJMSCs promote skin wound healing through paracrine signaling [246]. It was established by Azari *et al.* that, when WJMSCs from a goat were transplanted on a 3 cm full thickness wound on goat, there was less inflammation, thinner granulation tissue with minimum scar formation compared to the controls with no MSCs [247].

Therefore, in this study, Decellularized Wharton's jelly Matrix (DWJM) with previously generated CK19 positive cells and hair like structures [213] are transplanted onto a full thickness wound on the back of a mice and evaluated for their wound healing and skin regeneration potential. An Alloderm® regenerative tissue matrix (Life Cell Inc.) was used to cover the wounds and keep the tissues hydrated. Alloderm dermal graft (DG) is an acellular human dermal tissue matrix that integrates into the patient's tissue and promotes repair with rapid revascularization and white cell migration [250]. It is easy to handle and has remarkable ability to form functional tissue that provide structural support. This dermal graft has been used in many soft tissue reconstructions like abdominal wall reconstruction, breast reconstruction, and head and neck plastic reconstruction [251]. Achauer *et al.* used this Alloderm dermal graft in 11 patients with soft tissue defects or scarring on the face. They showed that dermal graft acts as an

excellent augmentation material for soft tissue defects with no rejections, mobilization, absorption, dislocation or extrusion associated with other materials [252]. Alloderm can act as a substitute to minimize problems associated with donor site morbidity and lack of adequate tissue for reconstruction [252].

WJMSCs were seeded onto DWJM, DG, and DWJM+DG and cultured *in vitro* using osteogenic differentiation media (OD) or regular media for 4 weeks. The differentiated WJMSCs along with the matrix were transplanted onto a 1.5cm X 1.5cm wound on the back of C57BL/6J mice and studied for its wound healing capabilities. It was observed that mice transplanted with DG and differentiated WJMSCs demonstrated superior wound healing and hair growth compared to controls. Mice with DG+DWJM and differentiated WJMSCs also exhibited complete skin regeneration associated with minimally developed skin appendages.

Materials and Methods

Human umbilical cord collection, WJMSCs and WJ tissue harvest followed by decellularization were performed according to the IRB protocol # HSC 12129 of the university of Kansas Medical Center. Umbilical cords were collected from consented donor mothers with full-term pregnancy immediately after normal vaginal delivery. The umbilical cord was placed in a transport solution made of Lactated Ringer's solution supplemented with penicillin 800 U/ml (Sigma-Aldrich, St. Louis, MO), streptomycin 9.1 mg/ml (Sigma-Aldrich), and amphotericin 0.25 mg/ml (Sigma-Aldrich) and immediately refrigerated at 4°C. The decellularization process was initiated within 72 hours of umbilical cord collection.

Decellularization process

The decellularization procedure was carried out as described in our earlier publication [169]. Briefly, umbilical cords were dissected and subjected to two cycles of osmotic shock, by alternating with a hypertonic salt solution containing sodium chloride, mannitol, magnesium chloride, and KCl. The tissues were further subjected to an anionic detergent (Sodium lauryl) and, sodium succinate (Sigma L5777), alternating with a recombinant nucleic acid enzyme, (Benzonase™) in buffered (Tris Hcl) water for 16 hours. Following this, an organic solvent extraction was done and all of the detergent and other processing residuals were then removed utilizing ion exchange beads. The decellularized matrix was cryopreserved using 10% human recombinant albumin (Novozymes) and 10% DMSO (Sigma) solution in standard RPMI media, employing a material specific computer controlled freezing profile that was developed to freeze at -1°C/minute to -180°C [222].

Isolation, expansion, and MSCs seeding onto DWJM

Preparation of DWJM for seeding with MSCs

Freshly obtained fragments of DWJM were transferred to a large petri dish and covered with phosphate buffered saline (PBS). DWJM pieces (5-7mm in diameter) were obtained using a sterile 5-7 mm skin punch biopsy kit or 1.5 X 1.5 cm pieces were obtained by cutting the matrix into square pieces.

Preparation of Dermal graft for cell seeding

The Alloderm® dermal grafts were purchased from Life cell Inc. (Bridgewater, NJ) and cut into 1 X 1 cm or 1.5 X 1.5 cm scaffolds of 150-250µ in thickness. These scaffolds were soaked in sterile PBS solution before use for rehydration.

The control DWJM / dermal graft scaffolds were washed twice in PBS and pre-incubated in low glucose DMEM (Sigma-Aldrich) with 10% FBS (Atlanta Biologics) and 1% Penicillin/streptomycin (Sigma-Aldrich) for 24 hours at 37°C, 5% CO_2 and 90% relative humidity. After incubation, the scaffolds were washed multiple times in PBS to remove the media before transplantation in the mice.

MSC isolation and expansion

WJMSCs were isolated and expanded according to the procedures described by Wang *et al.* [171]. Briefly, the outer layer of the cord was carefully removed and the cord was cut into smaller segments. The blood vessels were dissected from these cord segments and then cut into smaller pieces and digested with Collagenases (Worthington Biochemical Corporation, Lakewood, NJ) in low glucose DMEM (Sigma-Aldrich, St. Louis, MO) with 10% FBS (Atlanta Biologics, Atlanta, GA) and 1% Penicillin/Streptomycin (Sigma-Aldrich, St. Louis, MO) overnight at 37°C to obtain WJMSCs. The WJMSCs were passaged and maintained in low

glucose DMEM with 10% FBS and 1% Penicillin/Streptomycin. WJMSCs from passages 2 - 5 were used for the experiments.

Labeling of WJMSCs with Indocyanine green

The undifferentiated WJMSCs were labeled with Indocyanine green (MP Biomedicals, Santa Anna, CA) before injecting into the mice wound. Indocyanine green is a negatively charged polymethine dye that forms non-covalent fluorescent complex with proteins. This FDA approved dye with psuedofluorogenic property has been used for clinical applications such as cancer treatments, reconstructive surgeries, coronary and retinal surgeries and angiography [253]. Previous studies demonstrated that a concentration greater than 0.5mg/ml was cytotoxic to the cells [254, 255]; hence a concentration of 0.2 mg/ml was used for these studies, as suggested by Sabapathy et al. [244]. WJMSCs were incubated with 0.2-mg/ml indocyanine green for 1 hour, washed twice with PBS and immediately injected around the mice wounds.

MSC seeding onto scaffolds

For each set of seeding experiments, single-donor (n=1) WJMSCs was used. Briefly 1 x 10^6 MSCs were suspended in 100-µl culture medium and seeded on each DWJM scaffold/dermal graft scaffold (average seeding density was 1.4 X 10^4 - 4 x 10^4/mm^3 DWJM scaffold) in a 24-well non- tissue culture treated plate. 1 ml of medium/well was added to the cells on the scaffolds. After 2 days, the media was changed to osteogenic differentiation media (OD) which is composed of regular media with 100 nM dexamethasone (Sigma-Aldrich, St. Louis, MO), 5mM β-glycerophosphate (Sigma-Aldrich, St. Louis, MO), 10nM 1α 25 di-hydroxy vitamin D3 (Enzo life sciences, Farmingdale, NY), 50 µg/ml ascorbic acid 2-phoshate (Sigma-Aldrich, St. Louis, MO) and the cells were cultured for 4 weeks.

Animal surgeries

All animal experiments were performed according to the University of Kansas Medical Center IACUC protocol # 2014.2192. 4 - 8 week old C57BL/6J mice were purchased from Jackson Laboratories. Mice were anesthetized with intraperitoneal injection (IP) of ketamine (90-150 mg/kg) (Vedco) and xylazine (7.5-16 mg/kg) or Isoflourane gas. Buprenorphine SR (0.15-0.5 mg/kg) (Zoopharm pharmacy) was given intraperitoneally pre-op. The back of the mice was shaved after applying a commercially available hair removal cream (Nair, Ewing, NJ).

Study I

For the first study, 10 C57BL/6J mice were employed and a 1 X 1 cm full thickness excisional wound was made on the back of the mice. The wound was transplanted with 7 mm diameter DWJM seeded with differentiated WJMSCs and covered with a DG (test)(n = 5) or left empty and covered with a DG (control)(n = 5). The graft material was sutured to the adherent skin.

Study II

In the second set of experiments, 50 C57BL/6J mice were used and 1.5 X 1.5 cm full thickness excisional skin wound was carefully made on the back of the mice. The defect was transplanted with grafts (DG/DWJM) of 1.5 X 1.5 cm dimensions, (Test) (n=5) or left covered with a tegaderm dressing (Control) (n = 5). Surgical wound clips were used to attach the graft to skin. Tegaderm transparent dressing (Nexcare, St.Paul, MN) was used to cover the wounds and keep the grafts hydrated. Mastisol liquid adhesive (Ferndale laboratories, MI) firmly attached the tegaderm in place. The mice were divided in 10 groups of n = 5, monitored for 2 weeks and tested as follows.

1. Wound alone
2. Dermal graft alone
3. DWJM alone
4. DWJM+DG alone

Control

5. DWJM with undifferentiated cells
6. DG with undifferentiated cells
7. DWJM+DG with undifferentiated cells

Undifferentiated WJMSCs

8. DWJM with differentiated cells
9. DG with differentiated cells
10. DWJM+DG with differentiated cells

Differentiated WJMSCs

Mice with wound-alone received 1.5 X 1.5 cm full thickness excisional skin wound that was covered with tegaderm transparent dressing and served as our controls. The mice with DG or DWJM or DG + DWJM received 1.5 X 1.5 cm defect, which was transplanted with the respective graft material and closed with wound clips. Experimental groups with undifferentiated cells comprised of $1X10^6$ WJMSCs in 1 ml PBS labeled with indocyanine green and injected at the corners of the defect at the time of surgery. Groups with differentiated WJMSCs had $1 X 10^6$ WJMSCs seeded on the scaffolds and cultured in regular media for 2 days, followed by media with osteogenic components for 4 weeks. These scaffolds were then used for transplantation in mice **(**Figure 30**)**.

IVIS Imaging

Mice with indocyanine green were imaged using IVIS imaging station (PerkinEmler) on day 1, 4, 7 and 14. Mice were anaesthetized with isofluorane gas prior to imaging. The animals

were euthanized after imaging according to the protocol and the newly regenerated skin sample with the adjoining tissue were collected after 2 weeks in 10% phosphate buffered formalin (Newcomen supply) for 24 hours.

Histology and Immunohistochemistry

The skin sections were fixed in 10% formalin embedded in paraffin, sectioned, and stained with H&E. The tissues were also stained with trichrome stain kit – Richard Allan 87020 (Thermo Fisher, Waltham, MA). Staining was performed as per the manufacturer's instructions. Using this stain, the nuclei were stained bluish-black to black; cytoplasm, muscle fibers and keratin stained red, while collagen and mucus stained blue. Slides were reviewed using Olympus BX40 microscope and pictures were acquired using DP72 digital camera.

Immunohistochemistry staining was performed using IntelliPATH FLX™ automated stainer (Biocare Medical, Concord, CA) at room temperature. Briefly, after deparaffinization and rehydration, the tissues were incubated with primary antibodies against CYTOKERATIN 19 (1:50 dilution; Biocare Medical, Concord, CA), HLA class 1 ABC (1:400 dilution, Abcam, Cambridge, MA), Mitochondria Ab-2 (1:100 dilution, Lab Vision, Fremont, CA) for 30 minutes at room temperature. After rinsing, the section was incubated with anti-mouse HRP-labeled polymer (EnVision™ + system, Dako, Carpinteria, CA). Finally, the staining was visualized by DAB (Dako, Carpinteria, CA) and nuclei were counterstained with hematoxylin.

Quantification of hair follicles and sebaceous glands

All tissue sections were observed under the microscope (10X) and the total numbers of newly generated appendages (hair follicles and sebaceous glands, evaluated separately) were counted between the wound edges. These numbers are reported as the total number of appendages in Table 9 (5 mice per group were evaluated.) To estimate the density of new hair

follicles and sebaceous glands, the appendages were counted in a 600 X 800μ area of each histological section. The average density of appendages in each mouse was calculated by examining 3 independent wound areas. For each group 5 mice were evaluated and their average was calculated and reported in Figure 39.

Statistical analysis

All data is expressed as means ± standard error of mean (SEM) and analyzed using, student's t-test, two-way analysis of variance (ANOVA) with Bonferroni post-test. A threshold of $p \leq 0.05$ determined statistical significance. The statistical analyses were performed utilizing Graph Pad Prism software version 6 (Graph Pad Software, Inc.).

Results

Development of acellular structures at the interface of DWJM and DG

In the first experiment, the differentiated WJMSCs on DWJM were transplanted onto a 1 X 1 cm full-thickness excisional skin wound on C57BL/6J mice and wound healing was studied for 7 days. The dermal graft and DWJM with differentiated cells were implanted as shown in the figure **(**Figure 30**)**. The matrix was placed inside the wound and a dermal graft was used to cover the wound and protect DWJM from dehydration. In the control group the wounds were covered with only dermal graft **(**Figure 30**)**. After 7 days, there was no significant change observed in the extent of wound healing between the control and test **(**Figure 31**)**. The wounds healed to similar extent and the dermal graft was detectable in both groups **(**Figure 32A, C), although, the group with DWJM and differentiated cells demonstrated acellular structures at the interface of DWJM and DG **(**Figure 32C, E). These structures looked morphologically similar to the cross-sections of hair follicles leading us to speculate that these may be rudimentary hair like structures. Some anti-human mitochondrial antibody positive cells surrounded these structures as observed by immunohistochemistry suggesting the cells of human origin with ectodermal potential might be producing these hair-like structures (Figure 32F). These structures also resembled the vibrissae follicle-like structures demonstrated by Morioka *et al.* [229], although SMA positive cells were not observed around them. Areas of cell condensations were also observed below these structures, suggesting possible ectodermal differentiation to form hair follicles. Areas of cell condensations were observed near DWJM (Figure 32E), suggesting that DWJM might be acting as a potential mesenchymal surface and dermal graft acting as an epithelial surface, leading to potential epithelial-mesenchymal interactions.

Since there was no difference in wound healing rates between the test and control groups **(**Figure 31**)**, we performed another experiment with an increased size of the wound and assessed wound healing for extended duration of 2 weeks.

Transplanting dermal graft seeded with differentiated WJMSCs enhances wound healing and hair growth

Wound assessment

Full thickness excisional skin wounds measuring 1.5 x 1.5 cm were performed on the back of 50 C57BL/6J mice that were divided into 10 groups (n = 5) and monitored for 14 days as described in Figure 33. After 14 days of healing wound dimensions were measured and the healing rate was calculated as follows –

$$Healing\ rate = 1 - \left(\frac{area\ of\ the\ residual\ wound}{area\ of\ original\ wound}\right) X\ 100\%$$

. The mice with DWJM and differentiated cells showed 97.64% healing and mice with DWJM and undifferentiated cells had 79.04% wound healing, while mice with DWJM only demonstrated 92.39% healing **(**Figure 37**)**. In DWJM with undifferentiated cells, the WJ matrix was found attached to the wound and the matrix prevented the wound contraction in 2 mice. It was interesting to note that the mice with DWJM did not demonstrate any hair regeneration at the wound site. It was observed that mice with DG and differentiated WJMSCs demonstrated the maximum wound healing of 98.71% along with fully regenerated hair at the wound site. Although DG with undifferentiated cells and DG alone groups achieved 94.4 % and 97.86% healing respectively, these groups did not regenerate hair (Figure 35). The mice group that received both DG+DWJM demonstrated 96.73% healing with differentiated cells, 87.75% with undifferentiated cells and only 47.61 % healing without any cells **(**Figure 36**)**. Also, it was noticed that mice transplanted with DWJM alone, showed the least wound contraction while

mice groups with wound alone also exhibited good wound healing without any hair growth (Figure 37, Figure 38, Figure 39).

Understanding the fate of transplanted undifferentiated WJMSCs

WJMSCs were cultured in regular media, labeled with indocyanine green and injected around the wound site before transplantation with the graft material (DG, DWJM, DG+DWJM). After transplantation, mice with labeled WJMSCs were imaged using IVIS imager and it was observed that on day 1, the green fluorescence signal was restricted to the wound surroundings. On day 4, fluorescence was observed in the area of the DG and DWJM indicating possible cellular infiltration into the grafts although no fluorescence was detected on the graft for mice with both DG and DWJM (Figure 40, Figure 41, Figure 42). But it was interesting to note that mice with DG and DWJM also demonstrated some fluorescence in the area of the grafts by day 14, suggesting delayed cellular infiltration into the wound site (Figure 42). The fluorescence intensity also decreased with time suggesting dilution of fluorescence signal due to WJMSCs proliferation or cell death.

Histopathological observations

After 14 days, DG group seeded with differentiated cells appeared to have completely healed with epithelialization and appearance of skin associated appendages. In the group with no intervention to the wound, we noticed incomplete epithelialization indicting that the wounds primarily healed by wound contraction (Figure 46, Figure 50). All the mice revealed blue collagen deposition using trichrome staining.

DWJM

Mice with DWJM demonstrated collagen deposition at the newly generated tissue in the wound bed but no new epidermis or appendage formation was observed (Figure 43). A hyper

proliferative epithelium was noticed at the wound corners. On the contrary, in the group of mice with DWJM and differentiated WJMSCs, the matrix was undetectable with an incomplete and hyper proliferative epithelium at the wound corners. In the mice group with DWJM alone, evidence of epithelialization was noticed at the wound edges only. Also, epithelial cells appeared to form below DWJM, and cellular infiltration was observed at the bottom layers of DWJM in contact with wound bed, while almost no cells were observed towards the exposed area. Immunohistochemistry revealed some cells in the wound bed of mice with DWJM and differentiated WJMSCs were stained positive for CK19 and human mitochondrial protein while, the mice wounds with DWJM and undifferentiated WJMSCs were only positive for CK19 (Figure 47). The mice with DWJM alone did not reveal any cells, which were of human origin or CK19 positive.

Dermal graft

The mice with DG showed 98%±2.8% wound healing grossly, and histologically demonstrated epithelialization (multi-layered epidermis regeneration) at the wound site, although no skin appendages were observed (Figure 44). The group transplanted with DG and undifferentiated cells revealed some epithelialization without any new appendage regeneration. However, the group with DG and differentiated cells achieved almost complete epithelialization with near total growth of hair and the associated appendages such as sebaceous glands. Histologically, there was continuous epithelialization with the associated skin appendages. Immunohistochemistry identified cells which are positive for CK19 and human mitochondrial protein in both the groups with DG + differentiated/undifferentiated WJMSCs, while no such cells were identified in mice with DG alone (Figure 48).

DG+DWJM

In this group, wounds were transplanted with DWJM and covered with dermal graft. DWJM was in direct contact with the wound and acted as a barrier between DG and the wound. When both the grafts were transplanted onto the wound site discontinuous epithelialization was observed. In mice with DG+DWJM and WJMSCs injected around the wound, the epidermal layer from the wound edges appeared to be growing below the DWJM at the ends of the graft, but this was also discontinuous. Finally, in mice with DG+DWJM and differentiated WJMSCs, the grafts were undetectable, while, complete epithelialization with skin appendages were observed (Figure 45). The immunohistochemistry were similar to the observations in the mice groups with DWJM, as mice with DG+DWJM and differentiated WJMSCs demonstrated CK19 and human mitochondrial positive staining, while in the case of DG+DWJM with undifferentiated cells, it only showed some cells positive for human mitochondria. Mice with DG+DWJM without any cells did not reveal any cells of human origin or CK19 positivity (Figure 49).

Quantification of the newly regenerated appendages

Wound areas were carefully evaluated for hair follicle and sebaceous gland formation. Mice groups with wound alone, grafts alone (DG/DWJM/DG+DWJM), and grafts with undifferentiated WJMSCs did not generate any new appendages. Mice with DG and differentiated WJMSCs and DG+DWJM with differentiated WJMSCs generated hair follicles and sebaceous glands at the wound site. However, mice with DWJM and differentiated WJMSCs did not show any appendage development. The total number of appendages were counted at the wound site and reported as in Table 9. The density of the hair appendages was calculated as described above and it was observed that the native skin of the mice had the 25 hair follicles and

9 sebaceous glands on average in a 600 X 800µ area examined under the microscope (10X). For our discussion the density of hair follicles or sebaceous glands will be referred to as the number of hair follicles or sebaceous glands per defined area. Mice group with DG and differentiated WJMSCs demonstrated approximately 17 new hair follicles and 7 sebaceous glands in 600 X 800µ area at the wound site, while the mice group with DG+DWJM and differentiated WJMSCs showed 10 new hair follicles and 4 sebaceous glands in a 600 X 800µ area (Figure 39). These results in combination with the other immunohistochemical observations suggest that the differentiated WJMSCs on DG and DG+DWJM have the potential to regenerate skin with all the associated appendages.

Discussion

Ectoderm is one of the three primary germ layers in the early embryo that differentiates into epidermis, parts of nervous system such as spine, peripheral nerves, and brain and exocrine glands such as mammary, sweat, salivary and lacrimal glands [212]. WJMSCs are multipotent, non-controversial source of stem cells, which can be obtained easily and are self-renewable, proliferative with immunosuppressive properties [128, 256]. WJMSCs are known to differentiate into cells of different lineages such as bone, cartilage and fat, upon exposure to appropriate stimuli [244, 256]. There has been an increasing research interest in the application of WJMSCs in wound healing and skin regeneration applications since it has been well established that MSCs produce a variety of proteins, cytokines and adhesion molecules that regulate aspects of hematopoiesis [243, 247]. MSCs are also known to alter tissue microenvironment and promote tissue repair by secretion of factors that enhance regeneration of injured cells by stimulating proliferation and differentiation and decreasing inflammatory and immune reactions [247, 257, 258]. It has been demonstrated from the proteomic analysis of MSC conditioned medium that MSCs secrete many known mediators of tissue repair including growth factors like vascular endothelial growth factor (VEGF), monocyte chemo-attractant protein-1 (MCP-1) and hepatocyte growth factor (HGF). These growth factors were reported to stimulate fibroblast proliferation, aid during the inflammatory response of wound healing and accelerate angiogenesis [258].

Liu *et al.* demonstrated that human WJMSCs did not express MHC-II and co-stimulatory molecules such as CD 40, CD 80 and CD 86, but moderately express MHC-I. They exhibited immune inhibitors such as HLA-G, IDO, PGE2 thereby demonstrating low immunogenicity and potential to induce to induce immune tolerance microenvironments in hosts [259]. While,

several researchers have demonstrated the role of undifferentiated WJMSCs in wound healing, we found that osteogenic differentiated WJMSCs resulted in superior results in our model. Arno *et al.* showed that WJMSCs promote skin wound healing by promoting paracrine signaling. When adult human skin fibroblasts were treated with WJMSC conditioned media they showed enhanced fibroblast migration, proliferation and promoted wound healing in mice [246]. It has also been demonstrated that paracrine signaling from MSCS promotes angiogenesis, immunomodulation and recruitment and differentiation of endogenous tissue stem/progenitor cells, thus encouraging wound healing [259, 260].

Thus, in this dissertation we explored the role of WJMSCs in ectodermal differentiation applications such as wound repair and skin regeneration. This was studied by two methods – by transplanting undifferentiated WJMSCs at the wound site or by transplanting the scaffolds with differentiated WJMSCs at the wound site. The cellular migration in cutaneous wound healing was studied by labeling the cells with indocyanine green. We demonstrate that WJMSCs can be successfully transplanted at the wound site and the WJMSCs infiltrated the graft (DG/DWJM) by labeling the cells with non-toxic, non-ionizing indocyanine green and studying fluorescence. Thus undifferentiated WJMSCs labeled with indocyanine green, were used to track WJMSCs injected at the wound site. Cellular infiltration was observed in both the graft materials, although the fluorescence intensity was reduced with time suggesting cellular division or cell death.

Herein, we show that WJMSCs could be successfully seeded on the graft materials and cultured *in vitro* and transplanted *in vivo*. In the mice with DWJM, there was hyper proliferative epithelium at the wound corners, which was interrupted. This could have resulted from the thickness of the DWJM (2-3mm) as opposed to the DG (250-500μ) which might have limited the availability of nutrients necessary for cellular proliferate and growth. The thickness of DWJM

might have also resulted in the drying of graft on the exposed surface. On the contrary, mice with dermal graft alone produced a continuous epidermis, although no skin appendages were observed.

The dermal graft seeded with WJMSCs and differentiated *in vitro* for 4 weeks followed by transplantation on mice wounds demonstrated the best healing and complete regeneration of skin with its associate structures such as hair follicles and sebaceous glands. The newly regenerated tissue also demonstrated some cells of human origin along with CK19 positive cells indicating these cells might have migrated from the graft. Although dermal graft alone also showed complete wound healing, hair follicles and sebaceous glands were undetected. Mice with DG and undifferentiated cells exhibited a proliferative epithelium and epithelialization at the wound edges, but failed to produce a continuous epithelium, thus suggesting that the differentiated cells play a key role in the development of skin appendages. Immunohistochemistry also identified some cells positive for human mitochondrial protein suggesting that the undifferentiated WJMSCs might have played some role in wound healing.

Although mice with DWJM and differentiated cells alone did not aid in wound healing, the DG+DWJM mice with differentiated cells demonstrated continuous epithelium. There was complete skin regeneration at the wound edges, but delayed in the center of the wound, signifying it was taking longer for the appendages to form compared to DG with differentiated cells alone. DG+DWJM with or without WJMSCs demonstrated hyper proliferative epithelium at the wound edges, intact DWJM matrix, which interrupted the growth of a continuous epithelium. Thus, DG was necessary to keep the DWJM matrix hydrated and support wound healing process. Undifferentiated WJMSCs on DWJM/DG/DWJM+DG showed a hyper proliferative epithelium at the wound edges. Mice groups with DG, DG+DWJM and

differentiated cells demonstrated almost complete epithelialization and appendage development although; very few cells of human origin were identified at the wound site. Thus, we believe that the differentiated cells played a key role in skin appendage development in this group too, thereby supporting our hypothesis that the WJMSCs differentiated in OD might be having a paracrine effect in promoting epithelial growth while playing a structural role in producing a continuous epidermis to help in wound healing. Further work needs to be performed to assess the role of undifferentiated WJMSCs in our model and optimizing DWJM thickness to aid in better wound healing.

Conclusion

WJMSCs differentiated using DWJM and OD and undifferentiated were successfully transplanted onto the wound site and exhibited differential wound healing results. WJMSCs infiltrated the graft materials and WJMSCs were detected at the wound site for 14 days. Dermal grafts with differentiated WJMSCs demonstrated superior reconstitution of dermis, allowed re-epithelialization of wounds along with the development of the associated skin appendages such as hair follicles. While the use of DWJM with differentiated WJMSCs in the wound bed without dermal graft did not promote complete wound healing, the addition of DG to DWJM with differentiated cells showed reconstitution of dermis and re-epithelialization of wounds, with some degree of appendage development. Thus, the presence of dermal grafts seeded with differentiated WJMSCs was essential for promoting complete wound healing, while the presence of DWJM at the wound bed might have negative effects on appendage development. Hence, further work is needed to optimize the use of DWJM matrix for promoting wound healing.

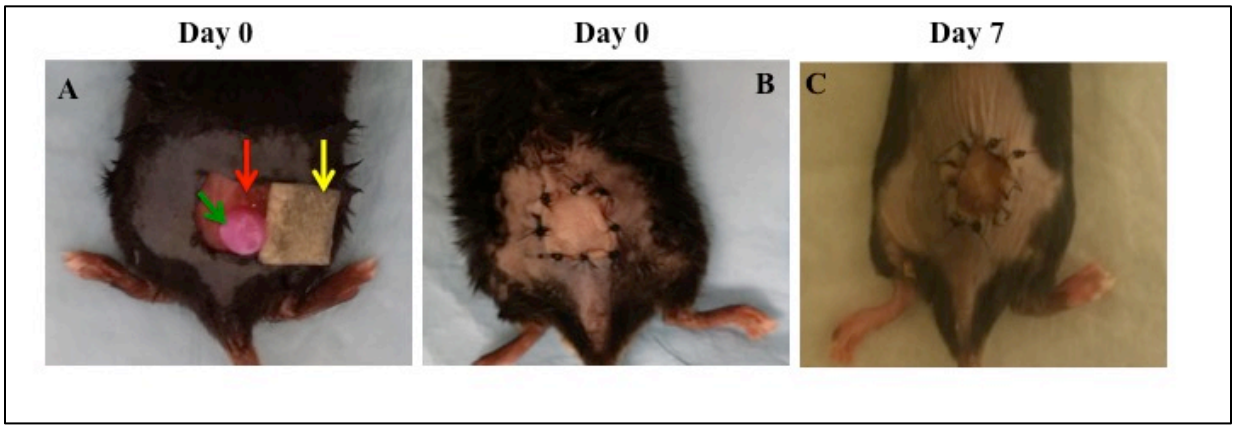

Figure 30 – Wound-healing study experimental design.

Image A shows mice with a 1 X 1 cm full thickness excisional wound. In this image, the green arrow points to DWJM, red arrow denotes the exposed wound area and yellow arrow shows DG during the surgery. Image B shows the wound after DG has been sutured and Image C shows the same wound 7 days post surgery.

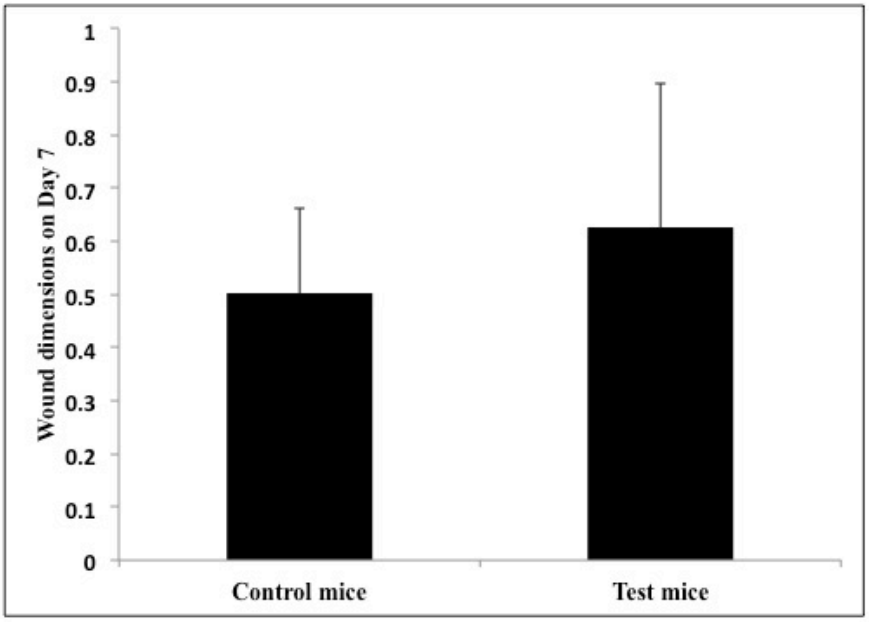

Figure 31 –Wound-healing assessment.

The control mice had DG alone, while the test group had mice with DWJM with differentiated cells and the wound was closed with DG. There was no significant difference noticed between the groups after 7 days. (Y-axis represents the area of wound in cm^2)

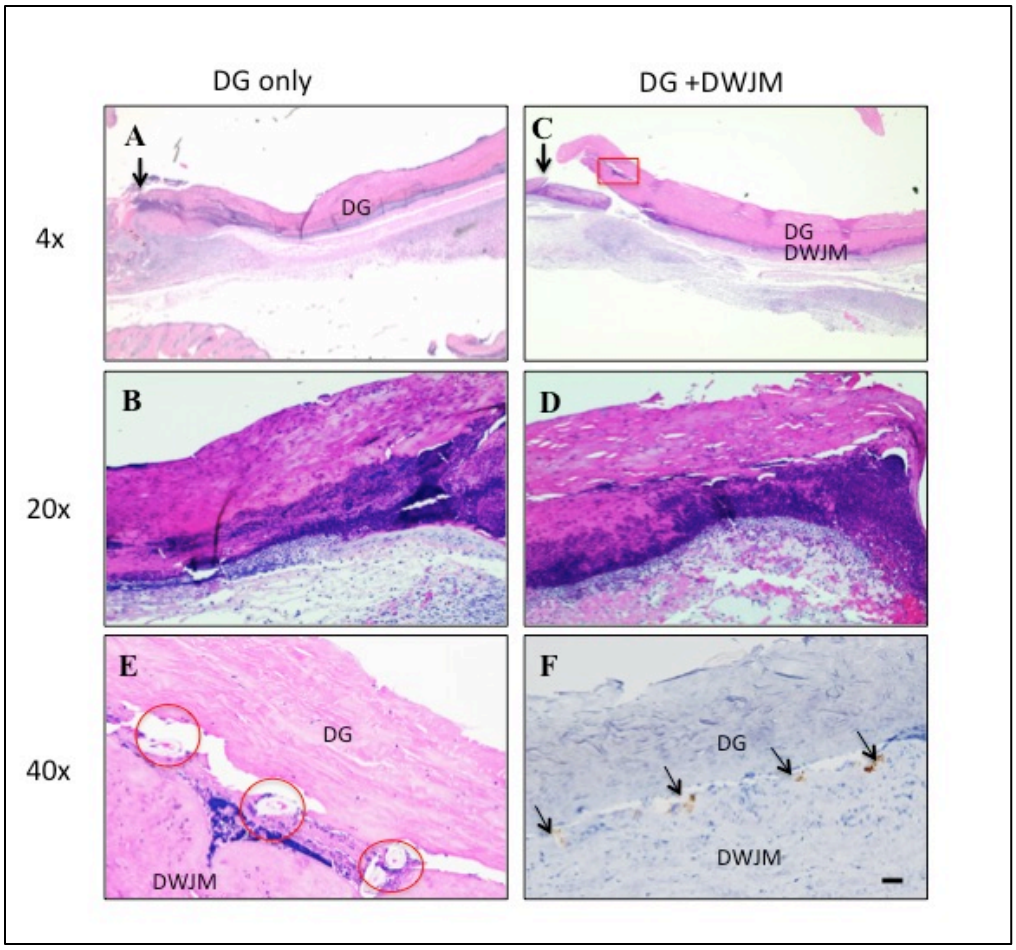

Figure 32 - Histological assessment of the wound bed across various groups.

Image A, B represents the wound with DG alone, while Images C-F show wound with DG and DWJM transplanted with differentiated WJMSCs. The black arrows in Image A and C denote the wound edges. The red box in Image C shows the acellular structures with cellular condensation below them. The red box is imaged at a higher resolution in Image E, and the blue circles on image E show the acellular structures. Image F demonstrates the immunohistochemical staining of the tissues with human mitochondrial protein. The arrows in Image F point to cells positive for human antibody. The scale bars in 4X represent 200µ, 20X is 50µ and 40X is 25µm respectively.

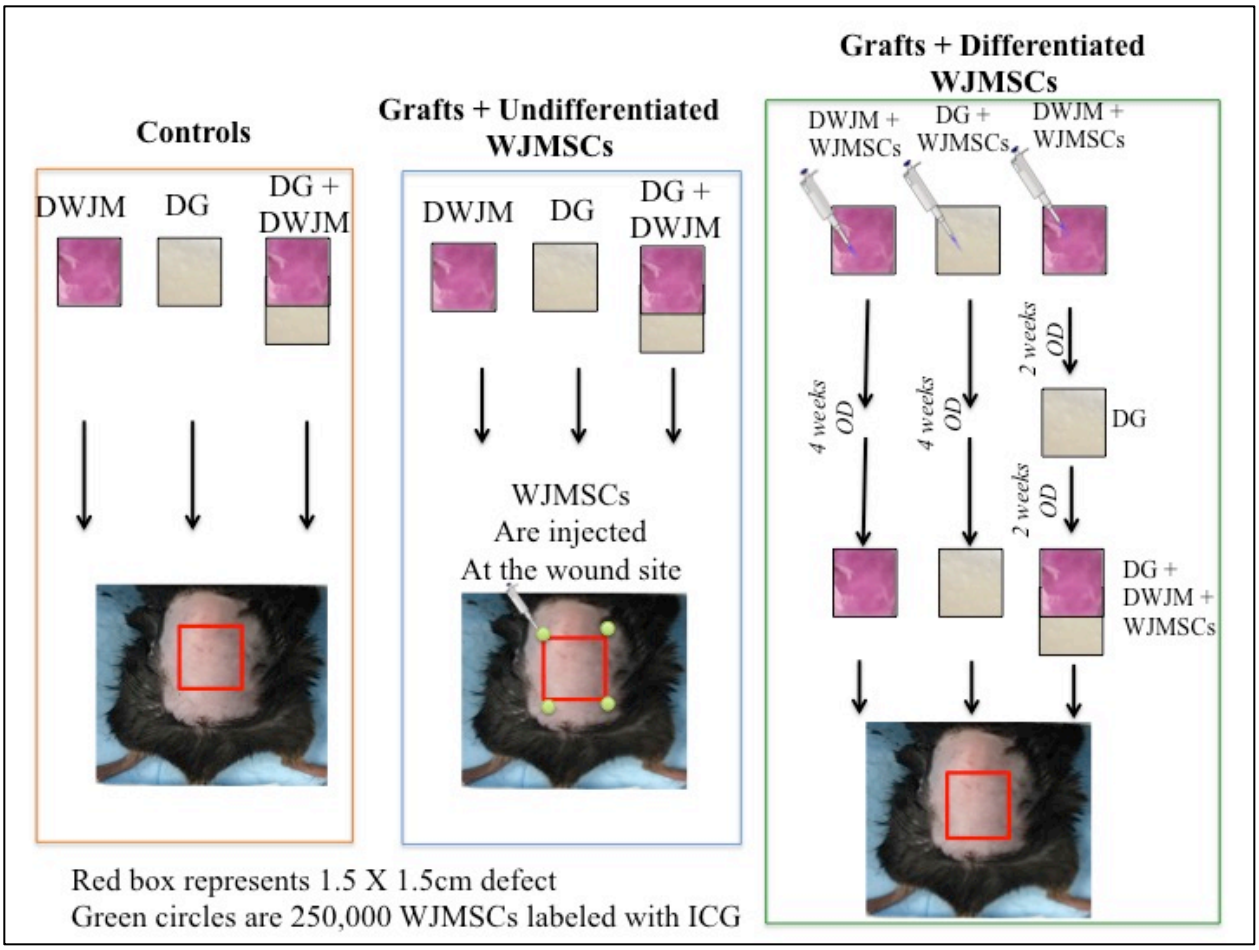

Figure 33 - Schematic representation of the experimental design of wound healing animal study.

The grafts were transplanted at the wound sites in controls. WJMSCs labeled with Indocyanine green (ICG) were injected at the wound site for imaging using IVIS imager. In the last group, WJMSCs were cultured on the grafts *in vitro* for 4 weeks as shown above and later transplanted onto full thickness wounds on mice.

DWJM – Decellularized Wharton's jelly matrix, DG- Alloderm dermal graft, OD – osteogenic differentiation media, WJMSCs – Wharton's jelly mesenchymal stem cells, ICG - Indocyanine green

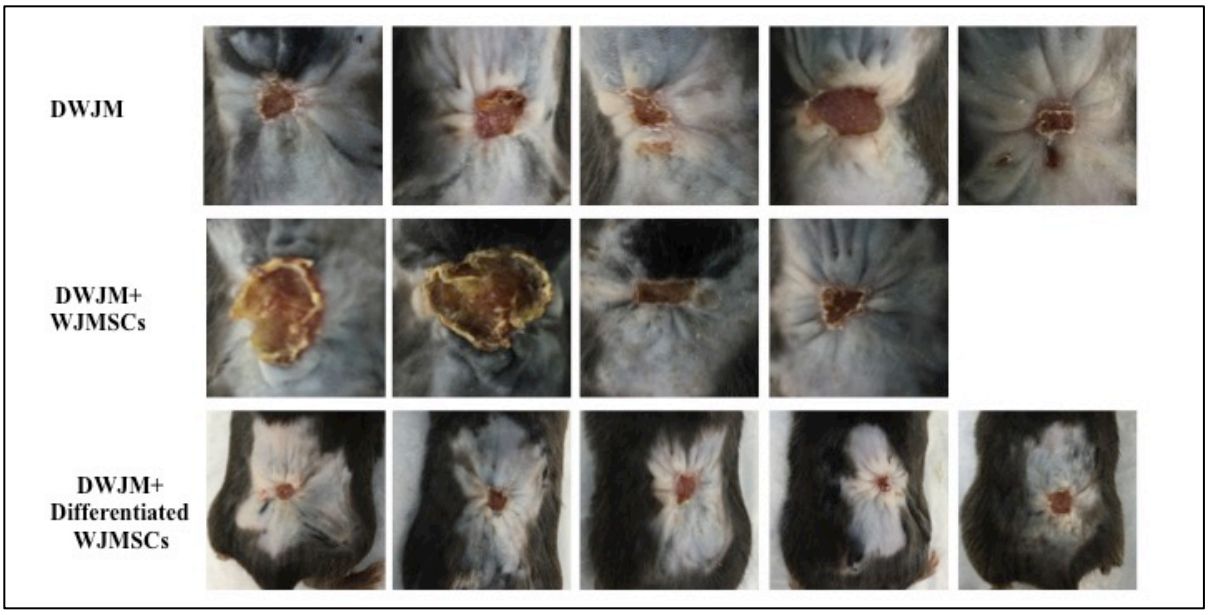

Figure 34 -Wound-healing assessment by gross appearance in mice groups with DWJM

Representative gross morphological images of all the experimental and control groups. They are divided into categories based on the type of graft. The mice wounds almost healed in most of the groups and hair regeneration was observed in groups with DG and differentiated cells and DG+DWJM and differentiated cells.

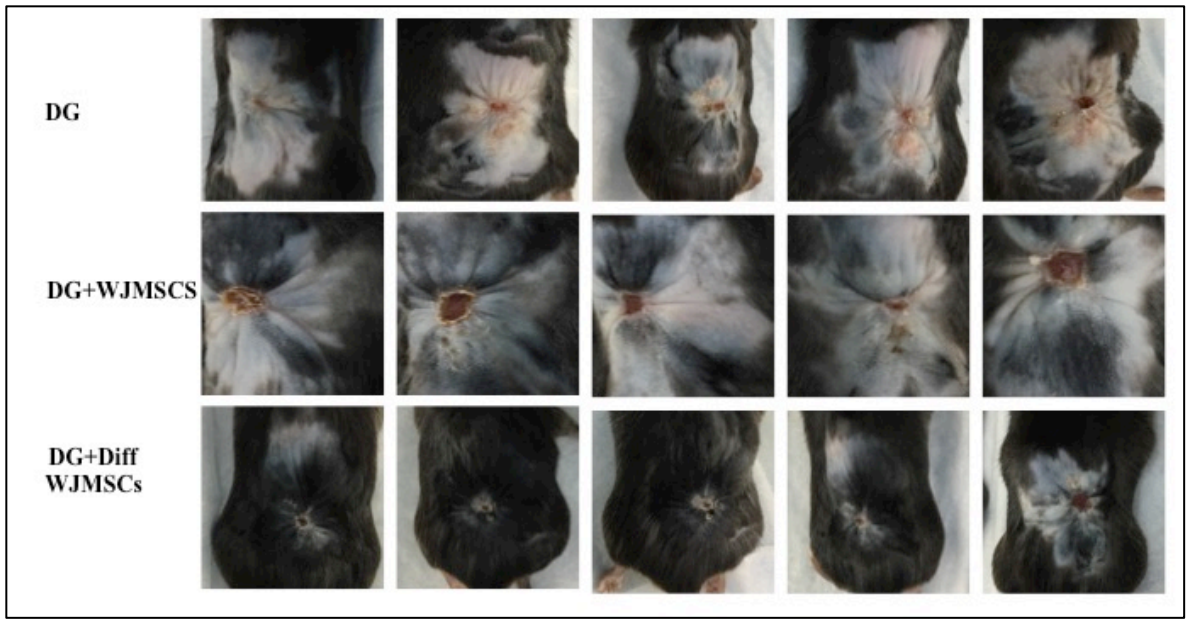

Figure 35 -Wound-healing assessment by gross appearance in mice groups with DG.

Representative gross morphological images of all the experimental and control groups. They are divided into categories based on the type of graft. The mice wounds almost healed in most of the groups and hair regeneration was observed in groups with DG and differentiated cells and DG+DWJM and differentiated cells.

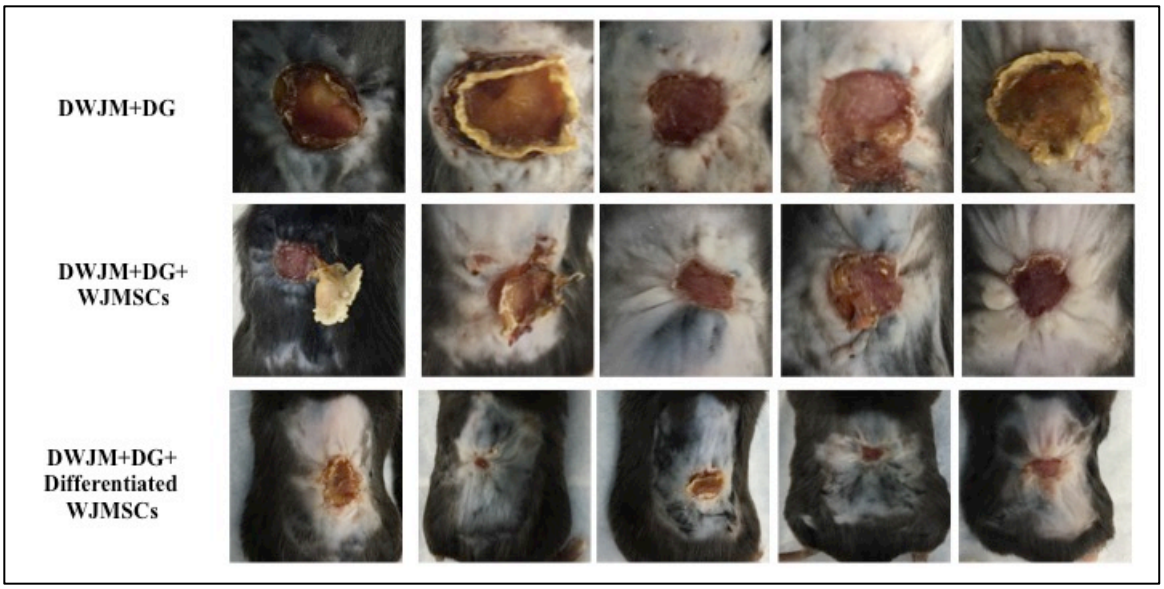

Figure 36 - Wound-healing assessment by gross appearance in mice groups with DG+DWJM.

Representative gross morphological images of all the experimental and control groups. They are divided into categories based on the type of graft. The mice wounds almost healed in most of the groups and hair regeneration was observed in groups with DG and differentiated cells and DG+DWJM and differentiated cells.

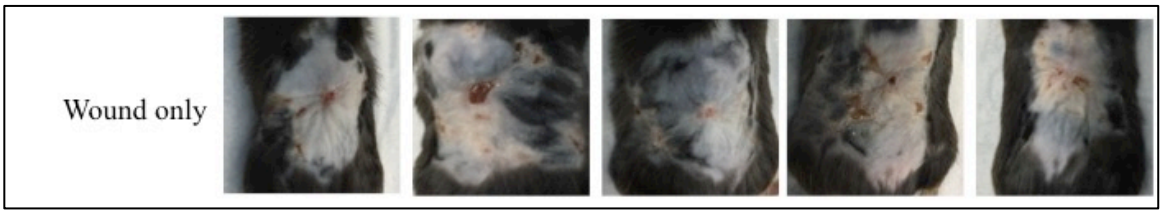

Figure 37 – Wound-healing assessment by gross appearance in mice with wound alone. Representative gross morphological images of all the experimental and control groups. They are divided into categories based on the type of graft. The mice wounds almost healed in most of the groups and hair regeneration was observed in groups with DG and differentiated cells and DG+DWJM and differentiated cells.

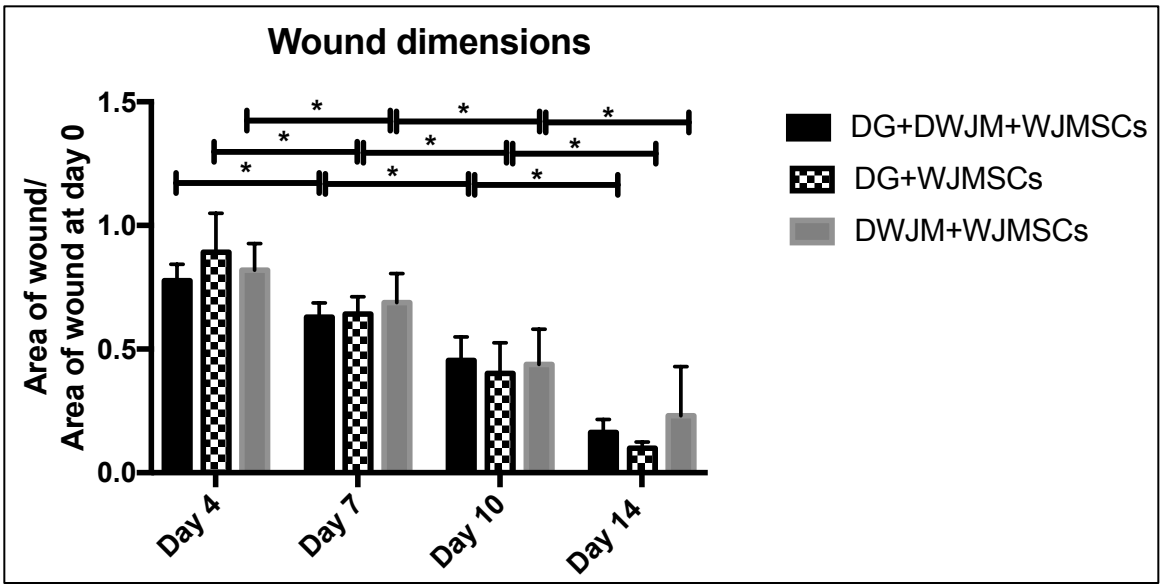

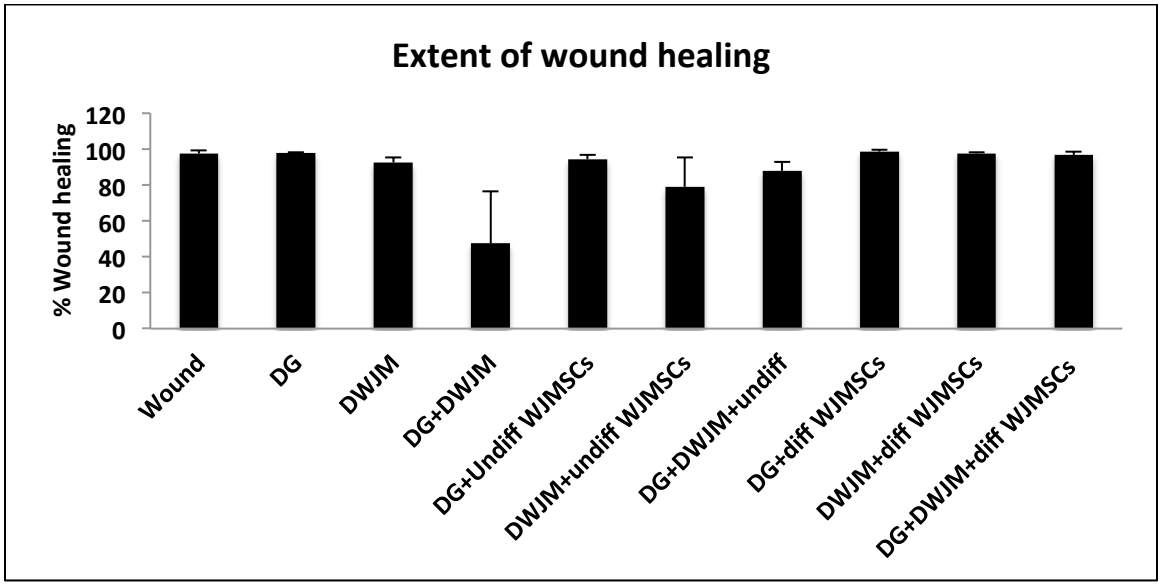

Figure 38 – Qualitative and quantitative assessment of wound healing by microscopy among various experimental conditions.

(* Indicates $p<0.05$)

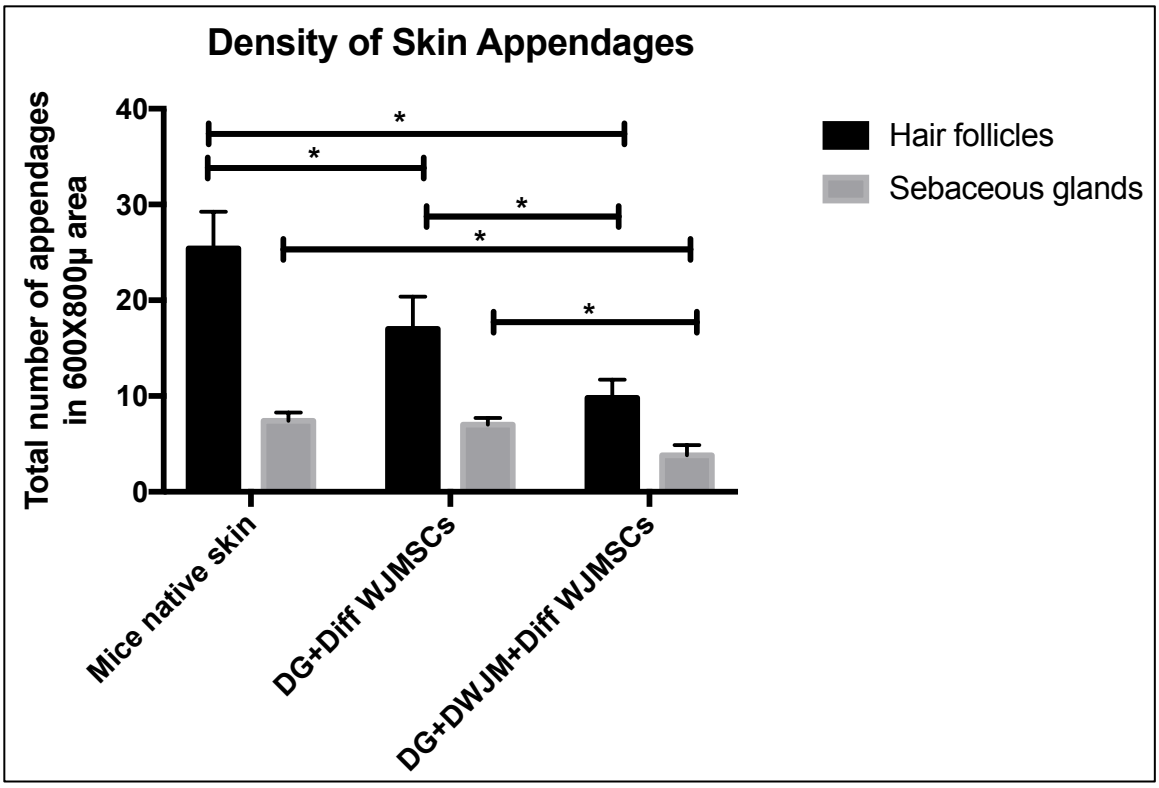

Figure 39 –Quantitative assessment of appendage development by microscopy among various experimental conditions.

The appendages were counted in a 600 X 800µ area of the newly regenerated skin. (* Indicates $p<0.05$). The other groups tested did not show any appendage development, hence are not shown in the graph.

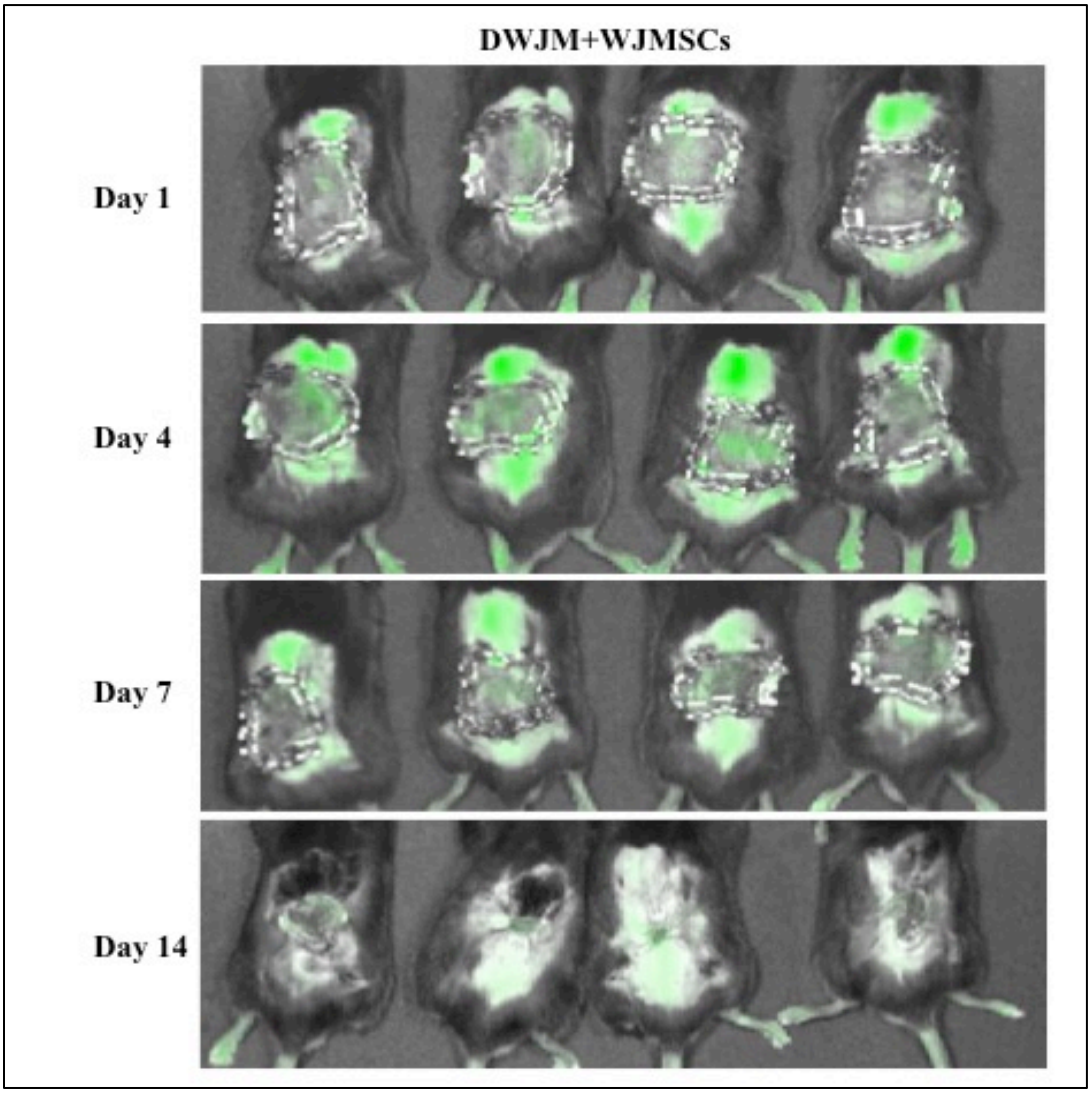

Figure 40 - Tracking the fate of transplanted WJMSCs in mice with DWJM using *in vivo* imaging.

The undifferentiated WJMSCs were labeled with indocyanine green prior to transplantation. Thus, green fluorescence was observed around the wound sites at day 1, while there was fluorescence on the graft material at day 4. The intensity of fluorescence decreased with time suggesting possible cellular proliferation / migration/mortality with time.

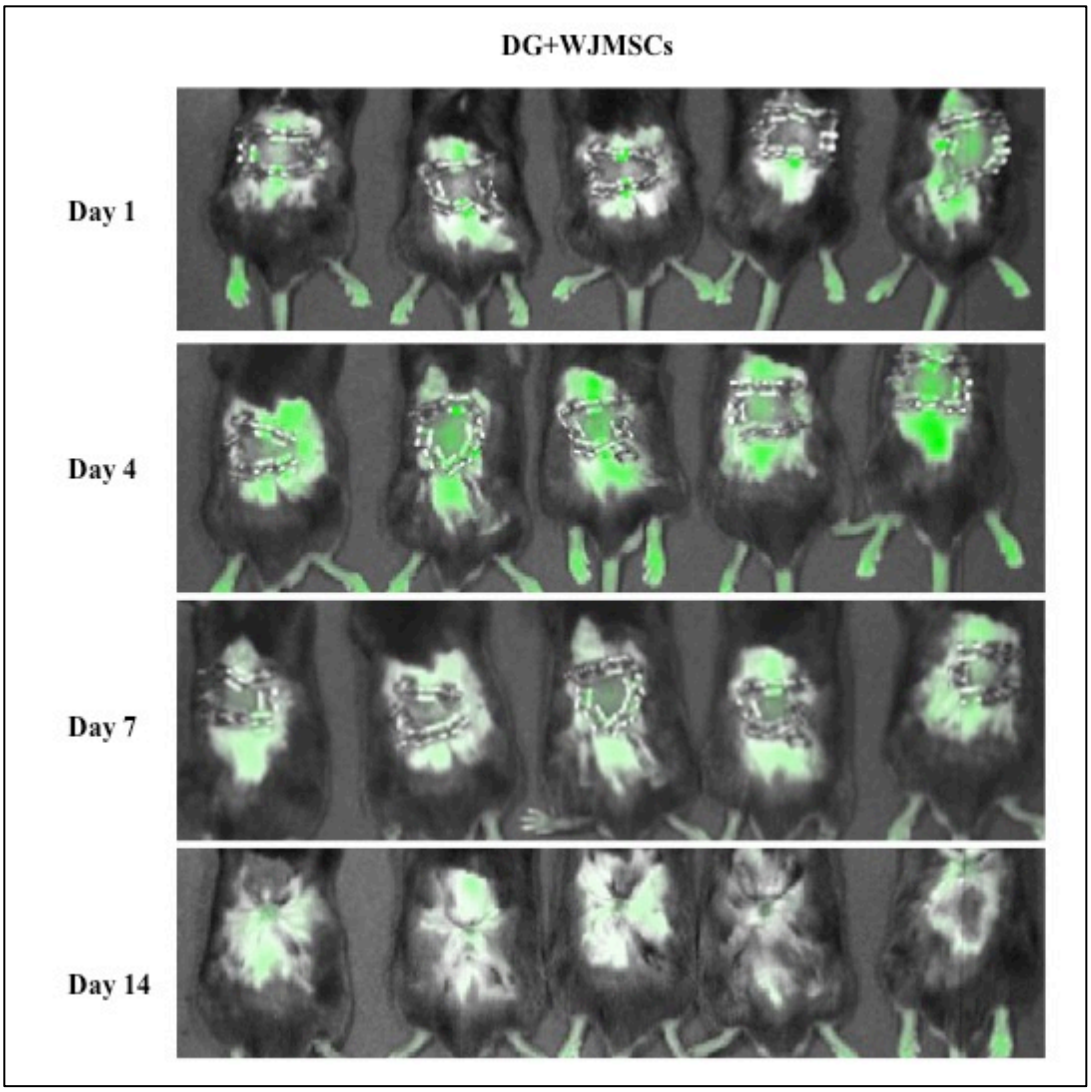

Figure 41 - Tracking the fate of transplanted WJMSCs in mice with DG using *in vivo* imaging.

The undifferentiated WJMSCs were labeled with Indocyanine green prior to transplantation. Thus, green fluorescence was observed around the wound sites at day 1, while there was fluorescence on the graft material at day 4. The intensity of fluorescence decreased with time suggesting possible cellular proliferation / migration/mortality with time.

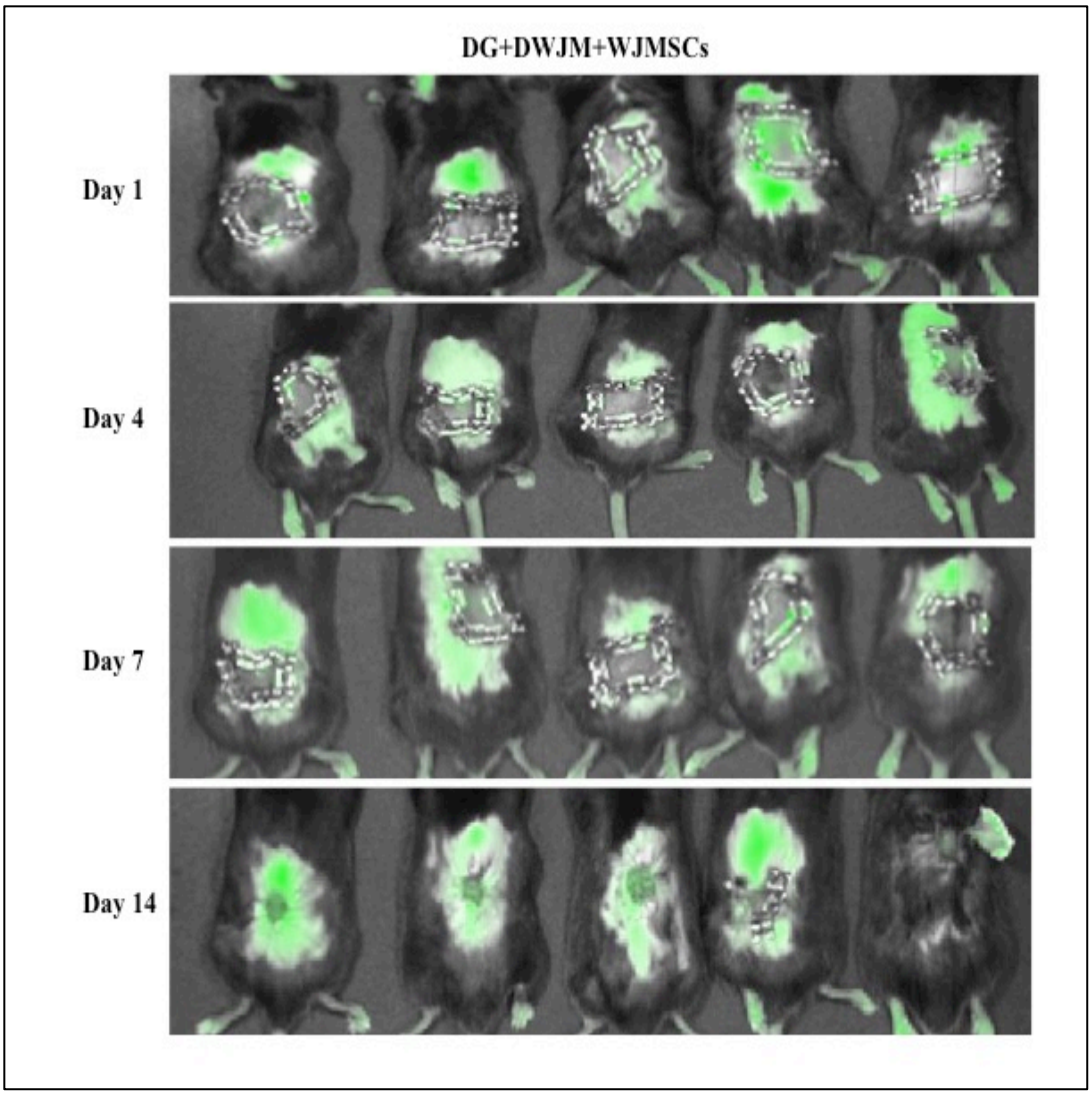

Figure 42 - Tracking the fate of transplanted WJMSCs in mice with DG+ DWJM using *in vivo* imaging.

The undifferentiated WJMSCs were labeled with indocyanine green prior to transplantation. Thus, green fluorescence was observed around the wound sites at day 1, while there was fluorescence on the graft material at day 4. The intensity of fluorescence decreased with time suggesting possible cellular proliferation / migration/mortality with time.

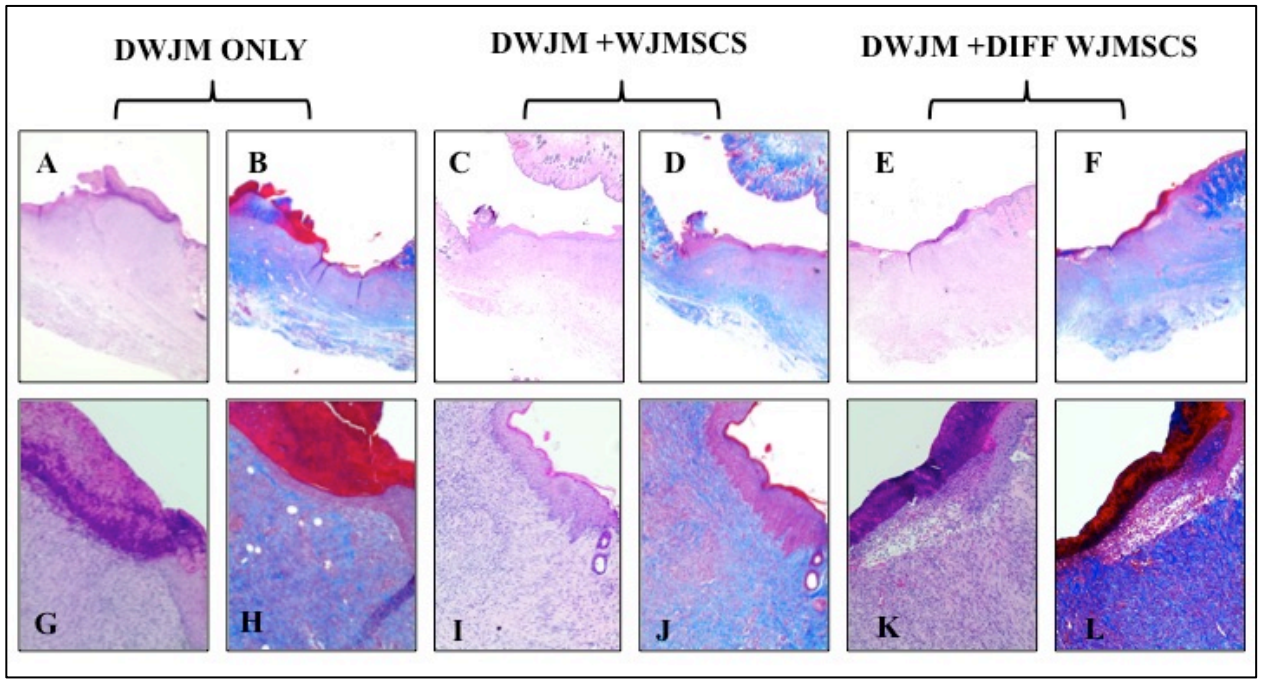

Figure 43 -Histological assessment of wound healing in mice groups with DWJM

Images A, C, E, G, I, K are tissue sections stained in H&E, with A, C and E are 4X magnification, while G, I and K are images at 20 X magnification. Images B, D, F, H, J, L are tissue sections in trichrome staining. Blue color represents collagen deposition, red is for keratin, cytoplasm is in light pink to red, and nuclei are in blue/black. The arrows in the images show the wound edges. The scale bar on 4X images is 200µ and 20X images are 50µ.

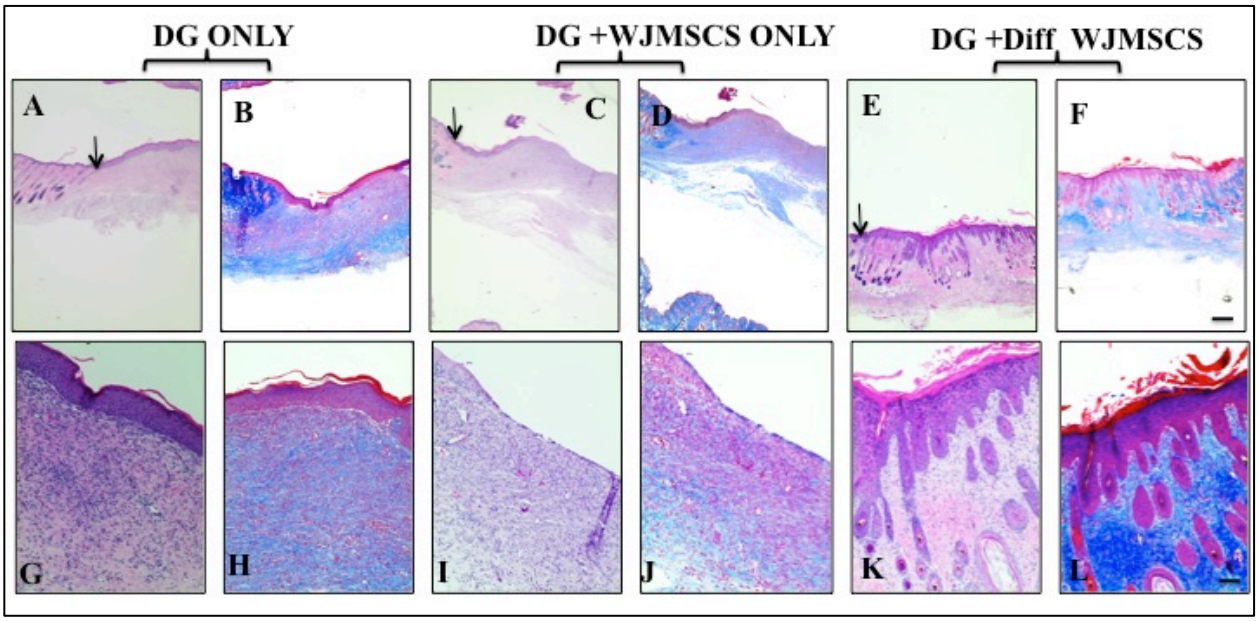

Figure 44 – Histological assessment of wound healing in mice groups with DG

Images A, C, E, G, I, K are tissue sections stained in H&E, with A, C and E are 4X magnification, while G, I and K are images at 20 X magnification. Images B, D, F, H, J, L are tissue sections in trichrome staining. Blue color represents collagen deposition, red is for keratin, cytoplasm is in light pink to red, and nuclei are in blue/black. The arrows in the images show the wound edges. The scale bar on 4X images is 200µ and 20X images are 50µ.

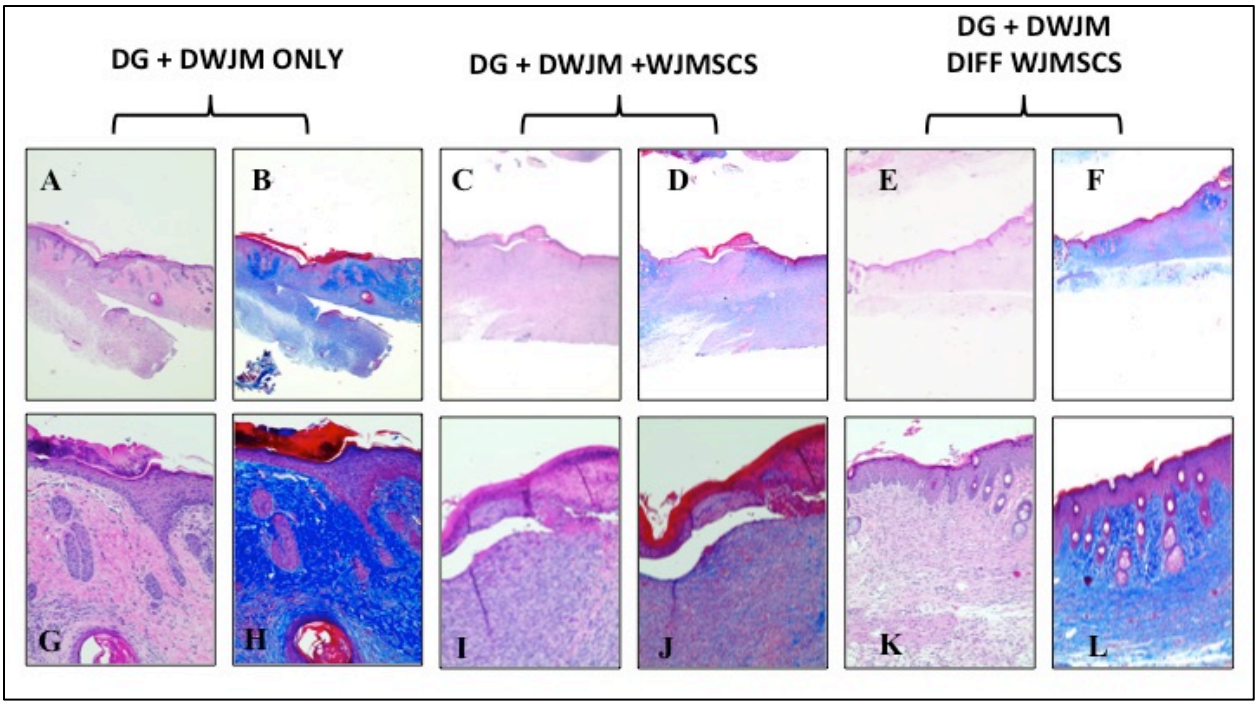

Figure 45 -Histological assessment of wound healing in mice groups with DG+DWJM

Images A, C, E, G, I, K are tissue sections stained in H&E, with A, C and E are 4X magnification, while G, I and K are images at 20 X magnification. Images B, D, F, H, J, L are tissue sections in trichrome staining. Blue color represents collagen deposition, red is for keratin, cytoplasm is in light pink to red, and nuclei are in blue/black. The arrows in the images show the wound edges. The scale bar on 4X images is 200µ and 20X images are 50µ

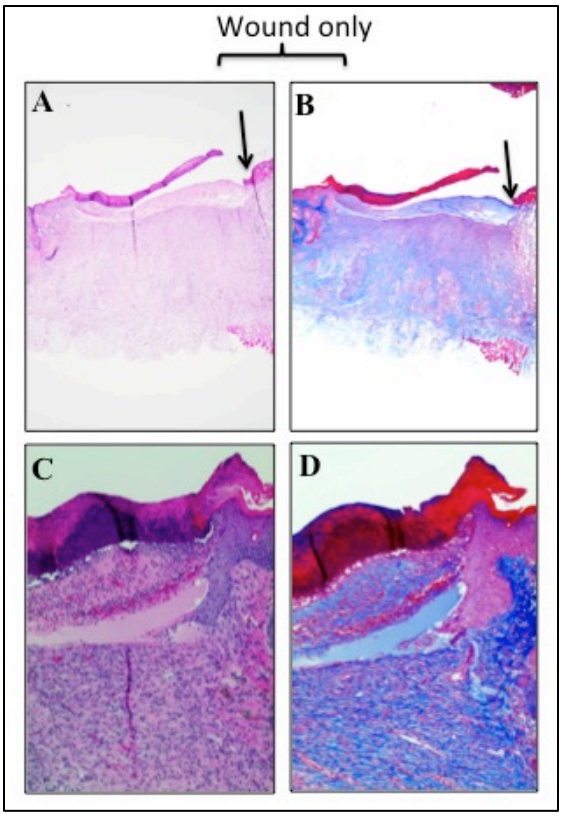

Figure 46 -Histological assessment of wound healing in mice with wound alone

Images A, C, E, G, I, K are tissue sections stained in H&E, with A, C and E are 4X magnification, while G, I and K are images at 20 X magnification. Images B, D, F, H, J, L are tissue sections in trichrome staining. Blue color represents collagen deposition, red is for keratin, cytoplasm is in light pink to red, and nuclei are in blue/black. The arrows in the images show the wound edges. The scale bar on 4X images is 200µ and 20X images are 50µ.

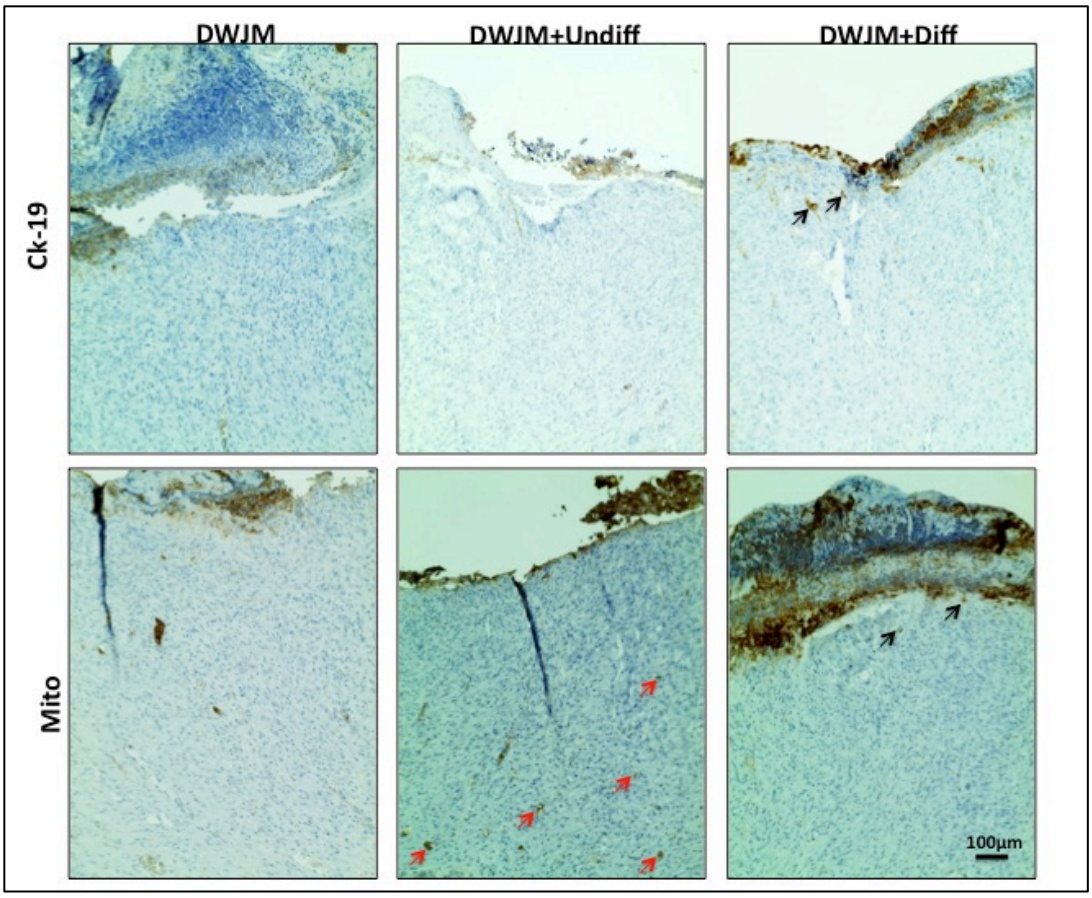

Figure 47 -Wound-healing assessment by immunohistochemistry in mice groups with DWJM

The tissue sections are stained with antibodies against Cytokeratin 19 and human mitochondrial protein. The positive cells are detected in brown. The black arrows represent cells positive CK19 and the red arrows indicate cells positive for mitochondrial staining.

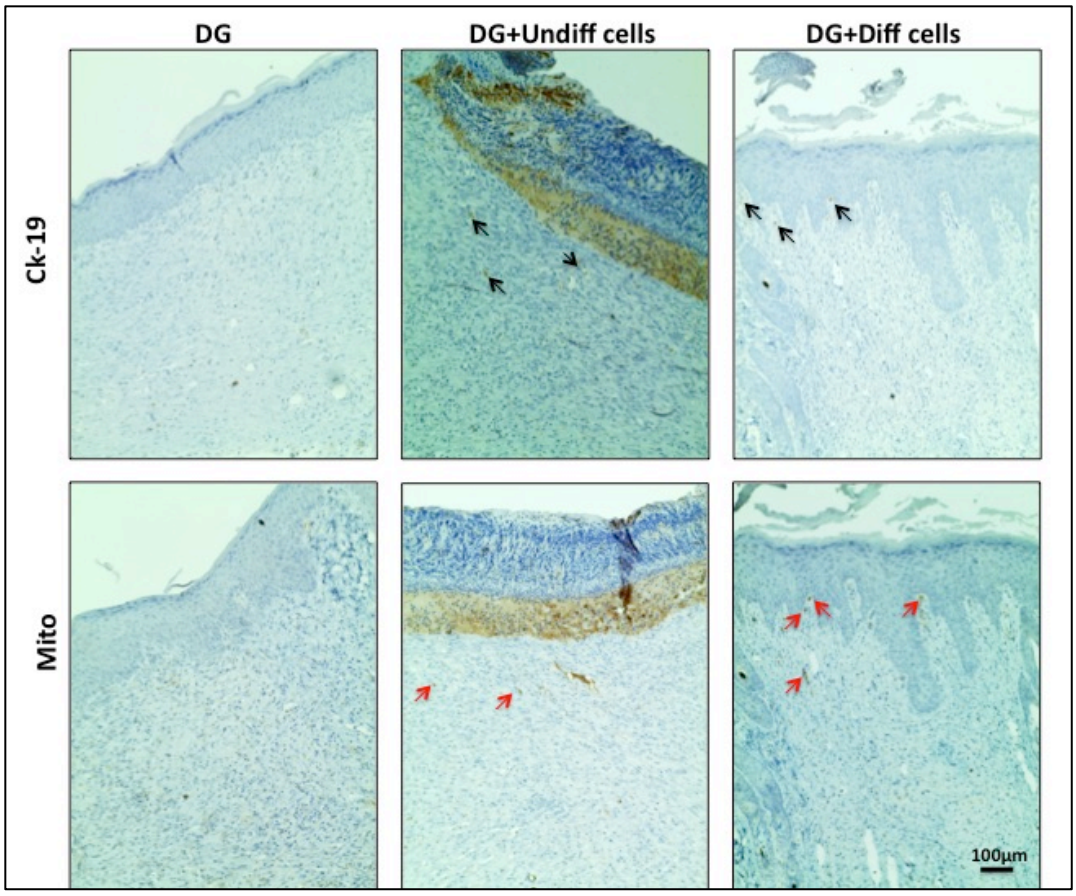

Figure 48 -Wound-healing assessment by immunohistochemistry in mice groups with DG

The tissue sections are stained with antibodies against Cytokeratin 19 and human mitochondrial protein. The positive cells are detected in brown. The black arrows represent cells positive CK19 and the red arrows indicate cells positive for mitochondrial staining.

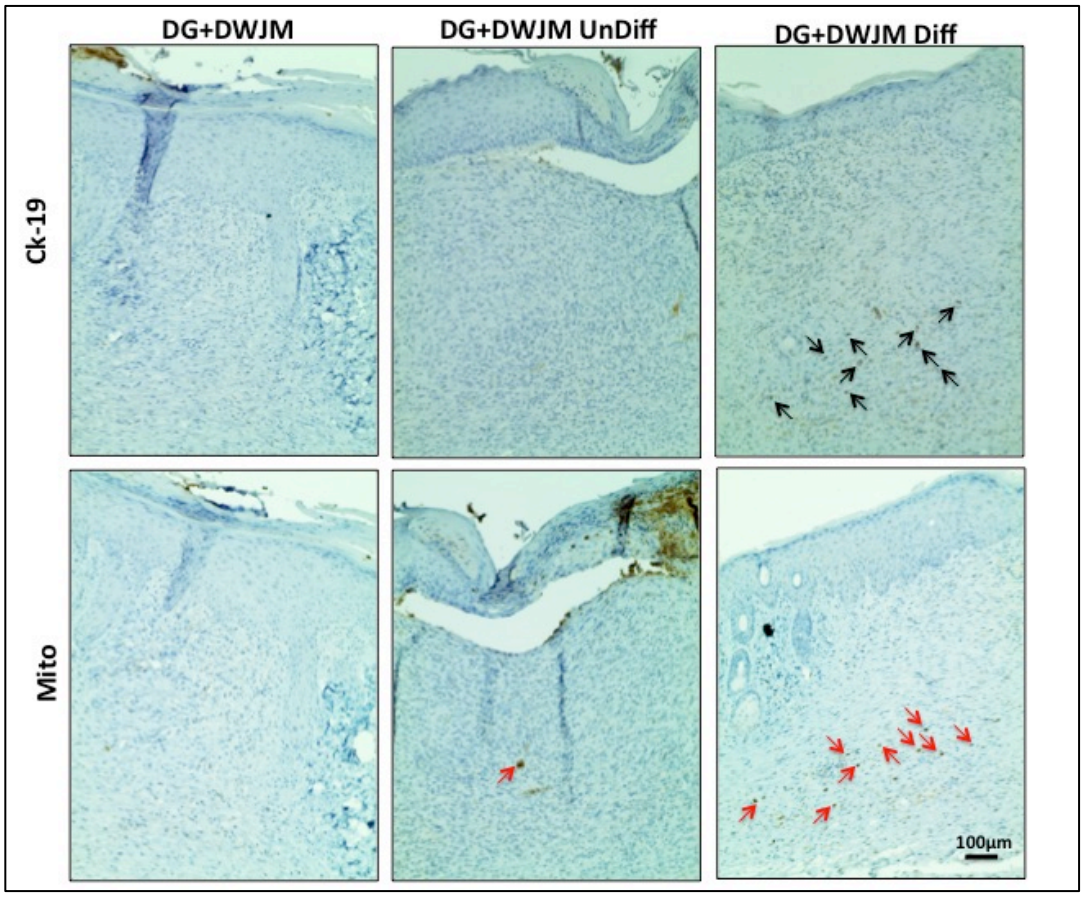

Figure 49 -Wound-healing assessment by immunohistochemistry in mice groups with DG + DWJM

The tissue sections are stained with antibodies against Cytokeratin 19 and human mitochondrial protein. The positive cells are detected in brown. The black arrows represent cells positive CK19 and the red arrows indicate cells positive for mitochondrial staining.

Wound alone

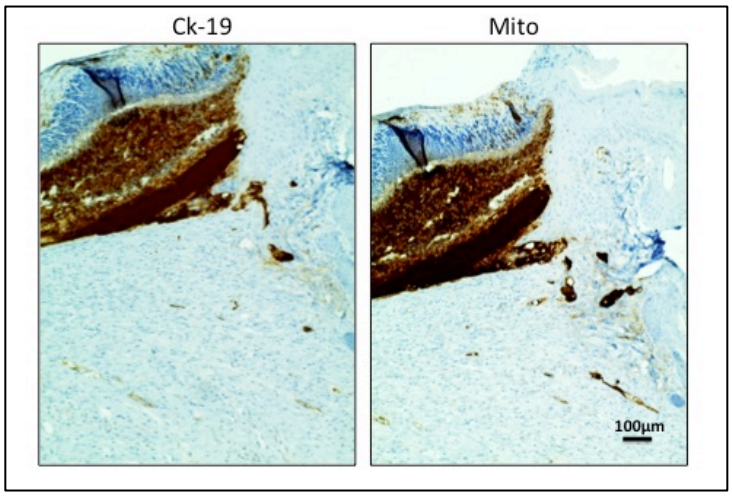

Figure 50 – Wound-healing assessment by immunohistochemistry in mice with wound alone

The tissue sections are stained with antibodies against Cytokeratin 19 and human mitochondrial protein. The positive cells are detected in brown. The black arrows represent cells positive CK19 and the red arrows indicate cells positive for mitochondrial staining.

Table 6 - Experimental design for animal study II.

Mice number	**Group**	**Cell type**	**Indocyanine green**
451-455	DG+Diff WJMSCs	Differentiated WJMSCs	Absent
456-460	DWJM+Diff WJMSCs	Differentiated WJMSCS	Absent
461-465	DG+DWJM+Diff WJMSCs	Differentiated WJMSCs	Absent
486-490	DG+ WJMSCs	WJMSCs	Present
476-480	DWJM+WJMSCs	WJMSCs	Present
496-500	DG+DWJM+ WJMSCs	WJMSCs	Present
491-495	DG+DWJM	No Cells	Absent
466-470	DG	No Cells	Absent
481-485	DWJM	No Cells	Absent
471-475	Wound	No Cells	Absent

Table 7 - Wound healing rates according to various study groups.

	Group	**Mice 1**	**Mice 2**	**Mice 3**	**Mice 4**	**Mice 5**	**Average Wound healing percentage**
1	Wound	98.6	95	98.6	98.6	97.2	97.6
2	DG	98.04	97.6	98.04	97.6	98.04	97.86
3	DWJM	94.40	90.87	94.08	87.91	94.71	92.39
4	DG+DWJM	70.91	16.4	76.04	57.6	17.1	47.61
5	DG+Undiff WJMSCs	95.47	93.2	93.4	98.04	92.1	94.44
6	DWJM+Undiff WJMSCs	67.91	62.35	91.64	94.24	-	79.03
7	DG+DWJM+ WJMSCs	94.56	86.10	90.82	80.94	86.31	87.75
8	DG+Diff WJMSCs	99.13	99.13	99.13	99.13	97	98.71
9	DWJM +Diff WJMSCs	97.72	97.95	96.95	98.72	96.87	97.64
10	DG+ DWJM+ Diff WJMSCs	94.13	98.8	95.90	98.13	96.70	96.73

Table 8 – Wound healing assessment according to various experimental groups.

(The total number of appendages in the newly regenerated skin were counted and represented below.)

	Group	Extent of Wound healing	Epithelialization	Collagen Deposition	Total number of hair follicles	Total number of sebaceous glands	CK19 positive cells	Cells of Human Origin
1	Wound	97.60%	Incomplete	+	-	-	-	-
2	DG	97.86%	Complete	+	-	-	-	-
3	DWJM	92.39%	Incomplete	+	-	-	-	-
4	DG+DWJM	47.61%	Incomplete	+	-	-	-	-
5	DG+Undiff WJMSCs	94.44%	Incomplete	+	-	-	+	+
6	DWJM+Undiff WJMSCs	79.04%	Incomplete	+	-	-	-	+
7	DG+DWJM+ Undiff WJMSCs	87.75%	Incomplete	+	-	-	-	+
8	DG+ Differentiated WJMSCs	98.71%	Complete	+	99±7.7	14±4.8	+	+
9	DWJM+ Differentiated WJMSCs	97.64%	Incomplete	+	-	-	+	+
10	DG+DWJM+ Differentiated WJMSCs	96.73%	Complete	+	10±3.7	5±1.6	+	+

+ Present, - Absent, Complete – complete epithelialization between the wound edges, Incomplete – No complete epithelialization between wound edges
DG- Dermal graft, DWJM – Decellularized Wharton's jelly matrix, WJMSCs- Wharton's jelly mesencymal stem cells.

Table 9 - Density of skin appendages according to the experimental groups.

		Mice 1		Mice 2		Mice 3		Mice 4		Mice 5		Average	
		HF	SG	HF	SG	HF	SG	HF	SG	HF	SG	HF	SG
1	Wound	-	-	-	-	-	-	-	-	-	-	-	-
2	DG	-	-	-	-	-	-	-	-	-	-	-	-
3	DWJM	-	-	-	-	-	-	-	-	-	-	-	-
4	DG+DWJM	-	-	-	-	-	-	-	-	-	-	-	-
5	DG+Undiff WJMSCs	-	-	-	-	-	-	-	-	-	-	-	-
6	DWJM+Undiff WJMSCs	-	-	-	-	-	-	-	-	-	-	-	-
7	DG+DWJM+Undiff WJMSCs	-	-	-	-	-	-	-	-	-	-	-	-
8	DG+ Differentiated WJMSCs	20	7	19	7	12	8	19	6	15	7	17	7
9	DWJM+ Differentiated WJMSCs	-	-	-	-	-	-	-	-	-	-	-	-
10	DG+DWJM+ Differentiated WJMSCs	9	2	10	5	8	4	9	4	13	4	9.8	3.8

HF- Hair follicle, SG – Sebaceous glands, DG- Dermal graft, DWJM – Decellularized Wharton's jelly matrix, WJMSCs- Wharton's jelly mesencymal stem cells.

Chapter 5: Conclusions and Final Perspective

The goal of tissue engineering and regenerative medicine is to restore structure and function to a defect by utilizing the body's natural response. These approaches require a 3D bio-scaffold that can provide the necessary structural support and mimic the natural environment, by promoting interaction and integration with the tissue through appropriate physical and cellular signals. This work is performed on the hypothesis that *decellularized Wharton's jelly matrix can be used as a three dimensional scaffold for culturing MSCs and when provided with the necessary cues, will enable their differentiation to the suitable cell types/tissues.* This dissertation demonstrates a novel way to culture WJMSCs to promote their differentiation towards ectodermal lineage. The success of this work would facilitate wound healing by promoting complete skin regeneration along with its associated structures such as hair follicles and sebaceous glands in full thickness defects from chronic wounds, burns and help in treating conditions like alopecia/baldness which are experienced by a large population.

Human umbilical cords were obtained from consented mothers, after normal vaginal delivery, and used for isolating Wharton's jelly matrix and decellularizing it following a series of chemical and osmotic treatments and extraction of Wharton's jelly mesenchymal stem cells (WJMSCs). Human umbilical cords are typically discarded after delivery and therefore are easy to obtain and their use is non-controversial without ethical constraints associated with other sources of stem cells. Wharton's jelly that is extracted and decellularized is called decellularized Wharton's jelly matrix (DWJM). The obtained DWJM is porous, completely devoid of cells, and comprised of 0.66 μg/mg of sulfated glycosaminoglycans along with hyaluronic acid, collagen and fibronectin. Mass spectrometry also identified a variety of extracellular matrix proteins such as collagen types I, II, VI, XII, fibronectin I, and lumican I in DWJM. This matrix demonstrated

mechanical properties similar to elastomeric scaffolds and when transplanted *in vivo* in a mice cranial defect, attracted neighboring GFP positive cells as early as 24 hours. When implanted at the mice cranial defect, the matrix was degraded after 14 days thus proving to be a biocompatible and biodegradable scaffold.

The extracted WJMSCs were plastic adherent and positive for markers such as CD73, CD90 and CD105 and negative for hematopoietic stem cell markers CD45, CD13, CD14 and CD19. As these MSCs are seeded on DWJM, evidence suggests they attach to and penetrate the porous matrix when cultured *in vitro*. WJMSCs were found at various planes along the thickness of the matrix and were viable and motile. Thus, this novel three-dimensional scaffold provided the necessary mechanical support to promote growth of cells.

The potential of WJMSC's to differentiate into bone, cartilage, and fat has been extensively researched. Recent evidence suggests that these cells can undergo ectodermal differentiation. In this dissertation, WJMSCs were cultured on DWJM in an osteogenic differentiation media to promote their ectodermal differentiation and assist in regeneration of skin and hair for wound healing applications to treat defects resulting from burns or chronic wounds. After 2 weeks of *in vitro* culture, the differentiated cells formed cellular condensations and were positive for cytokeratin-19 (CK19), α-smooth muscle actin (SMA) and collagen creating a microenvironment conducive for epithelial (CK19) and mesenchymal (SMA) interactions. The matrix also produced hair-like structures, which were either coiled underneath and 10 - 30 μ in length or straight, 30 – 100 μ wide and protruding out. The potential of other MSC's such as bone marrow mesenchymal stem cells (BMMSCs) to produce these hair-like structures was also investigated. We observed that BMMSCs did not possess such potential. WJMSCs were also cultured on an acellular dermal graft (Alloderm®) (DG) in osteogenic media

and differentiated to similar CK19, SMA and collagen positive cells but hair like structures were not observed. The components of osteogenic differentiation media were explored and it was noted that while dexamethasone was dispensable, β-glycerophosphate, vitamin C and vitamin D might be playing an important role in ectodermal differentiation.

We also investigated well-known pathways essential for hair follicle formation and showed that the up regulation of *β-catenin* gene and the lower expression of *BMP4* gene were the key players in our model. β-catenin is the early signal responsible for hair follicle formation and is accompanied by higher expression of noggin, a BMP4 inhibitor. In our model we show that, at week 2, WJMSCs cultured on DWJM in osteogenic media exhibited an increase in β-catenin expression followed by an up regulation of *noggin* mRNA, while *BMP4* mRNA expression was undetectable. On the other hand, in BMMSCs, BMP4 mRNA was detected at significant levels, which we believe plays a role in their inability to differentiate to hair-like structures.

Finally, the potential of these *in vitro* generated hair-like structures and associated cells that are CK19 and SMA positive to develop hair follicles and regenerate epithelial tissue was investigated *in vivo* using C57BL/6J mice. A 1.5 X 1.5 cm full thickness excisional skin wound was made on the back of the mice and DG/DWJM/ DG+DWJM grafts were transplanted with osteogenic undifferentiated or differentiated WJMSCs. After 2 weeks, it was observed that the mice with DG and differentiated WJMSCs, and mice with DG+DWJM and differentiated WJMSCs cells, achieved 98.71% and 96.73% wound healing, respectively. These groups completely regenerated the epidermis along with the associated appendages such as hair follicles and sebaceous glands although, the quantity of these appendages was observed to be higher in mice with DG and differentiated cells alone. Hair regeneration was mice own hair, suggesting that observed effect was probably related to paracrine effects produced by the transplanted

differentiated WJMSCs. This observation should be further investigated to optimize wound healing.

Interestingly, the presence of DWJM in the wound bed prevented wound healing by contraction in the presence of undifferentiated cells or in the case when DWJM was used alone. Cells were noted to have migrated into the lower region of DWJM that was in contact with wound; however, there was no cellular infiltration towards the outer exposed surface. This could possibly be due to the thickness of graft that might have limited the essential nutrient supply to the uppermost layers to support cellular infiltration and proliferation.

One of the inadequacies of this work has been difficult to obtain uniform DWJM scaffolds. Wharton's jelly is a mucoid, porous, gelatinous connective tissue, which is smooth and slippery and very difficult to manually alter the height, width or thickness of the matrix. Although care was taken to keep the scaffolds at 7mm diameter and 2mm thickness, attaining uniform scaffolds was challenging. Also, it was also difficult to fully utilize the complete Wharton's jelly matrix as a large portion was wasted due to the circular shape and also the non-uniformity in the various cords used in these studies. Procuring larger scaffolds such as 1.5 X 1.5 cm was difficult, thus several smaller pieces were sewn together using sutures. The variations in the animal studies between the groups can be attributed to the differences in compositions of different umbilical cords from individuals of diverse age groups and ethnicity. Therefore, 3D bio printing is an option for future engineers or scientists working on this model. If Wharton's jelly matrix can be lyophilized into powder form, it might be possible to 3D print the scaffolds in required shapes and dimensions. Multiple cords can be processed to obtain enough material with the desired quantity that can be combined together to eliminate the sample-to-sample variation. Scaffolds can be tailored to enhance the applications and the best possible scaffold for wound

regeneration and appendage formation can be constructed and tested. This also gives an opportunity to customize the scaffold according to patient needs since all injuries present a unique challenge.

Another area for future research is to isolate CK19 and SMA positive cells and transplant them directly at the wound site to evaluate healing. It would be remarkable to see if these cells have the potential to survive at the wound site and promote wound healing independent of DWJM or dermal graft.

Finally, this thesis presents a novel way to promote ectodermal differentiation of WJMSCs to CK19 and SMA positive cells, aiding in wound healing and skin regeneration. Perhaps, most importantly, the work presented here has shown a way to bridge the gap between the bench and bedside, by examining the transplantation of *in vitro* generated cells in mice. This study can be extended further and the potential of these cells in wound healing and hair follicle formation can be explored in other animal models. If proven successful, our model can be translated for direct application in victims with burns or chronic ulcers, needing full thickness grafts.

References

[1] Kanitakis J. Anatomy, histology and immunohistochemistry of normal human skin. Eur J Dermatol. 2002;12:390-9; quiz 400-1.

[2] Prevention FdaifsCfDCa. Web: U.S.Separtment of Health and Human services, 11 Oct 2011; 20 Dec 2014.

[3] "Burn incidence and treatement in the United states :2012 fact sheet." American Burn Association. Web: American Burn Association; 20 Dec 2014.

[4] Yano S, Komine M, Fujimoto M, Okochi H, Tamaki K. Mechanical stretching in vitro regulates signal transduction pathways and cellular proliferation in human epidermal keratinocytes. J Invest Dermatol. 2004;122:783-90.

[5] Kobayashi H, Aiba S, Yoshino Y, Tagami H. Acute cutaneous barrier disruption activates epidermal p44/42 and p38 mitogen-activated protein kinases in human and hairless guinea pig skin. Exp Dermatol. 2003;12:734-46.

[6] Bahou WF, Gnatenko DV. Platelet transcriptome: the application of microarray analysis to platelets. Semin Thromb Hemost. 2004;30:473-84.

[7] Noli C, Miolo A. The role of mast cells in the early stages of wound healing. Int Wound J. 2010;7:540.

[8] Cumberbatch M, Dearman RJ, Griffiths CE, Kimber I. Langerhans cell migration. Clin Exp Dermatol. 2000;25:413-8.

[9] Kim MH, Liu W, Borjesson DL, Curry FR, Miller LS, Cheung AL, et al. Dynamics of neutrophil infiltration during cutaneous wound healing and infection using fluorescence imaging. J Invest Dermatol. 2008;128:1812-20.

[10] Mori R, Shaw TJ, Martin P. Molecular mechanisms linking wound inflammation and fibrosis: knockdown of osteopontin leads to rapid repair and reduced scarring. J Exp Med. 2008;205:43-51.

[11] Tonnesen MG, Feng X, Clark RA. Angiogenesis in wound healing. J Investig Dermatol Symp Proc. 2000;5:40-6.

[12] Fuchs E. Skin stem cells: rising to the surface. J Cell Biol. 2008;180:273-84.

[13] Matoltsy AG, Viziam CB. Further observations on epithelialization of small wounds: an autoradiographic study of incorporation and distribution of 3H-thymidine in the epithelium covering skin wounds. J Invest Dermatol. 1970;55:20-5.

[14] Ilina O, Friedl P. Mechanisms of collective cell migration at a glance. J Cell Sci. 2009;122:3203-8.

[15] Nguyen BP, Gil SG, Carter WG. Deposition of laminin 5 by keratinocytes regulates integrin adhesion and signaling. J Biol Chem. 2000;275:31896-907.

[16] Hinz B. Formation and function of the myofibroblast during tissue repair. J Invest Dermatol. 2007;127:526-37.

[17] Fernandes KJ, McKenzie IA, Mill P, Smith KM, Akhavan M, Barnabe-Heider F, et al. A dermal niche for multipotent adult skin-derived precursor cells. Nature cell biology. 2004;6:1082-93.

[18] Adams RH, Alitalo K. Molecular regulation of angiogenesis and lymphangiogenesis. Nat Rev Mol Cell Biol. 2007;8:464-78.

[19] Haslett C. Resolution of acute inflammation and the role of apoptosis in the tissue fate of granulocytes. Clin Sci (Lond). 1992;83:639-48.

[20] Coussens LM, Werb Z. Inflammation and cancer. Nature. 2002;420:860-7.

[21] Loss M, Wedler V, Kunzi W, Meuli-Simmen C, Meyer VE. Artificial skin, split-thickness autograft and cultured autologous keratinocytes combined to treat a severe burn injury of 93% of TBSA. Burns. 2000;26:644-52.

[22] Bottcher-Haberzeth S, Biedermann T, Reichmann E. Tissue engineering of skin. Burns. 2010;36:450-60.

[23] Lee CH, Singla A, Lee Y. Biomedical applications of collagen. Int J Pharm. 2001;221:1-22.

[24] Chevallay B, Herbage D. Collagen-based biomaterials as 3D scaffold for cell cultures: applications for tissue engineering and gene therapy. Med Biol Eng Comput. 2000;38:211-8.

[25] Eyre DR. Collagen: molecular diversity in the body's protein scaffold. Science. 1980;207:1315-22.

[26] Kemp PD. Tissue engineering and cell-populated collagen matrices. Methods Mol Biol. 2009;522:363-70.

[27] Lynn AK, Yannas IV, Bonfield W. Antigenicity and immunogenicity of collagen. J Biomed Mater Res B Appl Biomater. 2004;71:343-54.

[28] Ito A, Mase A, Takizawa Y, Shinkai M, Honda H, Hata K, et al. Transglutaminase-mediated gelatin matrices incorporating cell adhesion factors as a biomaterial for tissue engineering. J Biosci Bioeng. 2003;95:196-9.

[29] Hinman MB, Jones JA, Lewis RV. Synthetic spider silk: a modular fiber. Trends Biotechnol. 2000;18:374-9.

[30] Altman GH, Diaz F, Jakuba C, Calabro T, Horan RL, Chen J, et al. Silk-based biomaterials. Biomaterials. 2003;24:401-16.

[31] Dal Pra I, Freddi G, Minic J, Chiarini A, Armato U. De novo engineering of reticular connective tissue in vivo by silk fibroin nonwoven materials. Biomaterials. 2005;26:1987-99.

[32] Horan RL, Antle K, Collette AL, Wang Y, Huang J, Moreau JE, et al. In vitro degradation of silk fibroin. Biomaterials. 2005;26:3385-93.

[33] Min BM, Lee G, Kim SH, Nam YS, Lee TS, Park WH. Electrospinning of silk fibroin nanofibers and its effect on the adhesion and spreading of normal human keratinocytes and fibroblasts in vitro. Biomaterials. 2004;25:1289-97.

[34] Aper T, Schmidt A, Duchrow M, Bruch HP. Autologous blood vessels engineered from peripheral blood sample. Eur J Vasc Endovasc Surg. 2007;33:33-9.

[35] Le Nihouannen D, Guehennec LL, Rouillon T, Pilet P, Bilban M, Layrolle P, et al. Micro-architecture of calcium phosphate granules and fibrin glue composites for bone tissue engineering. Biomaterials. 2006;27:2716-22.

[36] Neidert MR, Lee ES, Oegema TR, Tranquillo RT. Enhanced fibrin remodeling in vitro with TGF-beta1, insulin and plasmin for improved tissue-equivalents. Biomaterials. 2002;23:3717-31.

[37] Lu Q, Ganesan K, Simionescu DT, Vyavahare NR. Novel porous aortic elastin and collagen scaffolds for tissue engineering. Biomaterials. 2004;25:5227-37.

[38] Katsuyoshi Nishinari RT. Interaction in polysaccharide solutions and gels. Current opinion in colloid and interface science. 2003;8:396-400.

[39] Cascone MG, Barbani N, Cristallini C, Giusti P, Ciardelli G, Lazzeri L. Bioartificial polymeric materials based on polysaccharides. J Biomater Sci Polym Ed. 2001;12:267-81.

[40] Venugopal J, Ramakrishna S. Applications of polymer nanofibers in biomedicine and biotechnology. Appl Biochem Biotechnol. 2005;125:147-58.

[41] Khor E, Lim LY. Implantable applications of chitin and chitosan. Biomaterials. 2003;24:2339-49.

[42] Kweon DK, Song SB, Park YY. Preparation of water-soluble chitosan/heparin complex and its application as wound healing accelerator. Biomaterials. 2003;24:1595-601.

[43] Mayol L, De Stefano D, Campani V, De Falco F, Ferrari E, Cencetti C, et al. Design and characterization of a chitosan physical gel promoting wound healing in mice. J Mater Sci Mater Med. 2014;25:1483-93.

[44] Burkatovskaya M, Tegos GP, Swietlik E, Demidova TN, A PC, Hamblin MR. Use of chitosan bandage to prevent fatal infections developing from highly contaminated wounds in mice. Biomaterials. 2006;27:4157-64.

[45] Dai T, Tanaka M, Huang YY, Hamblin MR. Chitosan preparations for wounds and burns: antimicrobial and wound-healing effects. Expert Rev Anti Infect Ther. 2011;9:857-79.

[46] Dai T, Tegos GP, Burkatovskaya M, Castano AP, Hamblin MR. Chitosan acetate bandage as a topical antimicrobial dressing for infected burns. Antimicrob Agents Chemother. 2009;53:393-400.

[47] Ong SY, Wu J, Moochhala SM, Tan MH, Lu J. Development of a chitosan-based wound dressing with improved hemostatic and antimicrobial properties. Biomaterials. 2008;29:4323-32.

[48] Cakmak A, Cirpanli Y, Bilensoy E, Yorganci K, Calis S, Saribas Z, et al. Antibacterial activity of triclosan chitosan coated graft on hernia graft infection model. Int J Pharm. 2009;381:214-9.

[49] Ueno H, Mori T, Fujinaga T. Topical formulations and wound healing applications of chitosan. Adv Drug Deliv Rev. 2001;52:105-15.

[50] Liao YH, Jones SA, Forbes B, Martin GP, Brown MB. Hyaluronan: pharmaceutical characterization and drug delivery. Drug Deliv. 2005;12:327-42.

[51] Pianigiani E, Andreassi A, Taddeucci P, Alessandrini C, Fimiani M, Andreassi L. A new model for studying differentiation and growth of epidermal cultures on hyaluronan-based carrier. Biomaterials. 1999;20:1689-94.

[52] Mineda K, Feng J, Ishimine H, Takada H, Doi K, Kuno S, et al. Therapeutic Potential of Human Adipose-Derived Stem/Stromal Cell Microspheroids Prepared by Three-Dimensional Culture in Non-Cross-Linked Hyaluronic Acid Gel. Stem Cells Transl Med. 2015;4:1511-22.

[53] Chih-Ta Lee P-HK, Yu-Der Lee. Preparation of poly(vinyl alcohol)-chondroitin sulfate hydrogel as matrices in tissue engineering. Carbohydrate Polymers. 2005;61:348-54.

[54] Reis TC, Castleberry S, Rego AM, Aguiar-Ricardo A, Hammond PT. Three-dimensional multilayered fibrous constructs for wound healing applications. Biomater Sci. 2016;4:319-30.

[55] Wang TW, Wu HC, Huang YC, Sun JS, Lin FH. Biomimetic bilayered gelatin-chondroitin 6 sulfate-hyaluronic acid biopolymer as a scaffold for skin equivalent tissue engineering. Artif Organs. 2006;30:141-9.

[56] Marino D, Reichmann E, Meuli M. Skingineering. Eur J Pediatr Surg. 2014;24:205-13.

[57] Metcalfe AD, Ferguson MW. Tissue engineering of replacement skin: the crossroads of biomaterials, wound healing, embryonic development, stem cells and regeneration. J R Soc Interface. 2007;4:413-37.

[58] Osaka N, Takahashi T, Murakami S, Matsuzawa A, Noguchi T, Fujiwara T, et al. ASK1-dependent recruitment and activation of macrophages induce hair growth in skin wounds. J Cell Biol. 2007;176:903-9.

[59] Hadshiew IM, Foitzik K, Arck PC, Paus R. Burden of hair loss: stress and the underestimated psychosocial impact of telogen effluvium and androgenetic alopecia. J Invest Dermatol. 2004;123:455-7.

[60] de Koning EB, Passchier J, Dekker FW. Psychological problems with hair loss in general practice and the treatment policies of general practitioners. Psychol Rep. 1990;67:775-8.

[61] Cash TF. The psychology of hair loss and its implications for patient care. Clin Dermatol. 2001;19:161-6.

[62] Mahjour SB, Ghaffarpasand F, Wang H. Hair follicle regeneration in skin grafts: current concepts and future perspectives. Tissue Eng Part B Rev. 2012;18:15-23.

[63] Paus R, Foitzik K. In search of the "hair cycle clock": a guided tour. Differentiation. 2004;72:489-511.

[64] Mayer JA, Chuong CM, Widelitz R. Rooster feathering, androgenic alopecia, and hormone-dependent tumor growth: what is in common? Differentiation. 2004;72:474-88.

[65] Zheng Y, Nace A, Chen W, Watkins K, Sergott L, Homan Y, et al. Mature hair follicles generated from dissociated cells: a universal mechanism of folliculoneogenesis. Dev Dyn. 2010;239:2619-26.

[66] Krause K, Foitzik K. Biology of the hair follicle: the basics. Semin Cutan Med Surg. 2006;25:2-10.

[67] Mikkola ML. Genetic basis of skin appendage development. Semin Cell Dev Biol. 2007;18:225-36.

[68] Fuchs E. Scratching the surface of skin development. Nature. 2007;445:834-42.

[69] Schmidt-Ullrich R, Paus R. Molecular principles of hair follicle induction and morphogenesis. Bioessays. 2005;27:247-61.

[70] Rishikaysh P, Dev K, Diaz D, Qureshi WM, Filip S, Mokry J. Signaling involved in hair follicle morphogenesis and development. Int J Mol Sci. 2014;15:1647-70.

[71] Greco V, Chen T, Rendl M, Schober M, Pasolli HA, Stokes N, et al. A two-step mechanism for stem cell activation during hair regeneration. Cell Stem Cell. 2009;4:155-69.

[72] Rendl M, Lewis L, Fuchs E. Molecular dissection of mesenchymal-epithelial interactions in the hair follicle. PLoS Biol. 2005;3:e331.

[73] Jahoda CA, Horne KA, Oliver RF. Induction of hair growth by implantation of cultured dermal papilla cells. Nature. 1984;311:560-2.

[74] Andl T, Reddy ST, Gaddapara T, Millar SE. WNT signals are required for the initiation of hair follicle development. Dev Cell. 2002;2:643-53.

[75] Huelsken J, Vogel R, Erdmann B, Cotsarelis G, Birchmeier W. beta-Catenin controls hair follicle morphogenesis and stem cell differentiation in the skin. Cell. 2001;105:533-45.

[76] Narhi K, Jarvinen E, Birchmeier W, Taketo MM, Mikkola ML, Thesleff I. Sustained epithelial beta-catenin activity induces precocious hair development but disrupts hair follicle down-growth and hair shaft formation. Development. 2008;135:1019-28.

[77] Zhang Y, Andl T, Yang SH, Teta M, Liu F, Seykora JT, et al. Activation of beta-catenin signaling programs embryonic epidermis to hair follicle fate. Development. 2008;135:2161-72.

[78] Pummila M, Fliniaux I, Jaatinen R, James MJ, Laurikkala J, Schneider P, et al. Ectodysplasin has a dual role in ectodermal organogenesis: inhibition of Bmp activity and induction of Shh expression. Development. 2007;134:117-25.

[79] Munemitsu S, Albert I, Rubinfeld B, Polakis P. Deletion of an amino-terminal sequence beta-catenin in vivo and promotes hyperphosporylation of the adenomatous polyposis coli tumor suppressor protein. Molecular and cellular biology. 1996;16:4088-94.

[80] Aberle H, Bauer A, Stappert J, Kispert A, Kemler R. beta-catenin is a target for the ubiquitin-proteasome pathway. EMBO J. 1997;16:3797-804.

[81] Behrens J, von Kries JP, Kuhl M, Bruhn L, Wedlich D, Grosschedl R, et al. Functional interaction of beta-catenin with the transcription factor LEF-1. Nature. 1996;382:638-42.

[82] van de Wetering M, Cavallo R, Dooijes D, van Beest M, van Es J, Loureiro J, et al. Armadillo coactivates transcription driven by the product of the Drosophila segment polarity gene dTCF. Cell. 1997;88:789-99.

[83] Silva-Vargas V, Lo Celso C, Giangreco A, Ofstad T, Prowse DM, Braun KM, et al. Beta-catenin and Hedgehog signal strength can specify number and location of hair follicles in adult epidermis without recruitment of bulge stem cells. Dev Cell. 2005;9:121-31.

[84] Gat U, DasGupta R, Degenstein L, Fuchs E. De Novo hair follicle morphogenesis and hair tumors in mice expressing a truncated beta-catenin in skin. Cell. 1998;95:605-14.

[85] Chiang C, Swan RZ, Grachtchouk M, Bolinger M, Litingtung Y, Robertson EK, et al. Essential role for Sonic hedgehog during hair follicle morphogenesis. Dev Biol. 1999;205:1-9.

[86] St-Jacques B, Dassule HR, Karavanova I, Botchkarev VA, Li J, Danielian PS, et al. Sonic hedgehog signaling is essential for hair development. Curr Biol. 1998;8:1058-68.

[87] Schneider MR, Schmidt-Ullrich R, Paus R. The hair follicle as a dynamic miniorgan. Curr Biol. 2009;19:R132-42.

[88] Botchkarev VA, Kishimoto J. Molecular control of epithelial-mesenchymal interactions during hair follicle cycling. J Investig Dermatol Symp Proc. 2003;8:46-55.

[89] Li AG, Koster MI, Wang XJ. Roles of TGFbeta signaling in epidermal/appendage development. Cytokine Growth Factor Rev. 2003;14:99-111.

[90] Mishina Y. Function of bone morphogenetic protein signaling during mouse development. Front Biosci. 2003;8:d855-69.

[91] Miyazono K, Kusanagi K, Inoue H. Divergence and convergence of TGF-beta/BMP signaling. Journal of cellular physiology. 2001;187:265-76.

[92] Botchkarev VA, Botchkareva NV, Nakamura M, Huber O, Funa K, Lauster R, et al. Noggin is required for induction of the hair follicle growth phase in postnatal skin. FASEB J. 2001;15:2205-14.

[93] Botchkarev VA, Botchkareva NV, Roth W, Nakamura M, Chen LH, Herzog W, et al. Noggin is a mesenchymally derived stimulator of hair-follicle induction. Nature cell biology. 1999;1:158-64.

[94] Kobielak K, Pasolli HA, Alonso L, Polak L, Fuchs E. Defining BMP functions in the hair follicle by conditional ablation of BMP receptor IA. J Cell Biol. 2003;163:609-23.

[95] Oro AE, Higgins K. Hair cycle regulation of Hedgehog signal reception. Dev Biol. 2003;255:238-48.

[96] McMahon AP, Ingham PW, Tabin CJ. Developmental roles and clinical significance of hedgehog signaling. Curr Top Dev Biol. 2003;53:1-114.

[97] Dlugosz A. The Hedgehog and the hair follicle: a growing relationship. J Clin Invest. 1999;104:851-3.

[98] Sato N, Leopold PL, Crystal RG. Induction of the hair growth phase in postnatal mice by localized transient expression of Sonic hedgehog. J Clin Invest. 1999;104:855-64.

[99] Jamora C, Lee P, Kocieniewski P, Azhar M, Hosokawa R, Chai Y, et al. A signaling pathway involving TGF-beta2 and snail in hair follicle morphogenesis. PLoS Biol. 2005;3:e11.

[100] Millar SE. Molecular mechanisms regulating hair follicle development. J Invest Dermatol. 2002;118:216-25.

[101] Rabbani P, Takeo M, Chou W, Myung P, Bosenberg M, Chin L, et al. Coordinated activation of Wnt in epithelial and melanocyte stem cells initiates pigmented hair regeneration. Cell. 2011;145:941-55.

[102] Zhang J, He XC, Tong WG, Johnson T, Wiedemann LM, Mishina Y, et al. Bone morphogenetic protein signaling inhibits hair follicle anagen induction by restricting epithelial stem/progenitor cell activation and expansion. Stem cells. 2006;24:2826-39.

[103] Enshell-Seijffers D, Lindon C, Kashiwagi M, Morgan BA. beta-catenin activity in the dermal papilla regulates morphogenesis and regeneration of hair. Dev Cell. 2010;18:633-42.

[104] Oshimori N, Fuchs E. Paracrine TGF-beta signaling counterbalances BMP-mediated repression in hair follicle stem cell activation. Cell Stem Cell. 2012;10:63-75.

[105] Jahoda C, Oliver RF. The growth of vibrissa dermal papilla cells in vitro. Br J Dermatol. 1981;105:623-7.

[106] Reynolds AJ, Jahoda CA. Cultured dermal papilla cells induce follicle formation and hair growth by transdifferentiation of an adult epidermis. Development. 1992;115:587-93.

[107] Wu JJ, Zhu TY, Lu YG, Liu RQ, Mai Y, Cheng B, et al. Hair follicle reformation induced by dermal papilla cells from human scalp skin. Arch Dermatol Res. 2006;298:183-90.

[108] Havlickova B, Biro T, Mescalchin A, Arenberger P, Paus R. Towards optimization of an organotypic assay system that imitates human hair follicle-like epithelial-mesenchymal interactions. Br J Dermatol. 2004;151:753-65.

[109] Limat A, Breitkreutz D, Hunziker T, Klein CE, Noser F, Fusenig NE, et al. Outer root sheath (ORS) cells organize into epidermoid cyst-like spheroids when cultured inside Matrigel: a light-microscopic and immunohistological comparison between human ORS cells and interfollicular keratinocytes. Cell Tissue Res. 1994;275:169-76.

[110] Qiao J, Turetsky A, Kemp P, Teumer J. Hair morphogenesis in vitro: formation of hair structures suitable for implantation. Regen Med. 2008;3:683-92.

[111] Yoo BY, Shin YH, Yoon HH, Seo YK, Song KY, Park JK. Application of mesenchymal stem cells derived from bone marrow and umbilical cord in human hair multiplication. J Dermatol Sci. 2010;60:74-83.

[112] Cohen J. The transplantation of individual rat and guineapig whisker papillae. J Embryol Exp Morphol. 1961;9:117-27.

[113] Oliver RF. Histological studies of whisker regeneration in the hooded rat. J Embryol Exp Morphol. 1966;16:231-44.

[114] Ehama R, Ishimatsu-Tsuji Y, Iriyama S, Ideta R, Soma T, Yano K, et al. Hair follicle regeneration using grafted rodent and human cells. J Invest Dermatol. 2007;127:2106-15.

[115] Morris RJ, Liu Y, Marles L, Yang Z, Trempus C, Li S, et al. Capturing and profiling adult hair follicle stem cells. Nat Biotechnol. 2004;22:411-7.

[116] Lichti U, Anders J, Yuspa SH. Isolation and short-term culture of primary keratinocytes, hair follicle populations and dermal cells from newborn mice and keratinocytes from adult mice for in vitro analysis and for grafting to immunodeficient mice. Nat Protoc. 2008;3:799-810.

[117] Kishimoto J, Ehama R, Wu L, Jiang S, Jiang N, Burgeson RE. Selective activation of the versican promoter by epithelial- mesenchymal interactions during hair follicle development. Proc Natl Acad Sci U S A. 1999;96:7336-41.

[118] Zheng Y, Du X, Wang W, Boucher M, Parimoo S, Stenn K. Organogenesis from dissociated cells: generation of mature cycling hair follicles from skin-derived cells. J Invest Dermatol. 2005;124:867-76.

[119] Jahoda CA, Reynolds AJ. Dermal-epidermal interactions--follicle-derived cell populations in the study of hair-growth mechanisms. J Invest Dermatol. 1993;101:33S-8S.

[120] Pappa KI, Anagnou NP. Novel sources of fetal stem cells: where do they fit on the developmental continuum? Regen Med. 2009;4:423-33.

[121] De Miguel MP, Arnalich Montiel F, Lopez Iglesias P, Blazquez Martinez A, Nistal M. Epiblast-derived stem cells in embryonic and adult tissues. Int J Dev Biol. 2009;53:1529-40.

[122] Franc S, Garrone R, Bosch A, Franc JM. A routine method for contrasting elastin at the ultrastructural level. J Histochem Cytochem. 1984;32:251-8.

[123] Zhang H, Apfelroth SD, Hu W, Davis EC, Sanguineti C, Bonadio J, et al. Structure and expression of fibrillin-2, a novel microfibrillar component preferentially located in elastic matrices. J Cell Biol. 1994;124:855-63.

[124] Edmondson SR, Thumiger SP, Werther GA, Wraight CJ. Epidermal homeostasis: the role of the growth hormone and insulin-like growth factor systems. Endocr Rev. 2003;24:737-64.

[125] Shalitin N, Schlesinger H, Levy MJ, Kessler E, Kessler-Icekson G. Expression of procollagen C-proteinase enhancer in cultured rat heart fibroblasts: evidence for co-regulation with type I collagen. Journal of cellular biochemistry. 2003;90:397-407.

[126] Yu C, Wang F, Jin C, Huang X, Miller DL, Basilico C, et al. Role of fibroblast growth factor type 1 and 2 in carbon tetrachloride-induced hepatic injury and fibrogenesis. The American journal of pathology. 2003;163:1653-62.

[127] Sobolewski K, Malkowski A, Bankowski E, Jaworski S. Wharton's jelly as a reservoir of peptide growth factors. Placenta. 2005;26:747-52.

[128] Nekanti U, Rao VB, Bahirvani AG, Jan M, Totey S, Ta M. Long-term expansion and pluripotent marker array analysis of Wharton's jelly-derived mesenchymal stem cells. Stem Cells Dev. 2010;19:117-30.

[129] SB. Puranik ANaRG. ISOLATION OF MESENCHYMAL-LIKE CELLS FROM WHARTON'S JELLY OF UMBILICAL CORD INTERNATIONAL JOURNAL OF PHARMACEUTICAL, CHEMICAL AND BIOLOGICAL SCIENCES 2012;2:218-24.

[130] Kim DW, Staples M, Shinozuka K, Pantcheva P, Kang SD, Borlongan CV. Wharton's jelly-derived mesenchymal stem cells: phenotypic characterization and optimizing their therapeutic potential for clinical applications. Int J Mol Sci. 2013;14:11692-712.

[131] Troyer DL, Weiss ML. Wharton's jelly-derived cells are a primitive stromal cell population. Stem cells. 2008;26:591-9.

[132] Karahuseyinoglu S, Cinar O, Kilic E, Kara F, Akay GG, Demiralp DO, et al. Biology of stem cells in human umbilical cord stroma: in situ and in vitro surveys. Stem cells. 2007;25:319-31.

[133] Nanaev AK, Kohnen G, Milovanov AP, Domogatsky SP, Kaufmann P. Stromal differentiation and architecture of the human umbilical cord. Placenta. 1997;18:53-64.

[134] Zhang Y, Hao H, Liu J, Fu X, Han W. Repair and regeneration of skin injury by transplanting microparticles mixed with Wharton's jelly and MSCs from the human umbilical cord. Int J Low Extrem Wounds. 2012;11:264-70.

[135] Lund RD, Wang S, Lu B, Girman S, Holmes T, Sauve Y, et al. Cells isolated from umbilical cord tissue rescue photoreceptors and visual functions in a rodent model of retinal disease. Stem cells. 2007;25:602-11.

[136] Prasanna SJ, Gopalakrishnan D, Shankar SR, Vasandan AB. Pro-inflammatory cytokines, IFNgamma and TNFalpha, influence immune properties of human bone marrow and Wharton jelly mesenchymal stem cells differentially. PLoS One. 2010;5:e9016.

[137] Swamynathan P, Venugopal P, Kannan S, Thej C, Kolkundar U, Bhagwat S, et al. Are serum-free and xeno-free culture conditions ideal for large scale clinical grade expansion of Wharton's jelly derived mesenchymal stem cells? A comparative study. Stem Cell Res Ther. 2014;5:88.

[138] Baksh D, Yao R, Tuan RS. Comparison of proliferative and multilineage differentiation potential of human mesenchymal stem cells derived from umbilical cord and bone marrow. Stem cells. 2007;25:1384-92.

[139] Lu LL, Liu YJ, Yang SG, Zhao QJ, Wang X, Gong W, et al. Isolation and characterization of human umbilical cord mesenchymal stem cells with hematopoiesis-supportive function and other potentials. Haematologica. 2006;91:1017-26.

[140] Fong CY, Chak LL, Biswas A, Tan JH, Gauthaman K, Chan WK, et al. Human Wharton's jelly stem cells have unique transcriptome profiles compared to human embryonic stem cells and other mesenchymal stem cells. Stem Cell Rev. 2011;7:1-16.

[141] Kubota H, Avarbock MR, Brinster RL. Growth factors essential for self-renewal and expansion of mouse spermatogonial stem cells. Proc Natl Acad Sci U S A. 2004;101:16489-94.

[142] Magin AS, Korfer NR, Partenheimer H, Lange C, Zander A, Noll T. Primary cells as feeder cells for coculture expansion of human hematopoietic stem cells from umbilical cord blood--a comparative study. Stem Cells Dev. 2009;18:173-86.

[143] Saito S, Ugai H, Sawai K, Yamamoto Y, Minamihashi A, Kurosaka K, et al. Isolation of embryonic stem-like cells from equine blastocysts and their differentiation in vitro. FEBS letters. 2002;531:389-96.

[144] Zhang Z Y TS, Chong MS,Schantz JT, Fisk NM, Choolani MA, Chan J. Superior Osteogenic capacity for bone tissue engineering of fetal compared with perinatal and adult mesenchymal stem cells. Stem cells. 2009;27:126-37.

[145] Wang L, Ott L, Seshareddy K, Weiss ML, Detamore MS. Musculoskeletal tissue engineering with human umbilical cord mesenchymal stromal cells. Regen Med. 2011;6:95-109.

[146] Anzalone R, Lo Iacono M, Corrao S, Magno F, Loria T, Cappello F, et al. New emerging potentials for human Wharton's jelly mesenchymal stem cells: immunological features and hepatocyte-like differentiative capacity. Stem Cells Dev. 2010;19:423-38.

[147] Semenov OV, Breymann aC. Mesenchymal Stem Cells Derived from Wharton's Jelly and their Potential for Cardio-Vascular Tissue Engineering The Open Tissue Engineering and Regenerative Medicine Journal. 2011;4:64-71.

[148] Pispa J, Thesleff I. Mechanisms of ectodermal organogenesis. Dev Biol. 2003;262:195-205.

[149] Ramos-e-Silva M, Jacques C. Epidermal barrier function and systemic diseases. Clin Dermatol. 2012;30:277-9.

[150] Garzon I, Miyake J, Gonzalez-Andrades M, Carmona R, Carda C, Sanchez-Quevedo Mdel C, et al. Wharton's jelly stem cells: a novel cell source for oral mucosa and skin epithelia regeneration. Stem Cells Transl Med. 2013;2:625-32.

[151] Badiavas EV, Falanga V. Treatment of chronic wounds with bone marrow-derived cells. Arch Dermatol. 2003;139:510-6.

[152] Maxson S, Lopez EA, Yoo D, Danilkovitch-Miagkova A, Leroux MA. Concise review: role of mesenchymal stem cells in wound repair. Stem Cells Transl Med. 2012;1:142-9.

[153] Shaw TJ, Martin P. Wound repair at a glance. J Cell Sci. 2009;122:3209-13.

[154] Brower J, Blumberg S, Carroll E, Pastar I, Brem H, Chen W. Mesenchymal stem cell therapy and delivery systems in nonhealing wounds. Adv Skin Wound Care. 2011;24:524-32; quiz 33-4.

[155] Arno Al A-NS, Blit PH, Al-Shehad M, Belp C, Herer E, Tien CH, Jeschke MG. Human Wharton's jelly mesenchymal stem cels promote skin wound healing through paracrine signaling. Stem Cell Res Ther. 2014;5:28.

[156] Tam K, Cheyyatraviendran S, Venugopal J, Biswas A, Choolani M, Ramakrishna S, et al. A Nanoscaffold Impregnated With Human Wharton's Jelly Stem Cells or Its Secretions Improves Healing of Wounds. Journal of cellular biochemistry. 2014;115:794-803.

[157] Yang CC, Cotsarelis G. Review of hair follicle dermal cells. J Dermatol Sci. 2010;57:2-11.

[158] Bueno EM, Glowacki J. Cell-free and cell-based approaches for bone regeneration. Nature reviews Rheumatology. 2009;5:685-97.

[159] Li Z, Kawashita M. Current progress in inorganic artificial biomaterials. Journal of artificial organs : the official journal of the Japanese Society for Artificial Organs. 2011;14:163-70.

[160] Foschi F, Conserva E, Pera P, Canciani B, Cancedda R, Mastrogiacomo M. Graft Materials and Bone Marrow Stromal Cells in Bone Tissue Engineering. J Biomater Appl. 2011.

[161] Gloria A, De Santis R, Ambrosio L. Polymer-based composite scaffolds for tissue engineering. Journal of applied biomaterials & biomechanics : JABB. 2010;8:57-67.

[162] Baino F, Vitale-Brovarone C. Three-dimensional glass-derived scaffolds for bone tissue engineering: current trends and forecasts for the future. Journal of biomedical materials research Part A. 2011;97:514-35.

[163] Munarin F, Guerreiro SG, Grellier MA, Tanzi MC, Barbosa MA, Petrini P, et al. Pectin-based injectable biomaterials for bone tissue engineering. Biomacromolecules. 2011;12:568-77.

[164] Clarke SA, Walsh P, Maggs CA, Buchanan F. Designs from the deep: marine organisms for bone tissue engineering. Biotechnology advances. 2011;29:610-7.

[165] O'Brien FJ. Biomaterials & scaffolds for tissue engineering. Materials Today. 2011;14:88-95.

[166] Franc S, Rousseau JC, Garrone R, van der Rest M, Moradi-Ameli M. Microfibrillar composition of umbilical cord matrix: characterization of fibrillin, collagen VI and intact collagen V. Placenta. 1998;19:95-104.

[167] Bastow ER, Byers S, Golub SB, Clarkin CE, Pitsillides AA, Fosang AJ. Hyaluronan synthesis and degradation in cartilage and bone. Cellular and molecular life sciences : CMLS. 2008;65:395-413.

[168] Taipale J, Keski-Oja J. Growth factors in the extracellular matrix. The FASEB journal : official publication of the Federation of American Societies for Experimental Biology. 1997;11:51-9.

[169] Aljitawi O, Xiao Y, Zhang D, Stehno-Bittel L, Garimella R, Hopkins RA, et al. Generating CK 19 Positive Cells with Hair-like structures from Wharton's Jelly Mesenchymal Stromal Cells. Stem Cells Dev. 2012.

[170] Hopkins RA. Cardiac reconstructions with allograft tissues. 1 ed: Springer-Verlag New York; 2005.

[171] Wang L, Singh M, Bonewald LF, Detamore MS. Signalling strategies for osteogenic differentiation of human umbilical cord mesenchymal stromal cells for 3D bone tissue engineering. Journal of tissue engineering and regenerative medicine. 2009;3:398-404.

[172] Feng JQ, Scott G, Guo D, Jiang B, Harris M, Ward T, et al. Generation of a conditional null allele for Dmp1 in mouse. Genesis. 2008;46:87-91.

[173] Tan W, Krishnaraj R, Desai TA. Evaluation of nanostructured composite collagen--chitosan matrices for tissue engineering. Tissue engineering. 2001;7:203-10.

[174] Jackson RL, Busch SJ, Cardin AD. Glycosaminoglycans: molecular properties, protein interactions, and role in physiological processes. Physiological reviews. 1991;71:481-539.

[175] Kjellen L, Lindahl U. Proteoglycans: structures and interactions. Annu Rev Biochem. 1991;60:443-75.

[176] Chan BP, Leong KW. Scaffolding in tissue engineering: general approaches and tissue-specific considerations. Eur Spine J. 2008;17 Suppl 4:467-79.

[177] Foschi F, Conserva E, Pera P, Canciani B, Cancedda R, Mastrogiacomo M. Graft materials and bone marrow stromal cells in bone tissue engineering. Journal of biomaterials applications. 2012;26:1035-49.

[178] Chan RW, Rodriguez ML, McFetridge PS. The human umbilical vein with Wharton's jelly as an allogeneic, acellular construct for vocal fold restoration. Tissue engineering Part A. 2009;15:3537-46.

[179] Crapo PM, Gilbert TW, Badylak SF. An overview of tissue and whole organ decellularization processes. Biomaterials. 2011;32:3233-43.

[180] Altmann B, Steinberg T, Giselbrecht S, Gottwald E, Tomakidi P, Bachle-Haas M, et al. Promotion of osteoblast differentiation in 3D biomaterial micro-chip arrays comprising

fibronectin-coated poly(methyl methacrylate) polycarbonate. Biomaterials. 2011;32:8947-56.

[181] Burns JS, Rasmussen PL, Larsen KH, Schroder HD, Kassem M. Parameters in three-dimensional osteospheroids of telomerized human mesenchymal (stromal) stem cells grown on osteoconductive scaffolds that predict in vivo bone-forming potential. Tissue engineering Part A. 2010;16:2331-42.

[182] Scaglione S, Zerega B, Badano R, Benatti U, Fato M, Quarto R. A three-dimensional traction/torsion bioreactor system for tissue engineering. The International journal of artificial organs. 2010;33:362-9.

[183] Schagemann JC, Paul S, Casper ME, Rohwedel J, Kramer J, Kaps C, et al. Chondrogenic differentiation of bone marrow-derived mesenchymal stromal cells via biomimetic and bioactive poly-epsilon-caprolactone scaffolds. J Biomed Mater Res A. 2013;101:1620-8.

[184] Zhao L, Hantash BM. TGF-beta1 regulates differentiation of bone marrow mesenchymal stem cells. Vitamins and hormones. 2011;87:127-41.

[185] Kliemt S, Lange C, Otto W, Hintze V, Moller S, von Bergen M, et al. Sulfated hyaluronan containing collagen matrices enhance cell-matrix-interaction, endocytosis, and osteogenic differentiation of human mesenchymal stromal cells. Journal of proteome research. 2013;12:378-89.

[186] Derfoul A, Miyoshi AD, Freeman DE, Tuan RS. Glucosamine promotes chondrogenic phenotype in both chondrocytes and mesenchymal stem cells and inhibits MMP-13 expression and matrix degradation. Osteoarthritis and cartilage / OARS, Osteoarthritis Research Society. 2007;15:646-55.

[187] van Susante JLC, Pieper J, Buma P, van Kuppevelt TH, van Beuningen H, van Der Kraan PM, et al. Linkage of chondroitin-sulfate to type I collagen scaffolds stimulates the bioactivity of seeded chondrocytes in vitro. Biomaterials. 2001;22:2359-69.

[188] Goldring MB, Tsuchimochi K, Ijiri K. The control of chondrogenesis. Journal of cellular biochemistry. 2006;97:33-44.

[189] James AW, Xu Y, Lee JK, Wang R, Longaker MT. Differential effects of TGF-beta1 and TGF-beta3 on chondrogenesis in posterofrontal cranial suture-derived mesenchymal cells in vitro. Plastic and reconstructive surgery. 2009;123:31-43.

[190] Scaglione S, Braccini A, Wendt D, Jaquiery C, Beltrame F, Quarto R, et al. Engineering of osteoinductive grafts by isolation and expansion of ovine bone marrow stromal cells directly on 3D ceramic scaffolds. Biotechnology and bioengineering. 2006;93:181-7.

[191] Wang HS, Hung SC, Peng ST, Huang CC, Wei HM, Guo YJ, et al. Mesenchymal stem cells in the Wharton's jelly of the human umbilical cord. Stem cells. 2004;22:1330-7.

[192] Schieker M, Pautke C, Haasters F, Schieker J, Docheva D, Bocker W, et al. Human mesenchymal stem cells at the single-cell level: simultaneous seven-colour immunofluorescence. Journal of anatomy. 2007;210:592-9.

[193] Schieker M, Pautke C, Reitz K, Hemraj I, Neth P, Mutschler W, et al. The use of four-colour immunofluorescence techniques to identify mesenchymal stem cells. Journal of anatomy. 2004;204:133-9.

[194] Qian H, Le Blanc K, Sigvardsson M. Primary mesenchymal stem and progenitor cells from bone marrow lack expression of CD44 protein. J Biol Chem. 2012;287:25795-807.

[195] Lesley J, Hyman R, Kincade PW. CD44 and its interaction with extracellular matrix. Adv Immunol. 1993;54:271-335.

[196] Sobolewski K, Bankowski E, Chyczewski L, Jaworski S. Collagen and glycosaminoglycans of Wharton's jelly. Biol Neonate. 1997;71:11-21.

[197] Barry FP, Murphy JM. Mesenchymal stem cells: clinical applications and biological characterization. The international journal of biochemistry & cell biology. 2004;36:568-84.

[198] Bobis S, Jarocha D, Majka M. Mesenchymal stem cells: characteristics and clinical applications. Folia histochemica et cytobiologica / Polish Academy of Sciences, Polish Histochemical and Cytochemical Society. 2006;44:215-30.

[199] Yamaguchi A, Komori T, Suda T. Regulation of osteoblast differentiation mediated by bone morphogenetic proteins, hedgehogs, and Cbfa1. Endocr Rev. 2000;21:393-411.

[200] Ducy P. Cbfa1: a molecular switch in osteoblast biology. Dev Dyn. 2000;219:461-71.

[201] Zhou G, Zheng Q, Engin F, Munivez E, Chen Y, Sebald E, et al. Dominance of SOX9 function over RUNX2 during skeletogenesis. Proc Natl Acad Sci U S A. 2006;103:19004-9.

[202] Loebel C, Czekanska EM, Bruderer M, Salzmann G, Alini M, Stoddart MJ. In vitro osteogenic potential of human mesenchymal stem cells is predicted by Runx2/Sox9 ratio. Tissue Eng Part A. 2015;21:115-23.

[203] Conconi MT, Burra P, Di Liddo R, Calore C, Turetta M, Bellini S, et al. CD105(+) cells from Wharton's jelly show in vitro and in vivo myogenic differentiative potential. International journal of molecular medicine. 2006;18:1089-96.

[204] Bai J, Hu Y, Wang YR, Liu LF, Chen J, Su SP, et al. Comparison of human amniotic fluid-derived and umbilical cord Wharton's Jelly-derived mesenchymal stromal cells: Characterization and myocardial differentiation capacity. Journal of geriatric cardiology : JGC. 2012;9:166-71.

[205] Stenn KS, Paus R. Controls of hair follicle cycling. Physiological reviews. 2001;81:449-94.

[206] Dardour JC, Hennebert H. [Baldness surgery]. Annales de chirurgie plastique et esthetique. 2003;48:364-70.

[207] Lu ZF, Cai SQ, Wu JJ, Zheng M. Biological characterization of cultured dermal papilla cells and hair follicle regeneration in vitro and in vivo. Chinese medical journal. 2006;119:275-81.

[208] Matsuzaki T, Inamatsu M, Yoshizato K. The upper dermal sheath has a potential to regenerate the hair in the rat follicular epidermis. Differentiation; research in biological diversity. 1996;60:287-97.

[209] Osada A, Iwabuchi T, Kishimoto J, Hamazaki TS, Okochi H. Long-term culture of mouse vibrissal dermal papilla cells and de novo hair follicle induction. Tissue Eng. 2007;13:975-82.

[210] Horne KA, Jahoda CA, Oliver RF. Whisker growth induced by implantation of cultured vibrissa dermal papilla cells in the adult rat. J Embryol Exp Morphol. 1986;97:111-24.

[211] Osada A, Kobayashi K, Masui S, Hamazaki TS, Yasuda K, Okochi H. Cloned cells from the murine dermal papilla have hair-inducing ability. Journal of dermatological science. 2009;54:129-31.

[212] Jadalannagari S, Aljitawi OS. Ectodermal Differentiation of Wharton's Jelly Mesenchymal Stem Cells for Tissue Engineering and Regenerative Medicine Applications. Tissue Eng Part B Rev. 2015;21:314-22.

[213] Aljitawi OS, Xiao Y, Zhang D, Stehno-Bittel L, Garimella R, Hopkins RA, et al. Generating CK19-positive cells with hair-like structures from Wharton's jelly mesenchymal stromal cells. Stem Cells Dev. 2013;22:18-26.

[214] Aplin RT, Baldwin JE, Roach PL, Robinson CV, Schofield CJ. Investigations into the post-translational modification and mechanism of isopenicillin N:acyl-CoA acyltransferase using electrospray mass spectrometry. The Biochemical journal. 1993;294 (Pt 2):357-63.

[215] DasGupta R, Fuchs E. Multiple roles for activated LEF/TCF transcription complexes during hair follicle development and differentiation. Development. 1999;126:4557-68.

[216] Botchkarev VA, Botchkareva NV, Sharov AA, Funa K, Huber O, Gilchrest BA. Modulation of BMP signaling by noggin is required for induction of the secondary (nontylotrich) hair follicles. J Invest Dermatol. 2002;118:3-10.

[217] Fuchs E, Horsley V. More than one way to skin. Genes & development. 2008;22:976-85.

[218] Woo WM, Zhen HH, Oro AE. Shh maintains dermal papilla identity and hair morphogenesis via a Noggin-Shh regulatory loop. Genes & development. 2012;26:1235-46.

[219] Rendl M, Polak L, Fuchs E. BMP signaling in dermal papilla cells is required for their hair follicle-inductive properties. Genes & development. 2008;22:543-57.

[220] Plikus MV, Mayer JA, de la Cruz D, Baker RE, Maini PK, Maxson R, et al. Cyclic dermal BMP signalling regulates stem cell activation during hair regeneration. Nature. 2008;451:340-4.

[221] Owens P, Han G, Li AG, Wang XJ. The role of Smads in skin development. J Invest Dermatol. 2008;128:783-90.

[222] Hopkins RA. Cardiac reconstructions with allograft tissues. 2005.

[223] Baque CS, Zhou J, Gu W, Collaudin C, Kravtchenko S, Kempf JY, et al. Relationships between hair growth rate and morphological parameters of human straight hair: a same law above ethnical origins? Int J Cosmet Sci. 2012;34:111-6.

[224] Michel M, Torok N, Godbout MJ, Lussier M, Gaudreau P, Royal A, et al. Keratin 19 as a biochemical marker of skin stem cells in vivo and in vitro: keratin 19 expressing cells are differentially localized in function of anatomic sites, and their number varies with donor age and culture stage. J Cell Sci. 1996;109 (Pt 5):1017-28.

[225] Jahoda CA, Reynolds AJ, Chaponnier C, Forester JC, Gabbiani G. Smooth muscle alpha-actin is a marker for hair follicle dermis in vivo and in vitro. J Cell Sci. 1991;99 (Pt 3):627-36.

[226] Foitzik K, Lindner G, Mueller-Roever S, Maurer M, Botchkareva N, Botchkarev V, et al. Control of murine hair follicle regression (catagen) by TGF-beta1 in vivo. FASEB J. 2000;14:752-60.

[227] Kim SR, Cha SY, Kim MK, Kim JC, Sung YK. Induction of versican by ascorbic acid 2-phosphate in dermal papilla cells. J Dermatol Sci. 2006;43:60-2.

[228] Willert J, Epping M, Pollack JR, Brown PO, Nusse R. A transcriptional response to Wnt protein in human embryonic carcinoma cells. BMC Dev Biol. 2002;2:8.

[229] Morioka K, Arai M, Ihara S. Steady and temporary expressions of smooth muscle actin in hair, vibrissa, arrector pili muscle, and other hair appendages of developing rats. Acta Histochem Cytochem. 2011;44:141-53.

[230] Stasiak PC, Purkis PE, Leigh IM, Lane EB. Keratin 19: predicted amino acid sequence and broad tissue distribution suggest it evolved from keratinocyte keratins. J Invest Dermatol. 1989;92:707-16.

[231] Kishimoto J, Burgeson RE, Morgan BA. Wnt signaling maintains the hair-inducing activity of the dermal papilla. Genes & development. 2000;14:1181-5.

[232] Fuchs E, Merrill BJ, Jamora C, DasGupta R. At the roots of a never-ending cycle. Dev Cell. 2001;1:13-25.

[233] Van Mater D, Kolligs FT, Dlugosz AA, Fearon ER. Transient activation of beta -catenin signaling in cutaneous keratinocytes is sufficient to trigger the active growth phase of the hair cycle in mice. Genes & development. 2003;17:1219-24.

[234] Sung YK, Hwang SY, Cha SY, Kim SR, Park SY, Kim MK, et al. The hair growth promoting effect of ascorbic acid 2-phosphate, a long-acting Vitamin C derivative. J Dermatol Sci. 2006;41:150-2.

[235] Vegesna V, O'Kelly J, Uskokovic M, Said J, Lemp N, Saitoh T, et al. Vitamin D3 analogs stimulate hair growth in nude mice. Endocrinology. 2002;143:4389-96.

[236] Demay MB, MacDonald PN, Skorija K, Dowd DR, Cianferotti L, Cox M. Role of the vitamin D receptor in hair follicle biology. J Steroid Biochem Mol Biol. 2007;103:344-6.

[237] Fuchs E, Raghavan S. Getting under the skin of epidermal morphogenesis. Nat Rev Genet. 2002;3:199-209.

[238] Mundy G, Gutierrez G, Garrett R, Gallwitz W, Rossini G, Christiansen C, et al. Proteasome inhibitors stimulate both bone formation and hair growth by similar mechanisms. Annals of the New York Academy of Sciences. 2007;1117:298-301.

[239] Gurtner GC, Werner S, Barrandon Y, Longaker MT. Wound repair and regeneration. Nature. 2008;453:314-21.

[240] Aarabi S, Longaker MT, Gurtner GC. Hypertrophic scar formation following burns and trauma: new approaches to treatment. PLoS Med. 2007;4:e234.

[241] Berman B, Viera MH, Amini S, Huo R, Jones IS. Prevention and management of hypertrophic scars and keloids after burns in children. J Craniofac Surg. 2008;19:989-1006.

[242] Martin P. Wound healing--aiming for perfect skin regeneration. Science. 1997;276:75-81.

[243] Doi H, Kitajima Y, Luo L, Yan C, Tateishi S, Ono Y, et al. Potency of umbilical cord blood- and Wharton's jelly-derived mesenchymal stem cells for scarless wound healing. Sci Rep. 2016;6:18844.

[244] Sabapathy V, Sundaram B, V MS, Mankuzhy P, Kumar S. Human Wharton's Jelly Mesenchymal Stem Cells plasticity augments scar-free skin wound healing with hair growth. PLoS One. 2014;9:e93726.

[245] Pratheesh MD, Gade NE, Dubey PK, Nath A, Sivanarayanan TB, Madhu DN, et al. Molecular characterization and xenogenic application of Wharton's jelly derived caprine mesenchymal stem cells. Vet Res Commun. 2014;38:139-48.

[246] Arno AI, Amini-Nik S, Blit PH, Al-Shehab M, Belo C, Herer E, et al. Human Wharton's jelly mesenchymal stem cells promote skin wound healing through paracrine signaling. Stem Cell Res Ther. 2014;5:28.

[247] Azari O, Babaei H, Derakhshanfar A, Nematollahi-Mahani SN, Poursahebi R, Moshrefi M. Effects of transplanted mesenchymal stem cells isolated from Wharton's jelly of caprine umbilical cord on cutaneous wound healing; histopathological evaluation. Vet Res Commun. 2011;35:211-22.

[248] An Y, wei W, Jing H, Ming L, Liu S, Jin Y. Bone marrow mesenchymal stem cell aggregate: an optimal cell therapy for full-layer cutaneous wound vascularization and regeneration. Sci Rep. 2015;5:17036.

[249] Luo G, Cheng W, He W, Wang X, Tan J, Fitzgerald M, et al. Promotion of cutaneous wound healing by local application of mesenchymal stem cells derived from human umbilical cord blood. Wound Repair Regen. 2010;18:506-13.

[250] Lifecell. Alloderm tissue matrix defined. http://www.lifecell.com2016.

[251] Terino EO. Alloderm acellular dermal graft: applications in aesthetic soft-tissue augmentation. Clinics in plastic surgery. 2001;28:83-99.

[252] Achauer BM, VanderKam VM, Celikoz B, Jacobson DG. Augmentation of facial soft-tissue defects with Alloderm dermal graft. Annals of plastic surgery. 1998;41:503-7.

[253] Alander JT, Kaartinen I, Laakso A, Patila T, Spillmann T, Tuchin VV, et al. A review of indocyanine green fluorescent imaging in surgery. Int J Biomed Imaging. 2012;2012:940585.

[254] Kodjikian L, Richter T, Halberstadt M, Beby F, Flueckiger F, Boehnke M, et al. Toxic effects of indocyanine green, infracyanine green, and trypan blue on the human retinal pigmented epithelium. Graefes Arch Clin Exp Ophthalmol. 2005;243:917-25.

[255] Gale JS, Proulx AA, Gonder JR, Mao AJ, Hutnik CM. Comparison of the in vitro toxicity of indocyanine green to that of trypan blue in human retinal pigment epithelium cell cultures. Am J Ophthalmol. 2004;138:64-9.

[256] Bastawrous M, Pabón MM, Acosta S, de la Peña I, Hernandez-Ontiveros D, Staples M, et al. Wharton's Jelly Stem Cells. In: Fauza OD, Bani M, editors. Fetal Stem Cells in Regenerative Medicine: Principles and Translational Strategies. New York, NY: Springer New York; 2016. p. 257-76.

[257] Phinney DG, Prockop DJ. Concise review: mesenchymal stem/multipotent stromal cells: the state of transdifferentiation and modes of tissue repair--current views. Stem cells. 2007;25:2896-902.

[258] Mirotsou M, Jayawardena TM, Schmeckpeper J, Gnecchi M, Dzau VJ. Paracrine mechanisms of stem cell reparative and regenerative actions in the heart. J Mol Cell Cardiol. 2011;50:280-9.

[259] Liu S, Yuan M, Hou K, Zhang L, Zheng X, Zhao B, et al. Immune characterization of mesenchymal stem cells in human umbilical cord Wharton's jelly and derived cartilage cells. Cell Immunol. 2012;278:35-44.

[260] Khosrotehrani K. Mesenchymal stem cell therapy in skin: why and what for? Exp Dermatol. 2013;22:307-10.